

# Assessment of Steel-CLT Composite Floor Systems

Advancing material-efficient and environmentally friendly construction

van Rooij, N.H.

Delft University of Technology

Delft University of Technology

Advancing material-efficient and environmentally friendly construction

---

# Assessment of Steel-CLT Composite Floor Systems

---

*Author:*  
N.H. van Rooij

Monday 11<sup>th</sup> September, 2023

Thesis Committee	Prof. Dr. M. Veljkovic	TU Delft, Chair
	Dr. Ir. F. Kavoura	TU Delft, University Supervisor
	Dr. Ir. G.J.P. Ravenshorst	TU Delft
	CEng MIStructE T. Musson	WSP, Company Supervisor
	CEng FIStructE A. Woodward	WSP
	Pr Eng L. Ras	WSP

Cover: Construction site of the new Beaverton Public Safety Center (BPSC) by FFA Architecture and Interiors (Modified)



# Preface

The present report represents the culmination of my Masters thesis research on steel-timber composite floor systems, which satisfies the requirements for the completion of the Master's degree in Structural Engineering at the Faculty of Civil Engineering of Delft University of Technology.

Firstly, I extend my heartfelt thanks to T. Musson, my company supervisor, for his exceptional support, guidance, and professional insights throughout the research process. His expertise and encouragement have been invaluable in shaping this thesis. I am deeply grateful to Dr. Ir. F. Kavoura, my university supervisor, for her assistance and willingness to help me explore solutions during challenging situations. Her consistent guidance and scholarly input have significantly enriched this work. I extend my appreciation to Prof. Dr. M. Veljkovic and Dr. Ir. G.J.P. Ravenshorst, who served on my thesis committee. Their insightful perspectives, constructive criticism, and valuable feedback have greatly enhanced the quality of this research.

I would like to acknowledge WSP for providing me with the freedom to pursue the specific research area of my interest. I am grateful for their ongoing support, which has been instrumental in the success of this thesis. In particular, I would like to express my gratitude to A. Woodward and L. Ras from WSP in London for their openness and support regarding my thesis position. Their flexibility and willingness to accommodate my needs have contributed significantly to the overall success of this project.

Lastly, I would like to acknowledge my friends, family, and loved ones for their unwavering support and interest in my education. Their constant encouragement and presence have been a source of inspiration, motivating me to persevere and overcome challenges. Your love, understanding, and presence have always reminded me of what truly matters in life.

*Rooij, Nils  
Rotterdam, September 2023*

# Abstract

With the building and construction sector accounting for a significant portion of final energy use and emissions, and society's increasing focus on environmental awareness and improvements, the importance of sustainable construction has never been greater.

The utilisation of timber in construction offers clear sustainability benefits and has the potential to replace traditional functions of concrete. One notable replacement is the use of Cross-Laminated Timber (CLT) in composite structures with steel, enabling the potential creation of greatly performing floor systems which has seen a limited amount of research. The research explores the application of Steel-CLT Composite floor systems and assesses composite beam performance as well as predictive methods for analysing their behaviour in hopes of advancing the body of knowledge on this method of environmentally friendly construction.

The literature study revealed the current knowledge on steel-CLT composite floor systems and connections. Two particular floor systems, with and without the use of grout, are highlighted as well the potential for future exploration.

The steel-CLT composite connection utilised in the floor system significantly impacts performance and composite action as the use of grout is concluded to increase initial-, secondary stiffness and load carrying capacity of the connection. However, restricting the use of grout can promote circular construction practices.

In this research the behaviour of steel-CLT composite beams is predicted by the use of a numerical finite element model with shell elements and an analytical approach based on the simplified analysis of Eurocode 5(EN1995-1-1): Mechanically jointed beams.

The analytical method can predict the bending stiffness with a margin of error just slightly above 10%. However, it should be noted that the analytical method incorporates an incomplete representation of the composite connection used in the beam. On the other hand, the finite element model is able to accurately capture the pre-plasticity behaviour of the steel-CLT composite beam. This is achieved by incorporating the complete load-slip behaviour of the shear connection.

A parametric study was conducted to assess the importance of closely spacing composite shear connections in a steel-CLT composite beam to achieve a higher level of composite action. The study also demonstrates that by utilising connections with higher initial stiffness, secondary stiffness, and ultimate capacity, this effect can be further strengthened. As a result, the force resisted at the serviceability limit state experiences a notable boost due to the implementation of both a stronger and stiffer connection, as well as their close spacing. Shear connection position optimisation by concentration of connectors near the supports showed to have a small positive effect on beam deflection.

After evaluation of steel-CLT floor systems the research concludes that a steel-CLT composite floor system can be successfully constructed, offering environmental benefits and reduced structural weight while achieving the required structural performance for the set design conditions.

# Contents

<b>Preface</b>	<b>i</b>
<b>Abstract</b>	<b>ii</b>
<b>Nomenclature</b>	<b>ix</b>
<b>1 Introduction</b>	<b>1</b>
1.1 Relevance of the study	1
1.1.1 Construction with timber	1
1.1.2 Hybrid construction	2
1.1.3 Composite construction	3
1.1.4 Steel-timber composites	5
1.1.5 The debate on material efficiency and demountable construction	7
1.1.6 Problem statement	7
1.2 Research objective and questions	7
1.2.1 Objective	7
1.2.2 Research questions on Steel-CLT composite floors	8
1.3 Report structure	9
<b>2 State of the Art</b>	<b>10</b>
2.1 Background on composite beams	10
2.2 Shear connectors	11
2.3 Cross laminated timber	13
2.4 Effective flange width of T-sections	14
2.5 Steel-CLT composite floor systems	16
2.5.1 Floor system with continuous CLT panel	17
2.5.2 Floor system with transverse reinforced concrete slots with welded studs	18
2.6 Steel-CLT composite connections	22
2.6.1 Dowel-type fasteners for STC connections	22
2.6.2 Grout utilisation in STC connections	24
2.6.3 Comparison of experimentally tested steel-CLT connections	26
2.6.4 Spacing	28
<b>3 Analytical analysis</b>	<b>29</b>
3.1 Equivalent cross-section of the CLT panel	29
3.2 Effective bending stiffness with full- and no-composite action	30
3.3 Mechanically jointed steel-CLT composite beam	31
<b>4 Finite element model</b>	<b>32</b>
4.1 General	32
4.2 Material properties and behaviour	34
4.2.1 Cross laminated timber slab	34
4.2.2 Steel beam	36
4.3 Shear connection	36
4.3.1 No composite action	37
4.3.2 Full composite action	37
4.3.3 Rigid composite connection	37
4.3.4 Partial composite connection	37
4.4 Meshing	40
4.4.1 Elements	40

---

4.4.2	Mesh	40
4.5	Analysis and boundary conditions	41
4.5.1	Supports	41
4.5.2	Loading conditions	41
4.5.3	Iterative scheme	42
4.6	Validation of Numerical model	42
<b>5</b>	<b>Numerical study</b>	<b>45</b>
5.1	Parametric Study	45
5.1.1	Configurations	45
5.1.2	Material properties	46
5.2	Results	47
5.2.1	Overview of beam behaviour	47
5.2.2	Initial beam stiffness	52
5.2.3	Slip	53
5.2.4	Stress over cross-section height at midspan	55
5.2.5	Stress over width of CLT panel	59
5.2.6	Composite efficiency	63
5.3	Shear connection location optimisation study	64
5.4	Conclusions from numerical study	67
5.4.1	Spacing of composite connections	67
5.4.2	Characteristics of the composite connection	68
5.4.3	Width of the CLT panel	69
<b>6</b>	<b>Floor System Evaluation</b>	<b>70</b>
6.1	Floor system with transverse reinforced concrete slots with welded studs	70
6.2	Floor system with continuous CLT panel	73
6.3	Evaluation	75
<b>7</b>	<b>Conclusions</b>	<b>77</b>
<b>8</b>	<b>Discussion</b>	<b>81</b>
8.1	Numerical analysis	81
8.1.1	Scattering of numerical results	82
8.2	Analytical analysis	82
8.2.1	Scattering of analytical results	83
8.3	Recommendations and future research	83
	<b>References</b>	<b>85</b>



# List of Figures

1.1	Buildings and construction's share of global final energy and emissions in 2021[36], where "Buildings construction industry" is the portion (estimated) of overall industry devoted to manufacturing building construction materials such as steel, cement and glass	1
1.2	Pohlmann slab (1901) (from [14])	3
1.3	Typical steel-concrete composite (SCC) floor with a metal deck [3]	4
1.4	Examples of TCC & SCC slab systems (Adapted from [45])	4
1.5	STC slab system (Adapted from [45])	5
2.1	Cross sectional stress distribution due to (a) non-restricted and (b) fully-restricted slip (from [2])	10
2.2	Schematic illustration of the vertical strain distribution for cross-sections with (a) no composite action, (b) partial composite action and (c) no composite action.	11
2.3	Steel-CLT push-out test setup used by [68]	11
2.4	Loading protocol of push-out test by guidance of [21]	12
2.5	Load-slip curves of shear connectors	13
2.6	Construction detail of CLT panels [10]	13
2.7	Theoretical stress distribution (left) and Simplified rectangular stress distribution (right) with effective width( $b_E$ ) in T-sections (Adapted from [27])	15
2.8	Steel-CLT composite floor systems with (a) a continuous CLT panel connected with screws, (b) two CLT panels connected with the use of a grouted stud and transverse reinforcement and (c) two CLT panels compositely connected without the use of grout	17
2.9	View of modular steel-CLT hybrid construction proposed by [45]	17
2.10	Configuration II D-4 for a panel to panel connection [44]	18
2.11	Prototypes of floor components with custom-made U-shaped steel beam by [43]. (a) Composite connection with inclined screws and (b) steel plates with epoxy based resin	18
2.12	SCC floor system with precast HCS by [42]	19
2.13	The design for a steel-CLT composite floor system from WSP	20
2.14	The design for the composite connection from WSP	20
2.15	dowel-type fasteners in steel-CLT composites such as (a) screws and (b) bolts	22
2.16	Yielding modes (EYM) of the fastener considered for timber-to-steel connections (Adapted from [71])	23
2.17	Load-Slip curves for STC connection specimen (Adapted from [68]) with Group A: $6\phi$ 6.8 Bolts, Group B: $8\phi$ 6.8 Bolts, Group C: $5.5\phi$ Self drilling screws with other parameters unchanged	24
2.18	Side perspective on push-out test samples of BCGP, SCGP and GSC (L-R) (Adapted from [34], [73] and [72])	25
2.19	Load-Slip curves for STC connection specimen with changing diameters (Adapted from [28]) with (a) Coach screws, (b) Dog screws and (c) Bolt connectors in grouted pockets	25
2.20	Load-Slip curves for STC connection specimen with screws in grouted pockets (Adapted from [73]) with (a) screws, (b) screw in grouted pocket, (c) SCGP with increased depth and lastly (d) SCGP in pocket with increased radius	26
3.1	Cross-section of steel-CLT composite beam	29
3.2	Cross-section of steel-CLT composite beam with equivalent CLT panel	30
3.3	Schematic illustration of the vertical strain distribution for cross-sections and the corresponding distances $a_1$ & $a_2$	31

4.1	Extruded 3D finite element model, used for validation, of simply supported steel-CLT composite beam . . . . .	32
4.2	3D finite element model, used for validation, of simply supported steel-CLT composite beam . . . . .	33
4.3	Finite element mode: Cross-section of simply supported steel-CLT composite beam used for validation . . . . .	33
4.4	Finite element mode: Side view of simply supported steel-CLT composite beam used for validation . . . . .	34
4.5	Side view of 4-point bending tests on steel-CLT composite beam executed by (and figure adapted from:[31]) with instrumentation visual . . . . .	34
4.6	Stress-strain diagrams of the strengths in the Hashin damage model(Adapted from [65])	35
4.7	Uniaxial stress-strain relationship for the steel beam . . . . .	36
4.8	Zero-length spring, modelling with connector element 'Translator' that connects node of CLT panel with node of top flange of steel beam with a local axis system . . . . .	38
4.9	Connection type TRANSLATOR imposes kinematic constraints and uses local orientation definitions equivalent to combining connection types SLOT and ALIGN [11] . . . . .	38
4.10	Load-slip curve of two composite connections used in validation of the finite element model with data from [31] . . . . .	39
4.11	Piece-wise linear load-slip curve of two composite connections used in validation of the finite element model . . . . .	39
4.12	3D perspective on FEM with displayed mesh . . . . .	40
4.13	Side perspective on FEM with displayed mesh . . . . .	40
4.14	Top perspective on FEM with displayed mesh of the CLT panel . . . . .	40
4.15	Modelled support with the bottom section simply supported and central vertice laterally restrained . . . . .	41
4.16	Loading conditions of the finite element model zoomed in on position $z = 2L/3$ . . . . .	41
4.17	Numerical Results: Load-midspan deflection curve . . . . .	42
4.18	Load-Midspan deflection of experimental tests and numerical model (Experimental data from [31]) . . . . .	43
5.1	Uniaxial stress-strain relationship of S275 as defined by EN1993-1-1 §3.2.6 [17] . . . . .	47
5.2	Deflection of simply supported beam at different load levels in four-point flexural bending test numerically tested (I.E. force ( $P$ ) and deflection (solid black line) at load level 3 in the figure) . . . . .	47
5.3	Load-Midspan deflection of all configuration specified in Table 5.1 with parametric changes in length(red), slab width(blue), spacing(green), profile(purple) and connection type(orange)	48
5.4	Load-Midspan deflection of all configuration specified in Table 5.1 with parametric changes	49
5.5	Load-Midspan deflection of all configuration specified in Table 5.1 with parametric changes in slab width(blue), spacing(green) and connection type(orange) . . . . .	50
5.6	Load-midspan deflection of configuration 1 with force at serviceability limit state ( $P_{SLS}$ ) and angle of initial beam stiffness( $K_{b,ini}$ ) and stiffness per unit length( $k$ ) . . . . .	51
5.7	Cumulative maximum force at given displacement (load level) for the tested configurations	52
5.8	Initial beam stiffness of different configurations in numerical four-point bending test . . .	52
5.9	Initial beam stiffness of different configurations in numerical four-point bending test . . .	53
5.10	Configuration 2: The slip at material interface over the length of the beam . . . . .	54
5.11	The slip at the material interface over the length of beam configurations . . . . .	55
5.12	Side perspective of steel-CLT composite beam cross section of the numerical study with the connections: (a) dog screws and (b) BCGP (Further specified in Table 5.2 . . . . .	56
5.13	Longitudinal stress( $\sigma_{11}$ ) distribution at midspan over longitudinal axis of symmetry over the height of the cross-section . . . . .	56
5.14	Longitudinal stress( $\sigma_{11}$ ) distribution at midspan over longitudinal axis of symmetry over the height of the cross-section . . . . .	57
5.15	Longitudinal stress( $\sigma_{11}$ ) distribution at midspan over longitudinal axis of symmetry over the height of the cross-section . . . . .	58



5.16	Longitudinal stress( $\sigma_{11}$ ) distribution at midspan over longitudinal axis of symmetry over the height of the cross-section . . . . .	59
5.17	Example of cross-section of steel-CLT composite beam used in numerical analysis . . . . .	59
5.18	Stress development in compression at midspan at the top of the CLT panel of configuration 1 . . . . .	60
5.19	Stress development in tension at midspan at the bottom of the CLT panel of configuration 1 . . . . .	60
5.20	Stress development in compression at midspan at the top of the CLT panel of configuration 4 . . . . .	61
5.21	Stress development in tension at midspan at the bottom of the CLT panel of configuration 4 . . . . .	61
5.22	Stress development in compression at midspan at the top of the CLT panel of configuration 5 . . . . .	62
5.23	Stress development in tension at midspan at the bottom of the CLT panel of configuration 5 . . . . .	62
5.24	Stress development in compression at midspan at the top of the CLT panel of configuration 10 . . . . .	62
5.25	Stress development mostly in tension at midspan at the bottom of the CLT panel of configuration 10 . . . . .	63
5.26	Additional configurations ( $7_{O,1}$ , $12_{O,1}$ , $7_{O,2}$ , $12_{O,2}$ ) with different positions of shear connections in comparison to configurations 1,7,10 and 12 . . . . .	65
5.27	Load-Midspan deflection of configurations with non-uniform en uniform shear connection distribution . . . . .	65
5.28	The slip at the material interface over the length of the beam . . . . .	66
5.29	Load-midspan deflection of configurations with a changing spacing ( $s$ ) of composite connections type 'A' (left) and type 'B' (right) (Connection types clarified in Fig. 5.2) . . . . .	67
5.30	Initial beam stiffness of configuration 1,6 & 7 with composite connection A (left) and configuration 10,11 & 12 with composite connection B (right) with initial beam stiffness at full- and no-composite action . . . . .	68
5.31	Load-slip curve of two composite connections used in validation of the finite element model [31] . . . . .	68
6.1	The design for the composite connection from WSP . . . . .	70
6.2	Comparison(by [72]) between simulated results and test curves from literature[32] and finite element data from [72]. (a) BGP12 8.8 60; (b) BGP16 8.8 80 . . . . .	71
6.3	Estimation of the load-slip behaviour of the composite connection with transverse reinforced concrete slots with welded studs displayed in Fig. 6.1 . . . . .	72
6.4	Floor system segment from Section 2.5.2 with transverse reinforced concrete slots with welded studs numerically tested in four-point bending test . . . . .	73
6.5	Upper- and lower bound of the load-midspan deflection of the floor segment with transverse reinforced concrete slots and welded studs . . . . .	73
6.6	Floor system segment from Section 2.5.1 with screws (or BCGP) and panel-to-panel connection from [45] . . . . .	74
6.7	Load-midspan deflection of the floor segment with transverse reinforced concrete slots and welded studs and the segment with continuous CLT panel . . . . .	74

# List of Tables

1.1	Comparison of two different types of composite floor systems . . . . .	6
2.1	Comparison of existing experimental data on steel-CLT composite connections in push-out tests according to BS EN26891[21] . . . . .	27
4.1	Mechanical properties of the timber lamellae adopted in the validation model . . . . .	35
4.2	Hashin damage model parameters adopted in the validation model . . . . .	36
4.3	Properties of the 310UB32 profile . . . . .	36
4.4	Comparison beam behaviour of the numerical model, experimental test data, and analytical results . . . . .	44
5.1	Configurations of steel-CLT composite beams . . . . .	46
5.2	Properties of the composite connection . . . . .	46
5.3	Properties of the S275 steel grade . . . . .	46
5.4	Load level and Prescribed displacement . . . . .	47
5.5	Overview of configurations' beam behaviour . . . . .	50
5.6	Composite efficiency of configurations . . . . .	64
6.1	Evaluation . . . . .	75
6.2	Load categories and resulting design value of action . . . . .	75
6.3	Design value of resistance of floor systems compared to design value of action . . . . .	75

# Nomenclature

## Abbreviations

Abbreviation	Definition
BCGP	Bolt connectors embedded in grout pockets
CLT	Cross laminated timber
CS	Coach screw
DS	Dog screw
EN	European Norm
EYM	European Yield Model
GSC	Grouted stud connector
GLT	Glue laminated timber
HCS	Hollow core slabs
LCA	Life cycle assessment
LVL	Laminate veneer lumber
MPC	Multi point constraint
MOE	Modulus of elasticity
MSE	Mean squared error
SCC	Steel-concrete composite
SCGP	Screw connectors embedded in grout pockets
SDS	Self drilling screw
STC	Steel-timber composite
TCC	Timber-concrete composite
TTC	Timber-timber composite

## Symbols

Symbol	Definition	Unit
$a_i$	Distance layer $i$ to cross-sectional center	[mm]
$A$	Area	[mm <sup>2</sup> ]
$b$	Width	[mm]
$b_E$	Effective flange width (in T-sections)	[mm]
$b_f$	Flange width	[mm]
$C$	Composite efficiency	[%]
$CO_2\text{-eq}$	Carbon dioxide equivalent	[kg CO <sub>2</sub> -eq]
$d$	Depth	[mm]
$\Delta$	Deflection (or Displacement)	[mm]
$\delta$	Slip	[mm]
$E$	Young's modulus or Modulus of elasticity	[MPa]
$E_{h,CLT}$	MOE of the equivalent CLT cross-section	[MPa]
$E_s$	Young's modulus or Modulus of elasticity of steel	[MPa]
$EI_a$	Analytical bending stiffness	[Nmm <sup>2</sup> ]
$EI_{ini}$	Initial bending stiffness	[Nmm <sup>2</sup> ]
$EI_{n,ini}$	Numerical initial bending stiffness	[Nmm <sup>2</sup> ]
$E_1, E_2, E_3$	Directional Young's moduli	[MPa]

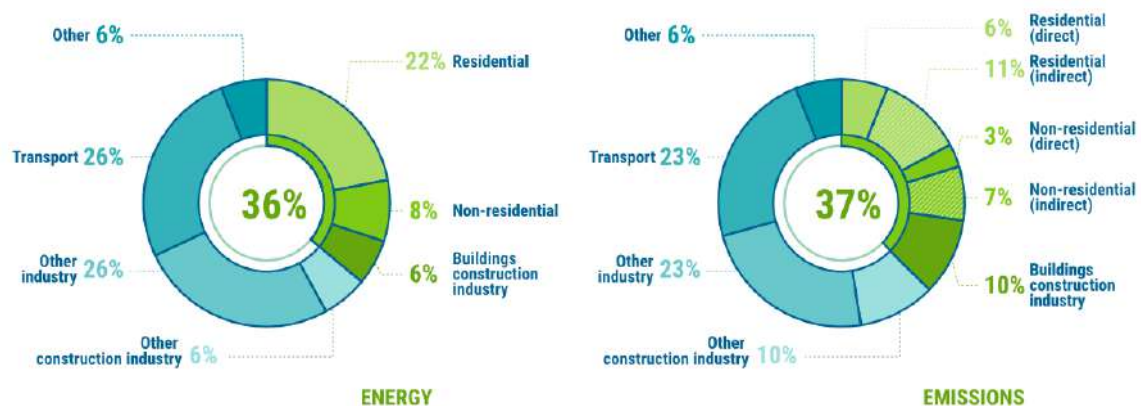
Symbol	Definition	Unit
$\varepsilon_{bottom}$	Strain at material interface of beam	[mm/mm]
$\varepsilon_{top}$	Strain at material interface of slab	[mm/mm]
$f_{u,s}$	Ultimate strength of steel	[MPa]
$f_{y,s}$	Nominal yield strength of steel	[MPa]
$G_{12}, G_{13}, G_{23}$	Directional Shear Moduli	[MPa]
$\gamma$	gamma-factor	[-]
$h$	Height	[mm]
$I$	Second moment of area	[mm <sup>4</sup> ]
$k$	Beam stiffness per unit length	[N/mm <sup>2</sup> ]
$k_{s,0.4}$	Initial stiffness at 40% of ultimate load	[kN/mm]
$k_{s,0.6}$	Ultimate stiffness at 60% of ultimate load	[kN/mm]
$K$	Slip modulus (in EN1995-1-1 Annex B)	[kN/mm]
$K_{b,ini}$	Initial beam stiffness	[kN/mm]
$L$	Length	[mm]
$n$	Number of connectors	[-]
$n_{ef}$	Effective number of connectors	[-]
$\nu$	Poisson's ratio	[-]
$P$	Load (or Force)	[kN]
$P_{Rk}$	Ultimate load carrying capacity	[kN]
$P_u$	Ultimate load carrying capacity	[kN]
$P_y$	Yield load	[kN]
$\phi$	Diameter	[mm]
$s$	Connector spacing	[mm]
$\sigma_{11}$	Principal stress in longitudinal direction	[MPa]
$\sigma_{c1}$	Longitudinal compressive strength	[MPa]
$\sigma_{c2}$	Transversal compressive strength	[MPa]
$\sigma_{t1}$	Longitudinal tensile strength	[MPa]
$\sigma_{t2}$	Transversal tensile strength	[MPa]
$\sigma_{v12}$	Longitudinal shear strength	[MPa]
$\sigma_{v23}$	Transversal shear strength	[MPa]
$t$	Thickness	[mm]
$t_f$	Flange thickness	[mm]
$t_w$	Web thickness	[mm]
$u_{bottom}$	Displacement at material interface of beam	[mm]
$u_{top}$	Displacement at material interface of slab	[mm]

# Introduction

## 1.1. Relevance of the study

### 1.1.1. Construction with timber

As humanity has developed, the presence of buildings and structures has grown exponentially. As of 2021, The buildings and construction sector accounted for 36% of global final energy use and 37% of the global carbon dioxide emissions at 3.6  $GtCO_2$ . 10% of which is a result of manufacturing important building materials such as steel and cement [36]. As we face the looming threat of permanent and catastrophic climate change, the urgency for sustainable and economical construction methods and technologies has never been greater. The buildings and construction sector worldwide needs to almost fully decarbonise by 2050 in order to meet the goals set forth in the Paris Agreement[36]. It is imperative for the the buildings and construction sector to take action now to minimise the carbon footprint and pave the way for a more sustainable future.



**Figure 1.1:** Buildings and construction's share of global final energy and emissions in 2021[36], where "Buildings construction industry" is the portion (estimated) of overall industry devoted to manufacturing building construction materials such as steel, cement and glass

While the environmental advantages of using timber as a construction material cannot be easily quantified for the present design, it still holds a considerable appeal due to its eco-friendliness. As a renewable resource timber has the additional advantage of storing carbon, with approximately 50% of its dry weight being carbon. Life cycle analysis allows the calculation of carbon-dioxide equivalent ( $CO_2-eq$ ) emissions for buildings and when comparing timber to more traditional construction methods such as use reinforced concrete in floors it is reported that it takes up to three times less energy and up to twelve times less fossil fuel to manufacture timber beams and floors[58]. Although deforestation,

largely caused by agriculture rather than logging, is of great concern there is sufficient supply of timber in the future as forests can be regrown with proper oversight and legislation.

In addition to the environmental benefits, the potential for construction with timber is vast, as engineered wood products offer a wide range of possibilities. They include a range of derivative wood products that are manufactured by bindings, fixing or orientating strands, particles, fibres, veneers or panels by methods of fixation to engineer a timber product with specific design specifications. Secondly, with application of timber in construction a significant reduction of the self-weight of the structure is achieved due to its lightweight property.

In summary, timber is a renewable material with fewer environmental impacts[58] when compared to concrete and steel and favorable construction attributes, such as a high strength-to-weight ratio when compared to traditional materials like steel and concrete. Additionally, engineered wood products offer a range of design possibilities. The potential for timber in construction is vast and it presents a great alternative due to its many benefits.

Despite the numerous advantages of using timber in construction, it is not without its constraints. Although it has a high strength-to-weight ratio in comparison to traditional construction materials like steel and concrete, its structural span when used as a sole material is limited due to its strength and stiffness, and material use quickly increases beyond this limit, which goes against the principle of sustainability. Additionally, the lightweight nature of timber can be a limitation, as it often requires additional mass to achieve acoustic or vibration limits. Moreover, fire is an issue with timber construction. Many countries limit the height of timber buildings due to concerns about fire performance, which further restricts its use in construction. These constraints suggest the need for alternative approaches that combine timber with other materials to achieve optimal structural performance and sustainability.

### 1.1.2. Hybrid construction

These promising engineered wood products can show even further improved sustainability and structural performance by using the product in conjunction with other materials, such as steel and reinforced concrete. Besides the increase in performance it tackles the constraint of timber as the sole material in use, such as the rapid increase of material use with an increasing span and required mass to combat acoustics, vibrations and fire requirements. Such hybrid construction elements and structures, systems where you combine different materials, enable an even wider range of structural solutions whilst optimising structural and building performance configurable to the design limitations at hand. Such hybrid structural solutions enable compensation of timber disadvantages such as its brittle failure in tension or shear.

Hybrid construction, where structural elements of different materials are used in a system, with timber, has shown great potential to utilise the previously mentioned(Section 1.1.1) beneficial properties of timber construction.

An example would be the designed steel-timber hybrid system, named the FFTT(Finding the Forest Through the Trees) system, that utilises timber products to resist gravity and lateral loads, essential in seismic reliability, with interconnection steel elements to provide ductility[25]. The steel elements allows dissipation of energy during, for example, intense ground motion where the timbers characteristic of non-ductile failure would be undesirable.

Similarly, more use of hybrid structural solutions is seen in steel-timber systems with cross-laminated timber, an engineered wood panel product made from gluing together at least three layers of solid-sawn lumber, used as infilled shear panels, to transfer shear force, in steel moment resisting frames [13].

Besides mixed-material solutions of steel and timber in structural systems research has shown the potential of the use steel and timber in jointed connections such as the use of post-tensioning technology, originally developed for precast concrete construction, in multi-story timber buildings [54] which resulted in a design procedure to guarantee control over the dissipative system of a multi-story timber building. Post-tensioning timber connections, thus hybridising steel, has been further developed to withstand significant horizontal loading[66].

In short, there are researched benefits of hybridisation of engineered wood products with steel and it has shown significant potential in application. Hybrid CLT-based construction is no longer in the stage of infancy, but practical and cost-effective steel-CLT assemblies for large scale mid to high-rise building application has not been fully explored.

### 1.1.3. Composite construction

As previously mentioned hybrid construction involves different materials in different parts of a structures such as a steel frame with timber floor. But such hybrid structural solutions can be done while combining two or more materials to create a single structural element; this is called composite construction. In short, composite construction, a broad term, is a form of a hybrid construction solution of materials in element build-up. The materials are used in conjunction to optimise a structural element, such as a reinforced beam or column.

Most notable, for this research, is the wide use of steel-concrete composite floors and systems, where compositely, through shear connectors, to connect the materials, the concrete works in compression and the steel beam in tension. This common system then utilises the beneficial properties of concrete in compression and steel in tension and has grown to be a common system in a variety of buildings. One of the first implementations is known as the Pohlmann slab(1901) [14] where flat metal hoops form shear connection as they restrict the movement of the concrete.

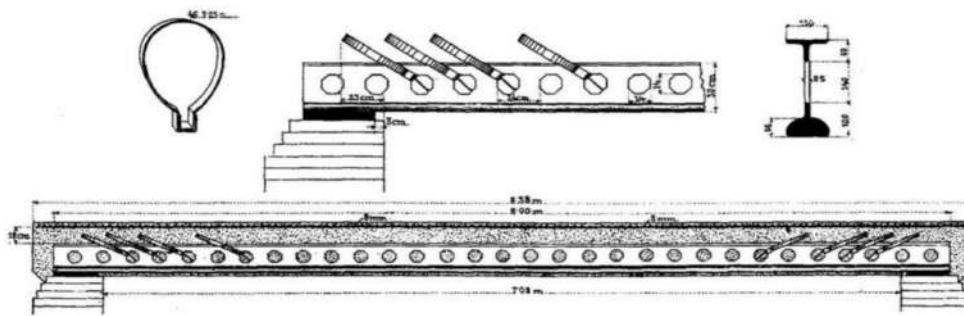
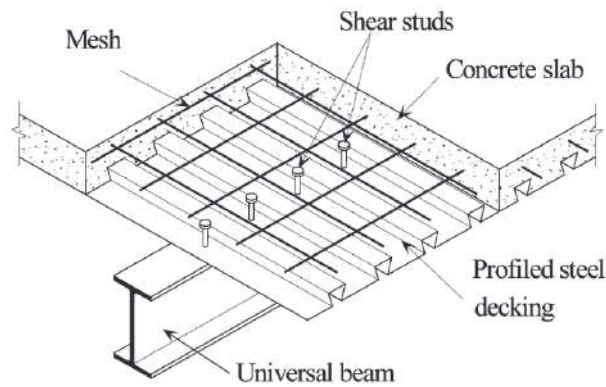


Figure 1.2: Pohlmann slab (1901) (from [14])

In a modern example of steel-concrete composite floor systems(Fig. 1.3), the steel beam is connected to the metal deck using shear studs that are welded to the top flange of the beam. The metal deck acts as a formwork during the construction stage, and later as a tensile reinforcement for the concrete slab. Once the steel beam and metal deck are in place, the concrete is poured onto the metal deck, which then sets and hardens to form a composite slab.

The shear connectors welded to the steel beam and embedded in the concrete slab prevent slip between the steel beam and the concrete slab, allowing for composite action between the two materials. The result is a floor system that is more efficient than a system with no-composite action , with a higher load-carrying capacity, increased stiffness, and improved deflection performance.



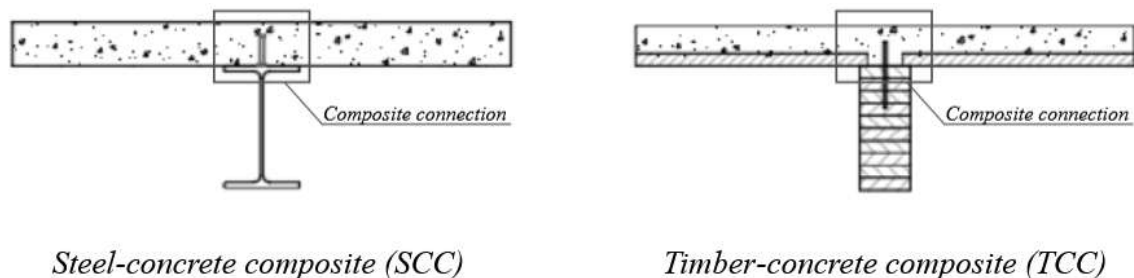


**Figure 1.3:** Typical steel-concrete composite (SCC) floor with a metal deck [3]

In composite construction, engineered wood products in conjunction with steel. Employing the engineered wood products can utilise beneficial properties such as freedom in design, a high-strength to weight ratio and lightweight in general, made from a renewable source (Section 1.1.1). Composite construction, utilising engineered wood products, could possibly rival conventional solutions, such as the above mentioned steel-concrete composite (SCC) floor system.

During the post-war periods there was a shortage of steel to reinforce concrete which was the origin of the TCC system in Europe as [49] presented a connection between a concrete slab with timber beams underneath.

Application of timber, in composite construction, has been researched extensively in the last 15 years. Both timber-concrete composites (TCC) and timber-timber composite (TTC) construction, has found extensive application because of ease of maintenance and low construction cost when comparing it to reinforced concrete and steel whilst being a efficient sustainable building solution [69] [40].



**Figure 1.4:** Examples of TCC & SCC slab systems (Adapted from [45])

The method of constructing TCC structures involves connecting a timber beam or deck to an upper concrete flange using various connectors. By combining the unique characteristics of both materials, TCC structures can withstand bending and tensile forces induced by gravity loads through the timber, while the concrete topping resists compression forces.

In short, TCC has potential as a sustainable effective floor solution. The subject has now been investigated at length but lacks economical solutions and prefabrication processes, fast erection and user-friendly design packages to compete within the construction industry [70].

Engineered wood products can be tailored to meet specific design requirements, allowing for the use of various timber elements with distinct engineered properties in composite construction. Cross-laminated timber (CLT) is a noteworthy product due to its slab of cross-layered laminates, providing two-way properties. Similarly, cross-banded laminate veneer lumber (LVL) panels can also achieve this two-directional resistance. By combining these two-directional engineered wood products as a top

surface with glue laminated timber (GLT) or LVL beams below, a timber-timber composite (TTC) floor can be created.

This TTC floor has advantageous timber properties such as being more lightweight, whilst comparing it to its TCC counterpart, while the CLT panel provides two-way action and the timber-beam underneath offers sufficient strength and stiffness. As previously stated, the composite connection is the leading influence on global performance of composite floors which therefor has been experimentally and numerically researched [55].

The advantages of using timber as a construction material are evident, particularly with the ability to engineer specific wood products and utilise composite construction techniques. Utilising composite construction with timber compensates for constraints such as the disadvantages of a brittle failure in tension or shear, the limited span capacity and the lightweight nature where mass is beneficial for acoustic or vibration limits.

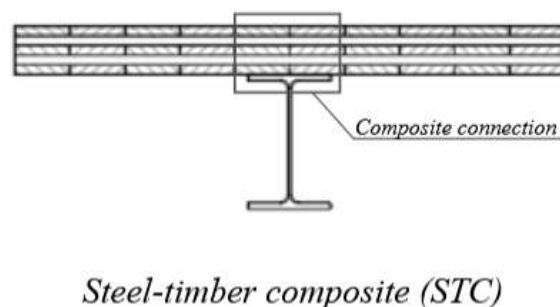
Other disadvantages of timber in construction should also be addressed in practical building solutions such as the susceptibility to moisture and decay, fire resistance and cost.

But in general using timber compositely in construction has promising potential. When combined with the benefits of steel, an entirely reusable strong material, in composite construction, it can result in a high-performance and eco-friendly floor solution. This approach allows for the incorporation of the best of both worlds as the flexibility of timber and the durability and strength of steel results in a sustainable and efficient floor design.

#### 1.1.4. Steel-timber composites

Research has demonstrated the structural benefits of hybridising, using different materials as different parts, with steel and engineered timber in various ways. Examples are the use of steel beams with timber columns [67], steel frames with timber wall panels [46][12]. Composite construction, on the other hand, combines multiple materials to create a single element. At this element level, the advantages of composite construction were evident in strengthening timber beams with steel plates or sheets [37] [8].

Therefore, it would be logical to explore the hybridisation of steel and timber at the composite construction level in floor systems to effectively integrate the two materials in a single structural element. Such research would allow for the best utilisation of both steel and timber's unique properties (Sections 1.1.1 and 1.1.2). Both materials have a height strength-to-weight ratio while steel has a high fire resistance and timber low thermal conductivity. Steel, as a material is also highly ductile and isotropic. In terms of sustainability steel is fully reuseable in many circumstances and completely recyclable while timber is a renewable resource with a low carbon footprint. Composite construction with steel and engineered timber products will potentially lead to innovative composite solutions with enhanced performance and sustainability.


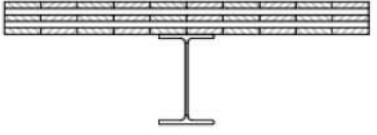


**Figure 1.5:** STC slab system (Adapted from [45])

Recent research [45][29] has explored steel-timber composite (STC) systems (Fig. 1.5) and their performance and feasibility, while four-point bending testing [32] has been conducted to support these

findings. The versatility of cold-formed thin-walled steel sections in combination with the numerous options available in engineered wood products allows for endless possibilities in compositely connecting the materials, providing freedom in shaping and design of an STC system.

**Table 1.1:** Comparison of two different types of composite floor systems

Steel-concrete composite system		Steel-CLT composite system	
			
Steel beam grade	S275	Steel beam grade	S275
Concrete grade	C25/30	Timber boards grade	C24
Profile	HEA160	Profile	HEA160
Slab height ( $h_c$ )	100 mm	Slab height ( $h_t$ )	5 x 20 mm
		Orientation ( $^\circ$ )	[0,90,0,90,0]
Spanning length	6 m	Spanning length	6 m
Width	2 m	Width	2 m
$w_{SLS} (l/250)$	24 mm	$w_{SLS} (l/250)$	24 mm
$EI_{k=0}$	$8.8 \cdot 10^{12} \text{ Nmm}^2$	$EI_{k=0}$	$4.9 \cdot 10^{12} \text{ Nmm}^2$
$EI_{k=\infty}$	$2.1 \cdot 10^{13} \text{ Nmm}^2$	$EI_{k=\infty}$	$1.2 \cdot 10^{13} \text{ Nmm}^2$
Selfweight	1.325 kN/m	Selfweight	0.28 kN/m
$Q_{SLS,k=0}$	12.5 kN/m	$Q_{SLS,k=0}$	7.0 kN/m
$Q_{SLS,k=\infty}$	29.3 kN/m	$Q_{SLS,k=\infty}$	17.7 kN/m
$(Q_{SLS}/\text{Self wgt.})_{k=0}$	9.4	$(Q_{SLS}/\text{Self wgt.})_{k=0}$	25.0
$(Q_{SLS}/\text{Self wgt.})_{k=\infty}$	22.1	$(Q_{SLS}/\text{Self wgt.})_{k=\infty}$	63.1
LCA: A1 & A3	554 $\text{kgCO}_2 - \text{eq}$	LCA: A1 & A3	375 $\text{kgCO}_2 - \text{eq}$
Biogenic carbon	0 $\text{kgCO}_2 - \text{eq}$	Biogenic carbon	-964 $\text{kgCO}_2 - \text{eq}$

\*The calculation is based on a simply supported beam. Thus  $w = \frac{5}{384} * \frac{q * l^4}{EI}$

\*\*A1 & A3 Life cycle assessment takes into a count Raw Material Acquisition, Manufacturing and Assembly

A comparative analysis, depicted in Table 1.1, highlights the results of a simply supported beam under flexural bending deformation for a steel-concrete composite system and a steel-CLT composite system. The allowable distributed load over the length of the beam has been calculated while considering the serviceability limit state ( $l/250$ ) for two scenarios: with a fully flexible composite connection ( $k=0$ ) and with a rigid composite connection ( $k=\infty$ ) which will be explained more extensively in Section 2.1. The load capacity to weight ratio indicates the previously mentioned benefit of lightweight construction in steel-CLT composites and thus the reduction of raw material use, in weight. The CLT, in this scenario, has two layers not working in parallel with the steel beam. Slightly over-designing the CLT panel to account for a lower modulus of elasticity and cross-lamination can result in comparable performance. For instance, increasing the thickness of the outer layers to 40 mm instead of 20 mm would yield similar bending stiffnesses to those observed in the steel-concrete composite system mentioned in Table 1.1.

Secondly, a brief Life Cycle Assessment (LCA)(Table 1.1) that evaluates stages A1 and A3, concerning raw material acquisition and manufacturing/assembly respectively, reveals the disparity in the environmental impact between the two options in terms of carbon dioxide equivalent ( $\text{kgCO}_2\text{e}$ ) as steel-concrete variant uses 48% more  $\text{kgCO}_2\text{e}$ . Furthermore, the timber variant exhibits a negative biogenic carbon dioxide equivalent of -964  $\text{kgCO}_2\text{e}$ . This indicates that the material has sequestered carbon during its growth phase, as trees absorb  $\text{CO}_2$  through photosynthesis and store the carbon in their structure. The stored carbon remains intact throughout the timber's use-life as a constructional element, resulting in a net reduction in  $\text{CO}_2$  emissions when utilising the steel-CLT composite system

instead of the steel-concrete composite system.

In composite systems, the performance of composite connections is crucial, as it directly affects the overall performance of the system, which can rival that of classical systems. In STC systems, the performance of these connections has been evaluated through push-out tests conducted on steel-LVL joints [30]. These tests have provided valuable insight into the behaviour of these connections and their effectiveness in transferring loads between the steel and timber elements in the composite system.

Another example of one of these numerous options in compositely connecting steel-timber in floor systems is a novel design by WSP (section 2.5.2), an engineering firm within the built and natural environment, that connects a CLT slab with a steel beam with studs in grouted slots with transverse reinforcement.

### 1.1.5. The debate on material efficiency and demountable construction

Improving material resource management within the built environment by utilising demountable design has been a topic of extensive discussion since the early 2000s, including at the International Conference on Global Built Environment [24]. However, an alternative environmental rationale aims to improve material resource management by prioritising material-efficient construction that achieves sustainable design through optimal structural performance and minimised material use. This second rationale is a key vision in the design of WSP their STC floor system.

These varying economic rationales currently affect design choices made by companies regarding steel-CLT composites, and this complex consideration will be kept in mind during the research.

Given the ongoing climate crisis, it is increasingly crucial to prioritise environmentally sustainable designs. As such, future engineers must gain a comprehensive understanding of the differing economic rationales, whether focusing on material efficiency or full demountability.

### 1.1.6. Problem statement

Following section 1.1.5, there is a pressing need for more sustainable construction practices, with steel-CLT composite floors recognised as a promising alternative to concrete slabs and steel-concrete composites as they can achieve implementable performance whilst decreasing the weight and environmental footprint. Achievement of wide implementation of steel-CLT composite floors is reliant on structural performance optimisation and incremental technological development in the subject.

This research will focus on the performance of steel-CLT composite floors, which is crucial to fulfilling this promise and shedding light on the debated rationales of material efficiency versus full demountability.

## 1.2. Research objective and questions

### 1.2.1. Objective

Given the context outlined in Section 1.1 and the identified problem, the primary objectives of this thesis are as follows:

- i. Assess and confirm the feasibility and benefits of constructing with steel-CLT composite floor systems.
- ii. Study the state of the art in steel-CLT composite connections and their influence on the behaviour of steel-CLT composite beams.
- iii. Investigate the behaviour of steel-CLT composite beams by examining important geometry and strength-related parameters.
- iv. Analyse available predictive methods, both analytical and numerical, for predicting the behaviour of steel-CLT composite beams.

### 1.2.2. Research questions on Steel-CLT composite floors

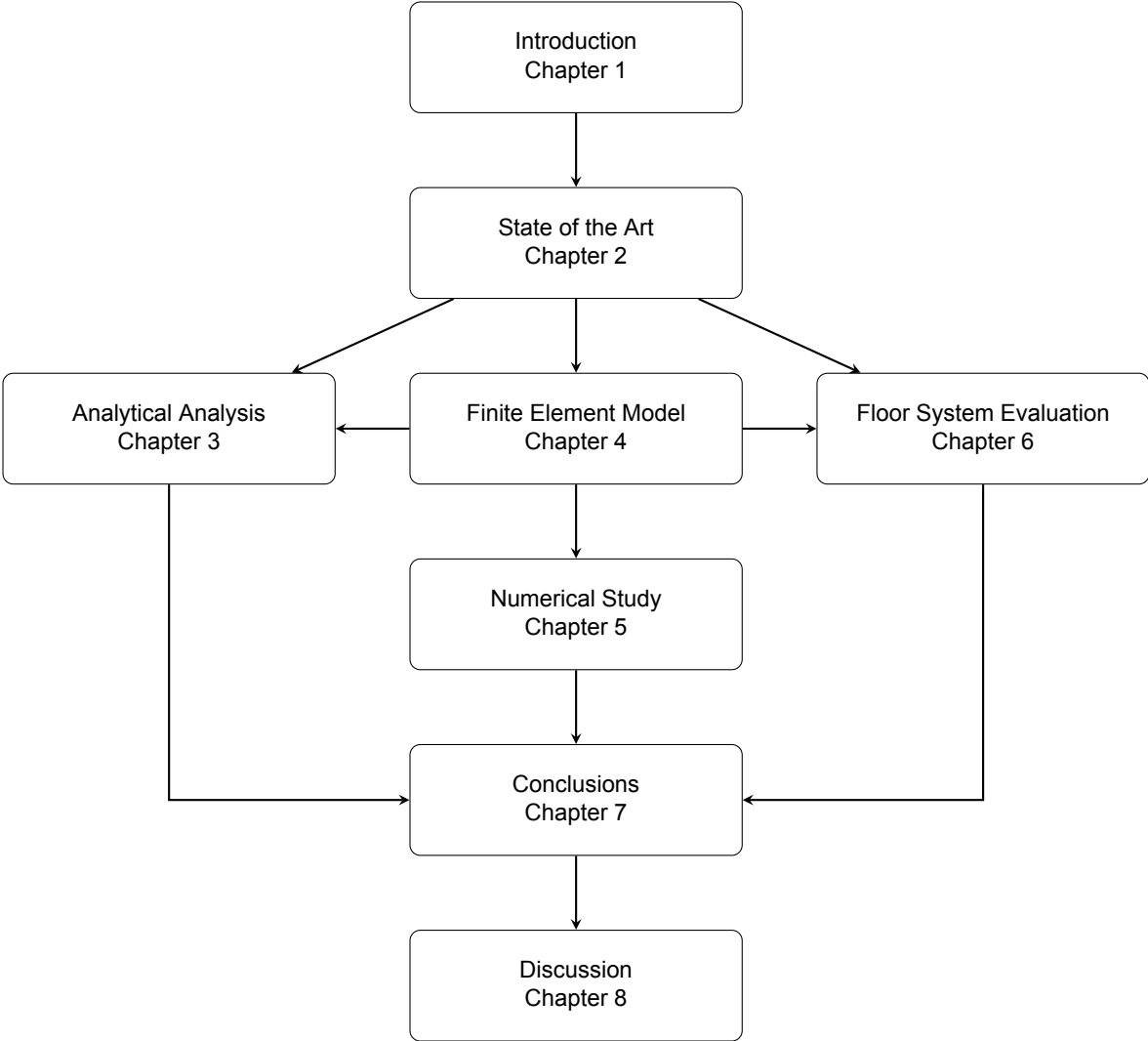
In order to explore the potential of steel-timber composite floor systems as a sustainable and efficient building solution, the following research questions aim to investigate their performance and feasibility in comparison to traditional building systems by answering the set out research objectives (1.2.1).

In order to answer the main research questions additional partial research questions will need answering:

1. How can a steel-CLT composite floor system be effectively constructed, considering the unique orthotropic properties of the CLT slab in contrast to traditional concrete?
  - (a) How can a floor system be constructed with steel-CLT composite beams?
  - (b) What are the environmental benefits and sustainability aspects of steel-CLT composite floor systems?
  - (c) What is the structural performance of steel-CLT composite floor systems under different loading conditions?
2. What are the different types of steel-CLT composite connections, their characteristics and their influence?
  - (a) How do different connection types, such as dowel-type connectors and grout implementations, affect the behaviour and performance of steel-CLT composite beams?
  - (b) How can the choice of connection type impact the overall performance and sustainability of steel-CLT composite floor systems?
3. How do geometry and strength-related parameters influence the behaviour and performance of steel-CLT composite beams?
  - (a) What is the effect of beam length, connector spacing, and steel profile on the structural response of steel-CLT beams?
  - (b) How does the CLT panel influence the behaviour of steel-CLT composite beams?
  - (c) What are the optimal design considerations and parameters for achieving greater performance in steel-CLT composite floor beams?
4. How can the behaviour of steel-CLT composite beams be predicted analytically and numerically?
  - (a) How accurate are analytical guidelines in predicting the behaviour of steel-CLT composite beams compared to experimental results?
  - (b) Can advanced numerical modeling techniques, such as finite element analysis, provide more accurate predictions of the behaviour of steel-CLT composite beams?
  - (c) What are the limitations and assumptions associated with analytical and numerical models used for predicting the behaviour of steel-CLT composite beams?

### 1.3. Report structure

The report consists of 8 chapters. Chapter 1, Introduction, provides the context and rationale for the study, along with the research objectives and questions. In Chapter 2, the State of the Art is explored, focusing on steel-CLT composite beams: their behaviour, factors influencing it, and methods for analytical and numerical prediction. Building on this knowledge, Chapter 3 examines the analytical analysis of a steel-CLT composite beam using existing guidelines. Chapter 4 delves into the construction of a finite element model specifically designed to study steel-CLT composite beams, leading to Chapter 5, the Numerical Study. This chapter compares the analytical and numerical approaches. In Chapter 6 the presented floor systems from Chapter 2 are evaluated based on the finite element method described in Chapter 4 and knowledge obtained in Chapter 2. The findings from the analytical analysis, finite element model, numerical study and floor system evaluation assemble in Chapter 7, the Conclusion. Following the conclusion, Chapter 8, the Discussion, reflects on the results, assesses the validity and risks associated with the analyses conducted, and proposes recommendations.



# 2

## State of the Art

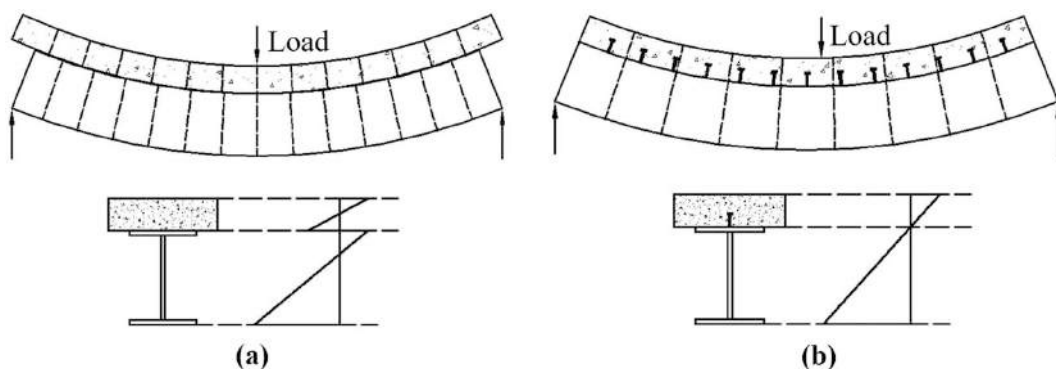
### 2.1. Background on composite beams

Firstly, it is essential to provide a brief introduction to composite beam behaviour to ensure all readers can understand the state-of-the-art regarding steel-CLT composite beams and floor systems. A composite floor system typically comprises a floor element (traditionally a concrete top slab), a supporting beam (typically made of steel), and connectors that facilitate shear interaction and transfer the longitudinal shear force. Secondly, they insure continuity of the curvature at the material interface.

The benefit of a composite beam lies within the composite action. Composite action could be defined as 'the interaction of the concrete slab with the steel beam as a function of the degree of connection of the two components. If there is no slip at the interface of the slab and beam, complete interaction is achieved. When the slab and beam are not rigidly interconnected, interfacial slip occurs and incomplete interaction results'[50]. Slip( $\delta$ ) is the relative change in position, at interface, in longitudinal direction of the beam between the two materials.

$$\delta = u_{top} - u_{bottom} \quad (2.1)$$

To resist slip at the interface between the slab and beam composite connections are used. The degree of shear connection, achieved through a composite connection often lies in between full composite action, resisting all slip, and no composite action and is called partial composite action. Fig. 2.1 displays the deflection of a simply supported beam with single concentrated force and the corresponding slip that occurs.



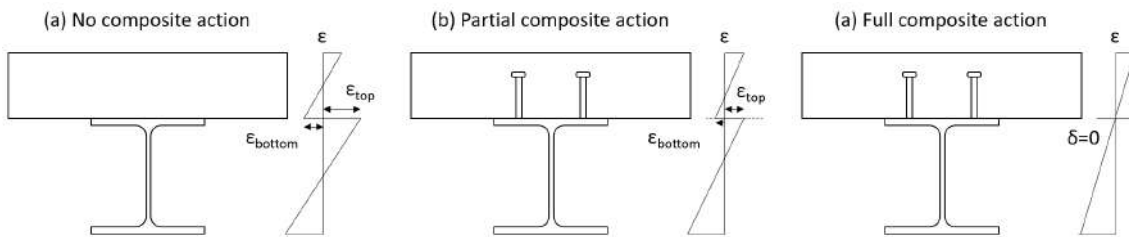
**Figure 2.1:** Cross sectional stress distribution due to (a) non-restricted and (b) fully-restricted slip (from [2])



Secondarily, at the material interface vertical separation could occur. This separation, space between the two materials, could occur as a result of difference in strain. The difference in strain of the two materials results in different vertical deformation which can be prevented with closely enough spaced shear connectors[50], although the vertical separation is limited in the elastic phase[50]. By definition, as slip is the difference in displacement, it can be related to the difference in strain over the length of the beam.

$$\delta = \int_0^L \varepsilon_{top} dx - \int_0^L \varepsilon_{bottom} dx \quad (2.2)$$

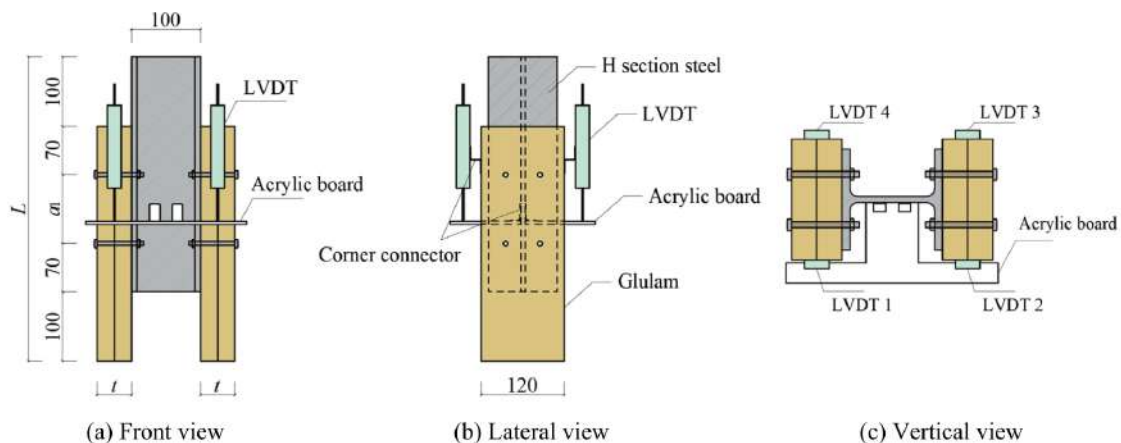
As displayed in Table 1.1 the bending stiffness, in the reference scenario, is between 2.5 and 4 times higher with full composite action than with no composite action. As a result the beam can carry much less distributed load in serviceability.



**Figure 2.2:** Schematic illustration of the vertical strain distribution for cross-sections with (a) no composite action, (b) partial composite action and (c) no composite action.

## 2.2. Shear connectors

Thus, the performance of a floor system depends heavily on the ability of its shear connector to resist slip, which can be evaluated by its force-displacement(force interchangeable with load and displacement interchangeable with slip, behaviour. This behaviour is commonly assessed through push-out tests, as specified in EN1994-1-1 for composite steel and concrete structures and in BS EN26891[21] for timber joints with mechanical fasteners. A load-displacement curve, as shown in Fig. 2.5, is often used to illustrate connection behaviour. Such a result from a push-out test is often used to identify three parameters: shear connector stiffness, the initial stiffness ( $k_{s,0.4}$ ) and secondary stiffness ( $k_{s,0.6}$ ) and the ultimate load carrying capacity ( $P_u$ ).



**Figure 2.3:** Steel-CLT push-out test setup used by [68]

Standard EN 26891 [21] states guiding principles for the determination of strength and deformation characteristics for joints with mechanical fasteners. Fig. 2.3 depicts the experimental set-up[68] for a steel-CLT composite connection in shear with bolts as mechanical fasteners in front view, side view and top view.

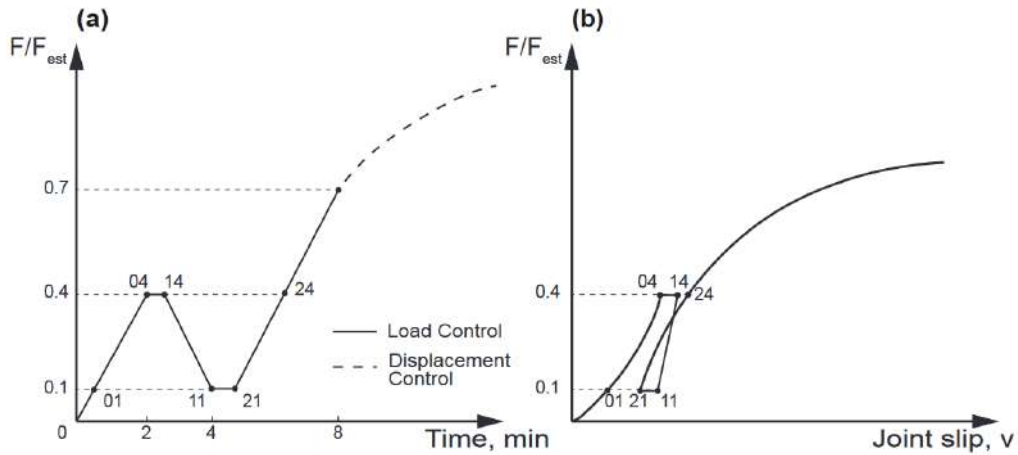


Figure 2.4: Loading protocol of push-out test by guidance of [21]

The loading protocol for such a tested connection is depicted in Fig. 2.4 and it is divided into several steps of loading. Initially, load-control is utilised until different load levels which are based on the estimated maximum force that the connection can resist,  $F_{est}(P_u)$ . From 0.7 times the estimated maximum force displacement-control is applied.

The initial stiffness is evaluated by considering the connection stiffness before 40% of  $P_u$  and the ultimate stiffness is calculated with connection stiffness before 60% of  $P_u$  in relation to the load at 10% based on EN26891 [21].

$$k_{s,0.4} = \frac{0.4P_u - 0.1P_u}{\Delta_{0.4} - \Delta_{0.1}} \quad (2.3)$$

$$k_{s,0.6} = \frac{0.6P_u - 0.1P_u}{\Delta_{0.6} - \Delta_{0.1}} \quad (2.4)$$

where

$0.4P_u$  and  $0.6P_u$  are the load at different load levels

$\Delta_{0.4}$  and  $\Delta_{0.6}$  are the slip at different load levels

The results of the testing procedure are often presented in the form of a load-slip curve, which illustrates the relationship between the applied force in shear per connector and the relative slip at the material interface, as shown in Figure 2.3. Figure 2.5 presents two distinct load-slip curves. In curve (a), a ductile connection is depicted, exhibiting a significant amount of slip before failure and featuring a yield plateau. On the other hand, curve (b) represents a brittle shear connector that fails with minimal slip. For it to be defined brittle in traditional steel-concrete composite connections to be slip has to be less than 6mm [18].

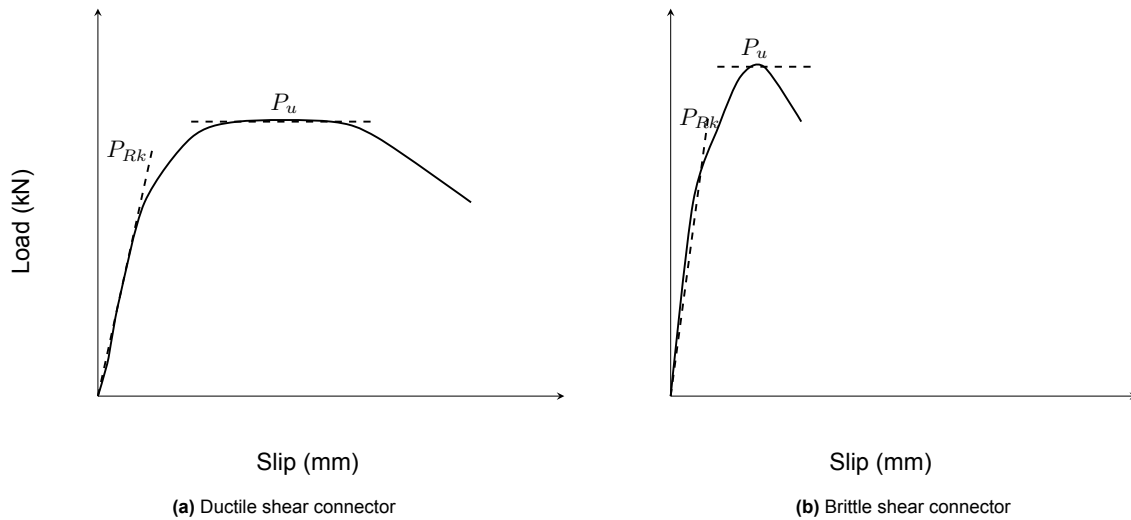


Figure 2.5: Load-slip curves of shear connectors

In a steel-CLT composite beam, the ductility of the connection plays a vital role in redistributing the longitudinal shear force between the steel beam and the CLT panel. Additionally, a connection with a high load capacity often enhances the stiffness of the connection.

### 2.3. Cross laminated timber

In steel-CLT composite construction the top slab is constructed with cross laminated timber (CLT). CLT is a building material made from layers of wood boards stacked in alternating perpendicular directions and glued together under high pressure as seen in Fig. 2.6. The resulting panel is a strong and rigid, plate-like, laminar, engineered timber product which is a composite slab that can be used for floors, walls and roofs.

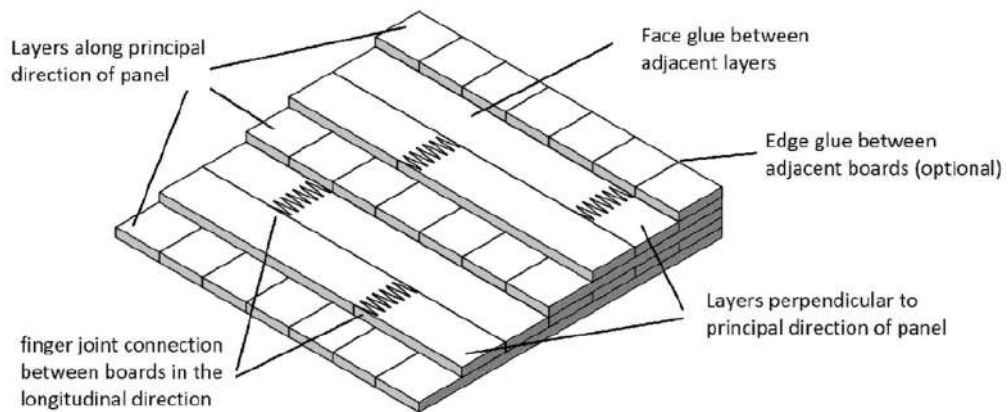


Figure 2.6: Construction detail of CLT panels [10]

CLT is typically made from softwood species such as spruce, pine, or fir, although hardwoods such as oak and maple can also be used. The individual boards used to create CLT panels are typically 15 to 50 millimeters thick, and are dried to a low moisture content to ensure stability.

The layers of wood boards in a CLT panel are typically arranged in an odd number, with the grain of the wood running parallel within each layer but perpendicular to the grain in the adjacent layer. This cross lamination creates a panel that is very stable, with little tendency to warp or twist.

CLT panels can be produced in a variety of sizes and shapes, making them suitable for a wide range of building applications. They are often used for walls, floors, and roofs in multi-story buildings,

as well as for prefabricated building components that can be quickly and easily assembled on site. In steel-CLT composite floor construction the CLT panel would be a prefabricated element which puts it in contrast to the use of in-situ concrete. As panels can be prefabricated off-site to precise specifications, and then assembled quickly and easily on site[6]. This reduces construction time and costs, while also minimising waste and disruption to the surrounding environment.

Research into CLT, its mechanical characteristics and behaviour spans the past three decades as CLT found its inception in the 1990s as the sawmill industry sought to find value for side boards at the time [38].

From a structural engineering perspective, CLT has several unique properties that make it an attractive building material. One of its key advantages is its high strength-to-weight ratio. CLT panels are lightweight[6] yet incredibly strong, which makes them an ideal material for use in tall buildings where weight can be a concern such as multi-story buildings undergoing ground motion [7].

The cross lamination of the boards in CLT also gives it exceptional dimensional stability. This means that it is less susceptible to changes in temperature and humidity than other building materials such as steel or concrete[9]. This makes CLT an excellent choice for buildings that need to maintain their structural integrity in a variety of environmental conditions.

CLT also has good fire resistance. Because it is made of solid wood, it will char on the surface when exposed to fire, creating an insulating layer that protects the underlying material. This charring can slow down the spread of fire, giving occupants more time to evacuate the building. In composite floors with a CLT slab the fire condition is often guiding for overall CLT layup design as the remaining reduced cross section has to remain load-bearing. However, in CLT, charring will incapacitate the layers exposed to fire. In design, one should recognise that the remaining internal layers, that in fire conditions will be protected, should be able to transfer the remaining load.

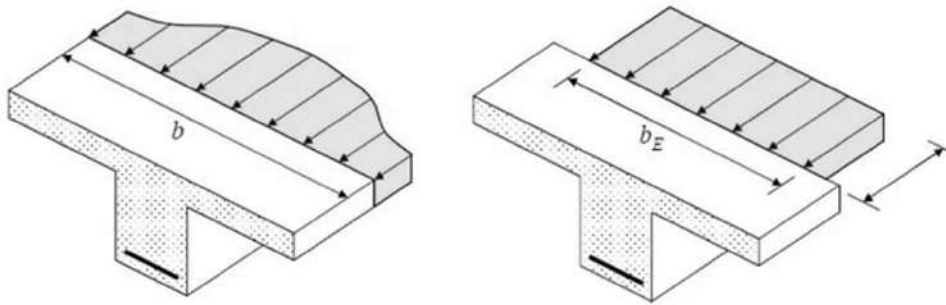
The behaviour of a CLT panel has been investigated in a wide array of circumstances. A European standard, EN14080, has been developed to comprehensively evaluate the performance of glulam, including its tensile strength perpendicular to the grain and out-of-plane shear strength [22].

Furthermore, the behaviour and compressive strength of cross-laminated timber (CLT) panels in the perpendicular to the grain direction have been extensively investigated in previous studies [61][59][4].

Additionally, the in-plane shear strength of CLT has been studied extensively in previous research [5] [23], and the behaviour of CLT panels under concentrated load has also been investigated [35]. These studies have provided valuable insights into the mechanical behaviour and performance of CLT and glulam, which are important factors to consider in the development of steel-CLT composite floor systems.

## 2.4. Effective flange width of T-sections

In structural members, with non-uniform cross-sections shear lag could occur when stress is not uniformly distributed when subjected to axial or bending load. This is more apparent in members with wide flanges and narrow webs, such as T-sections where the stiffness of the flanges decreases in areas near the web. Due to stiffness decreases of the flange as it approaches the web of the T-section the in-plane shear strain in the flange of the T-section causes smaller longitudinal displacements in the flange further away from the web when compared to near the web. As a result the displacement and stress estimates, using Euler bending theory, can become inaccurate [47].



**Figure 2.7:** Theoretical stress distribution (left) and Simplified rectangular stress distribution (right) with effective width( $b_E$ ) in T-sections (Adapted from [27])

The elastic stresses peak at the axis of symmetry of the T-shaped cross-section and reduces with the distance away from this axis as seen in Fig. 2.7. To account for the reduction in capacity of the flange due to this phenomenon there is use for the concept of effective width of the flange in analytical calculations. The effective width is the result of the assumption of a constant stress distribution over that width which result in an equal sum of stress as the realistic stress distribution.

As composite beams are examples of such T-sections this has to be accounted for in steel-CLT composite beam design. [47] researched a 1000mm wide CLT slab, with a height of 120mm, in a timber composite beam. In Steel-CLT composites [28] uses CLT panels of 800mm in width. [56] selected a width of 1000mm whilst looking at semi-rigid beam-to-column connections in steel-CLT composites.

## 2.5. Steel-CLT composite floor systems

A composite floor system refers to a type of structural flooring system that consists of multiple materials working together to form a unified and efficient structure. It typically involves the combination of two main components: a concrete slab and steel beams.

In a traditional composite floor system, the steel beams provide the primary structural support, while the concrete slab acts as the load-carrying element. The two materials work together to create a strong, rigid, and efficient flooring system that can withstand various loads, such as dead- and live loads.

In contrast, a steel-CLT composite floor system replaces the concrete slab with a CLT panel. The CLT panel offers unique characteristics (Section 2.3) that distinguish it from a traditional concrete slab. Each laminated timber lamella within the CLT panel exhibits orthotropic properties, resulting in a mechanical behaviour that is notably different from that of a concrete slab.

The distinct mechanical behavior of the CLT panel arises from its orthotropic nature. Unlike a concrete slab, which is considered isotropic at a macroscopic level, the CLT panel exhibits different mechanical properties along different axes. This means that the panel's response to loads and stresses varies depending on the direction in which they are applied.

In the case of a steel-CLT composite floor system, the orthotropic properties of the CLT panel introduce unique characteristics to the overall behavior of the floor system. The panel's stiffness, strength, and load-carrying capacity can vary depending on the orientation and arrangement of the laminated timber lamellae. This allows for optimized structural solutions that leverage the specific properties of the CLT panel in combination with the steel components.

The CLT slab and steel beams are connected using mechanical shear connectors, traditional dowel types connectors such as screws. These connectors transfer the shear forces (Section 2.1) between the steel beams and the concrete slab, allowing them to act together as a composite unit.

The composite action between the concrete slab and steel beams provides several advantages. It increases the load-carrying capacity of the floor system, improves the stiffness and strength whilst simultaneously reducing the deflections as explained in Section 2.1. A composite floor system is thus a floor system consisting of composite beams. Composite beams are often defined as: "elements resisting only flexure and shear that comprise of two longitudinal components connected together either continuously or by a series of discrete connectors"[53].

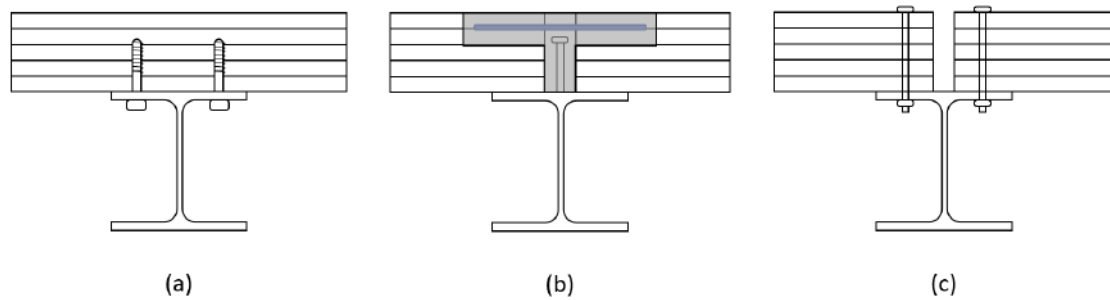
By that definition, a steel-CLT composite floor system, composed of composite beams, can be constructed in the following ways:

- Utilising steel beams connected with a single continuous CLT panel.
- Utilising CLT panels spanning between steel beams.

The design choice has a significant impact on the overall floor system, as it directly affects the behaviour of the composite elements. When utilising a continuous CLT panel over a steel beam, the inherent rigidity of the CLT panel contributes to the overall stiffness of the system. However, in the case of two CLT panels supported on a steel beam, the achievement of composite action relies on having a connection with sufficient rigidity and strength to ensure effective load transfer between the CLT panels and the steel beam while supporting the span of the CLT panel.

Previous research has proposed the use of the first option to construct a prefabricated modular steel-CLT composite floor system [45][44]. Alternatively a steel-CLT composite floor system where CLT panels span between steel beams is being designed by WSP.

Fig. 2.8 provides a brief introduction to the aforementioned options, while the subsequent sections (2.5.1 & 2.5.2) delve deeper into their explanations. In Fig. 2.8 (a), a continuous CLT panel is illustrated, supported by a steel beam and connected with a composite connection (e.g., screws, as shown in the example figure) [45][44]. Fig. 2.8 (b) depicts a design featuring two CLT panels on a steel beam,



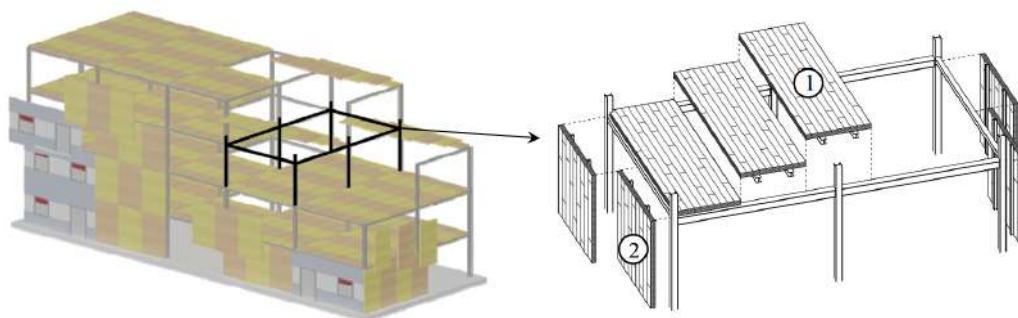
**Figure 2.8:** Steel-CLT composite floor systems with (a) a continuous CLT panel connected with screws, (b) two CLT panels connected with the use of a grouted stud and transverse reinforcement and (c) two CLT panels compositely connected without the use of grout

with the CLT spanning between two steel beams. In this case, grout is utilised to achieve composite connection between the elements and ensure floor continuity. Fig. 2.8 (c) presents a CLT composite system with a single steel beam supporting two CLT panels, similar to the configuration in (b), but without the use of grout for composite connection between the structural elements. This particular option for a potentially viable steel-CLT composite floor system remains unexplored at present.

Exploration and design of a novel steel-CLT composite connection, capable of activating composite interaction between two individual CLT panels resting on a single steel beam without the use of grout, is necessary. The development of such an innovative connection would facilitate the implementation of steel-CLT floor beams in floor systems and promote circular construction practices by eliminating the need for grout. However, it is important to note that grout-less connections may not always provide a comprehensive solution for achieving full circularity, as the drilling of screws and the preloading of bolts can result in permanent damage to the timber [57]. This adds complexity to the desired connection design objectives.

### 2.5.1. Floor system with continuous CLT panel

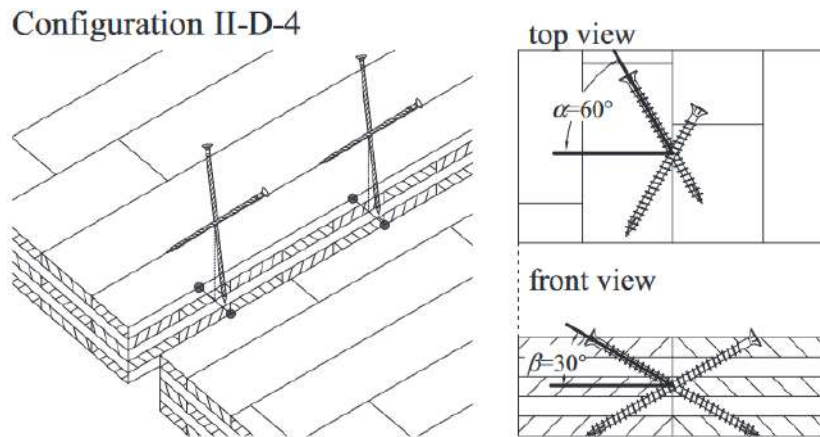
An example of steel-CLT composite floor system with a steel beam supporting a single CLT panel would be the modular steel-CLT composite floor system, proposed by [45][44]. The main structure is built by placing steel frames with a floor assembled from primary steel beams supporting secondary steel beams with CLT panels compositely connected to the secondary beams as seen in Fig. 2.9. The standard construction system is regular and very repeatable in space with linear steel elements and flat CLT components.



**Figure 2.9:** View of modular steel-CLT hybrid construction proposed by [45]

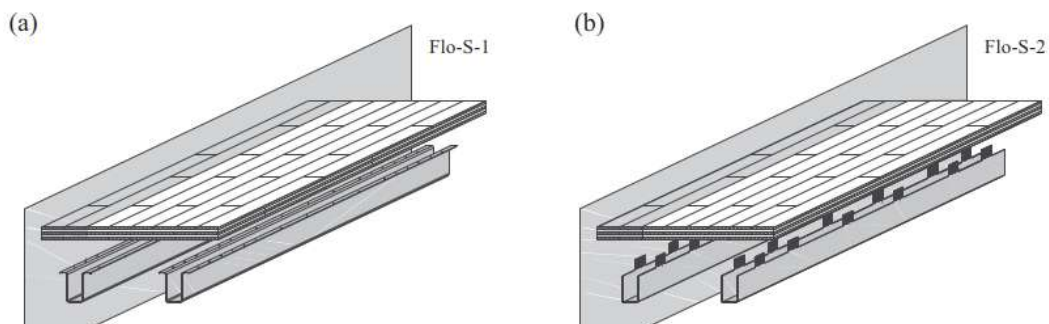
To ensure floor continuity screws are proposed to connect the floor elements together such as depicted in Fig. 2.10.





**Figure 2.10:** Configuration II D-4 for a panel to panel connection [44]

The proposed implementation of modular steel-timber floor elements can be realised with differently formed steel elements and different composite connections. Different steel beams proposed are a H-shaped hot-rolled symmetric steel beam, Q-shaped cold formed steel beam or even a more bespoke thin steel formed beam in a U-shape[43]. The design proposes a primary beam length of 10 meters between which the steel-CLT composite floor system spans with 6 meters in length. In Fig. 2.9 standardised H-shaped beam are used but alternatively a steel-CLT composite floor system could be achieved with an innovative U-shape as seen in Fig. 2.11.



**Figure 2.11:** Prototypes of floor components with custom-made U-shaped steel beam by [43]. (a) Composite connection with inclined screws and (b) steel plates with epoxy based resin

To enable transversal force transfer and activating the composite action of the floor system the CLT has both perpendicular as parallel lamellae, respectively. The proposed CLT panel has 5 layers of C24 timber with thickness per lamellae being respectively  $t = (20, 20, 20, 20, 20)$  mm. with orientation  $[0^\circ, 90^\circ, 0^\circ, 90^\circ, 0^\circ]$ . The two transverse lamellae are important for bi-directional force transfer while the longitudinal lamellae are the main contributors to the composite action of the steel-CLT composite beam. The investigations conclude that steel elements supporting CLT wood-based panels allow the construction for promising lightweight buildings.

### 2.5.2. Floor system with transverse reinforced concrete slots with welded studs

WSP, an engineering company focused on the built and natural environment, has recognised the potential of timber floor systems, particularly the STC floor systems. They have introduced a scalable design that can be easily implemented. Similar to the arguments mentioned in Section 1.1.4, their innovative floor system aims to be competitive in newly constructed buildings due to its low carbon intensity and in vertical extensions due to its high strength-to-weight ratio. The design differs from a previously explained floor system as the CLT panel spans two steel supporting element and a novel connection will enable composite action. Their main argument for this design was its practicality and ability to be

scalable.

In traditional construction, hollow core slabs (HCS), prefabricated structural elements, are commonly used in building construction. They are precast concrete slabs with hollow voids running longitudinally, which significantly reduce their weight while maintaining structural strength. These voids or cores also provide benefits such as enhanced thermal and acoustic insulation. Hollow core slabs are commonly used in various building applications, including residential, commercial, and institutional structures. They are often utilised as flooring and roofing systems, providing large spans and excellent load-carrying capacity. The installation of hollow core slabs is relatively fast and cost-effective, contributing to efficient construction processes.

To combine the benefits of the use of HCS and composite construction [42] investigated the use of two HCS supported by a steel beam connected together on site using a small amount of in-situ concrete. The connection, which activates the composite action, consists of shear studs welded on the steel beam, milled slots in the HCS with transverse reinforcement which would all be filled in with concrete.

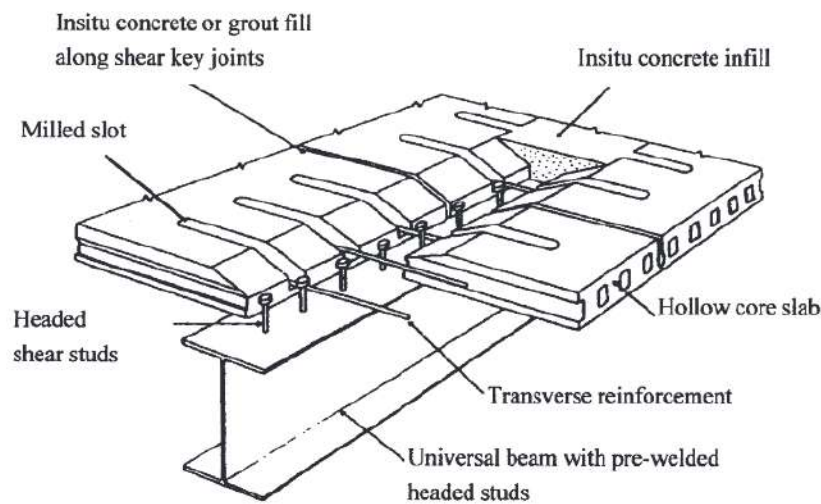


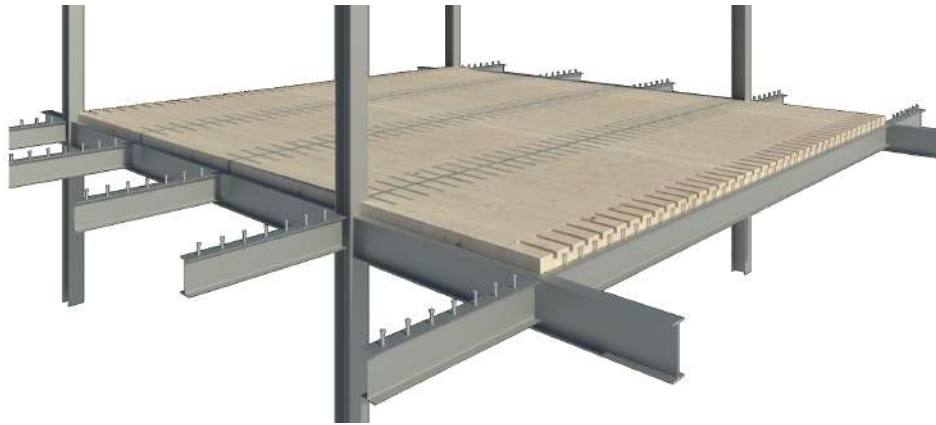
Figure 2.12: SCC floor system with precast HCS by [42]

The research[42] concluded that a floor comprising of precast HCS which are tied together with infilled concrete surrounding transverse reinforcement and welded studs on the supporting steel beam are a reliable and very cost-effective alternative for steel-concrete composite construction. This would have been the origin for steel-CLT composite floor system designed WSP which employs a similar composite connection.

To establish implementable design rules, WSP plans to conduct push-out experiments on the connection in 2023. While full-sized beam tests in the future will provide a comprehensive understanding of this steel-CLT composite beam design, accurate numerical modeling can already shed light on beam performance by utilising the push-out data obtained from the composite connection.

### The floor system

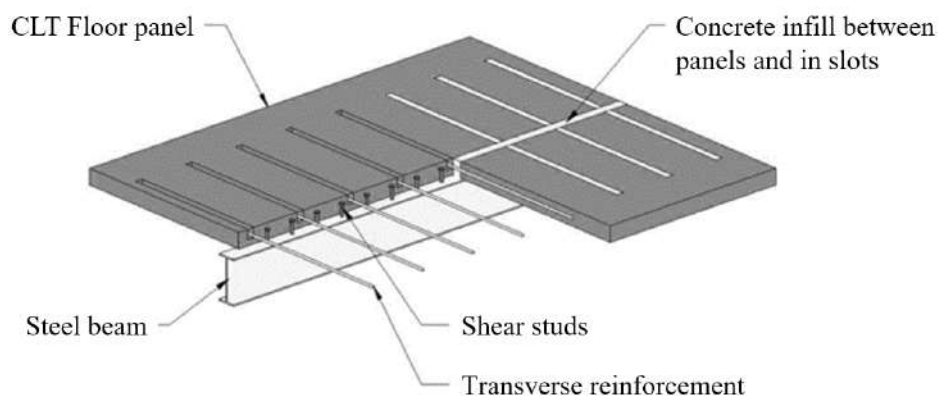
The objective of the composite beam is to provide longitudinal spans of up to 12 meters while maintaining a 3-meter span between the composite beams. The system is even able to support a 4 meter span. By utilising two CLT panels on a single beam, the steel-CLT composite beam becomes a more practical option for a floor system as the CLT panels can now span between two beams. However, this panel orientation and support present added complexities in building design and construction that must be accounted for, beyond solely considering the performance of the steel-CLT composite beam itself.



**Figure 2.13:** The design for a steel-CLT composite floor system from WSP

### The composite connection

The design uses normal shear studs pre-fixed to a steel beam while achieving the composite interaction with the CLT panel by grouted horizontal slots/notches with transverse reinforcement placed repetitively in longitudinal direction (Fig. 2.14). The design takes into account the ease of construction as studs and notches do not need to be aligned.



**Figure 2.14:** The design for the composite connection from WSP

The design differs from the rest as it refitted a traditional solution often used in conjunction with pre-fabricated concrete panels - the concrete slots - for use with a CLT panel. This allows for a more equal dispersion of the longitudinal shear force acting on the material interface onto the panel. A hypothesis is that, due to the use of more grout and transverse reinforcement, the connection would be significantly stiffer than previously mentioned composite connections (Section 2.6.1 & 2.6.2). This hypothesis is based on research on the utilisation of grout in composite connections. In both BCGP and GSC (Section 2.6.2), wider and larger grouted pockets achieve superior performance. As a result, the ultimate load capacity, stiffness, and ductility of the connection would be better.

### The CLT panel

The CLT panel is designed to be 160mm thick and composed of five layers. The outer and middle layers will be oriented in a transverse direction, meaning they will not primarily contribute to the composite effect that relies on the compressive strength of fibers aligned in parallel. Instead, these layers will span between the steel beams and each will be 40 mm thick. The second and fourth layers will be 20 mm thick and will be placed with their grain in parallel to the steel beam.

Thickness and direction of the timber panels significantly impact the composite connection and beam performance. Push-out tests have shown that behaviour differs over thickness [68], while connection stiffness can almost halve [55] in timber-timber composite connections when loaded perpendicular to the grain instead of in parallel.

Thus, the above-mentioned CLT panel results in less composite beam performance. However, WSP accounted for all real construction parameters and designed the floor system to accommodate panel boundary conditions and load-bearing capacity in fire conditions.

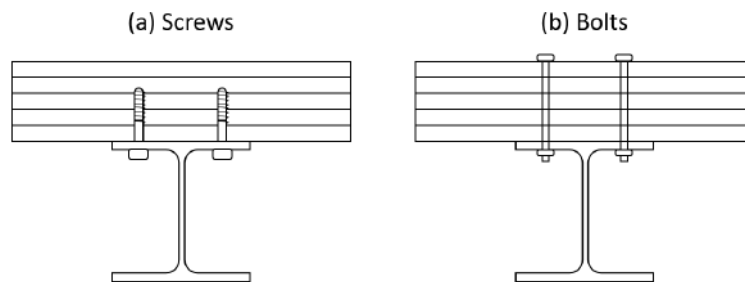
## 2.6. Steel-CLT composite connections

While most steel-CLT design choices are guided by structural requirements and regulations to ensure sufficient resistance against loads, and load in fire conditions, the influence of composite connections in CLT is more complex and ambiguous. A detailed perspective is needed to understand how different connections interact with the CLT panel and how they can affect the overall behaviour of the Steel-CLT composite beam system.

There is a need for innovative steel-CLT composite connections with greater strength, stiffness, ductility which result in beams with greater composite efficiency ( $C$ ). Different arrangements of screws, glue and other varieties of simple dowel-type connections have been proposed and tested in push-out test conditions [45][33]. Such tests revealed that screw and bolted shear connectors in steel-CLT composite connections only achieve medium composite efficiency. The application of grout in connections in timber has shown promising results [39] [60] [48] [51] to achieve greater strength, stiffness, ductility when compared to dowel-type composite steel-CLT shear connections.

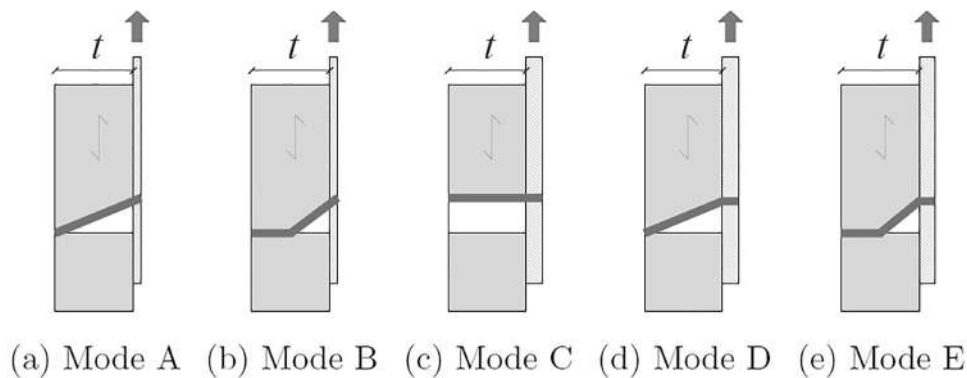
### 2.6.1. Dowel-type fasteners for STC connections

Most commonly used for composite connections are dowel-type fasteners, also known as mechanical connectors. In timber connections they are most often screw and bolt connectors. They transfer forces between members and in STC, between the steel and the timber. The main advantages of a dowel-type fastener, in STC, is their ease of installation, their versatility in terms of size, length and diameter and ability to transfer shear forces and bending moments between steel and timber elements.



**Figure 2.15:** dowel-type fasteners in steel-CLT composites such as (a) screws and (b) bolts

The previously mentioned research, based on push-out tests, on steel-CLT samples give an accurate depiction of the behaviour and failure of such connections. During such push-out tests on STC connections the failures are guided by the simultaneous lack of embedding strength of the glulam and the bending capacity of the connector [68]. Traditionally the corresponding failure modes, based on plastic embedding of wood and fastener yielding are based on the European Yield Model (EYM)[71]. The resulting failures are determined by the connector slenderness in relation to the strength ratio, of the connector to the primary material[33].



**Figure 2.16:** Yielding modes (EYM) of the fastener considered for timber-to-steel connections (Adapted from [71])

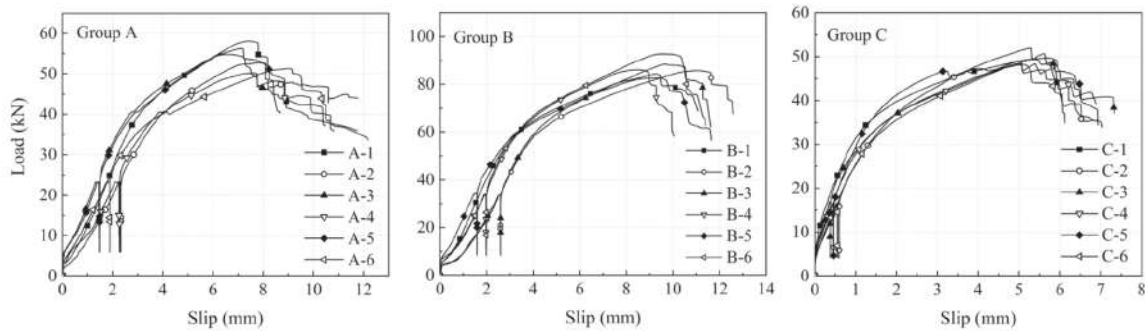
In EYM, failure mode A is a result of significant crushing of the timber alongside the fracture of the connector at the end of the connector. This failure mode is characterised as brittle. During failure mode B crushing of the timber is the result of two plastic hinges that occur, one at the end of the connector and one in the middle of the dowel. Failure mode C is related to the crushing of timber near the largely undeformed dowel, over its length in entirety (Fig. 2.16). In failure mode D a single plastic hinge forms, within the dowel, near the interaction surface between steel and timber. As a result we see the crushing of timber (in white) (Fig. 2.16) concentrated near the interaction surface. During failure mode E crushing of the timber is the result of two plastic hinges that occur, one at the interaction surface close to the end of the connector and one in the middle of the dowel.

When reflecting on steel-CLT composite joints [33] showed that in bolted connectors failure mode 1 was dominant. Similarly [33] also showed that smaller screws (12mm) were guided by failure mode E and larger screws (16 and 20mm) were dominated by failure mode D.

Thus when comparing the behaviour of screw connectors to bolted connectors in steel-CLT composites a rapid loss of stiffness with increasing load is observed in screws [68] while bolts maintain their stiffness longer over increasing load. Both, screws and bolts, mostly show a ductile response. However, in screws the failure occurs after a large post-peak branch in the load-slip curve, making failure of the connection more predictable. In screws, failure is caused by local timber crushing and developing plastic hinges. In contrast, failure in prestressed bolts is mostly associated with rupture and a sudden drop in load-slip response [33].

In terms of load-slip behaviour this is less elaborately depicted as the dimension of the connector plays a significant role in the load-slip curve. Fig. 2.17 below depicts the load-slip curves of a STC connection in a push-out test as described by BS EN26891[21](Section 2.2). In Group B we see a clear higher ultimate strength and stiffness, as a result of a greater diameter since sample Group B employed  $8\phi 6.8$  Bolts in comparison to Group A with  $6\phi 6.8$  Bolts.

Interestingly, when comparing Group A with Group C, in which  $5.5\phi$  Self drilling screws were used, it is difficult to conclusively identify the difference described by both [33] and [68] as behaviour of the STC connection is very similarly depicted in the load-slip curve of Fig. 2.17.



**Figure 2.17:** Load-Slip curves for STC connection specimen (Adapted from [68]) with Group A:  $6\phi$  6.8 Bolts, Group B:  $8\phi$  6.8 Bolts, Group C:  $5.5\phi$  Self drilling screws with other parameters unchanged

The dowel-type fasteners show moderate rates of composite efficiency [32], in STC beams with LVL slabs. Consequently that research showed that connector spacing, excluding the design of the composite connection, is a leading cause in achieving a high composite efficiency. In general, conventional methods, employing mechanical fasteners that rely on dowel action, do not transfer horizontal shear force very efficiently between steel and timber components in STC floor.

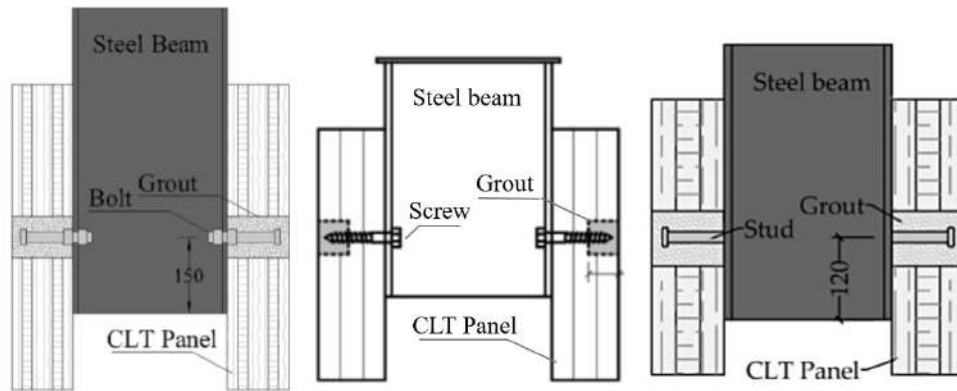
Composite connection adaptations can be done to achieve a better performing steel-timber, and steel-CLT, composite connection in regards to stiffness, load carrying capacity and ductility.

### 2.6.2. Grout utilisation in STC connections

Grout is dense fluid mixture, often used as a filler, consisting of cement, water (and often sand). Different additives and mixture quantities can make it more versatile in use or more resistant to moisture. The origin of applying grout to timber structures was for anchorage of timber structures to a foundation. Over the years it has developed, in timber structure application, as a way to increase stiffness and load capacity whilst it is also easily applicable on site.

Recent studies have identified the same recent wood-based construction advancements and corresponding need for the development of high-performance, reliable mass timber connections and as such have proposed novel grout-reinforced shear connectors for use in steel-CLT hybrid systems. [62] proposed a connector with steel rods embedded in grout in steel-CLT assemblies and experimented on 240 full-scale push-out shear tests which concluded that such connections allow for high performance in strength and stiffness to be attainable.

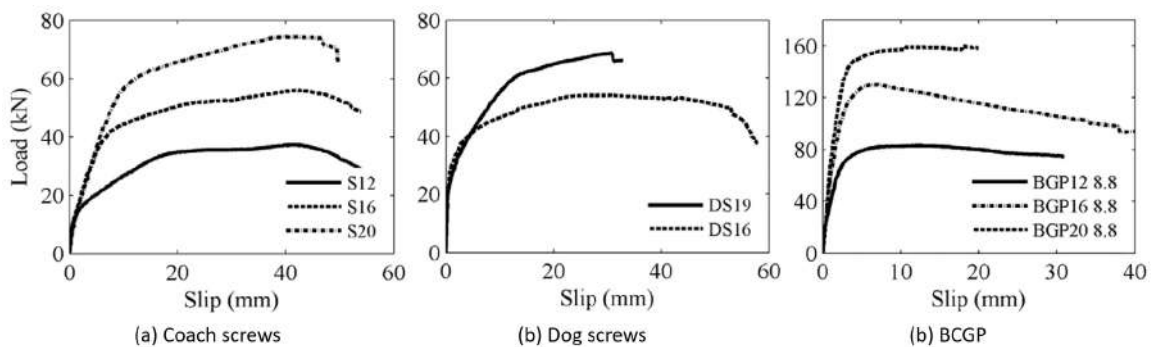
Further research in recent years has highlighted the potential to use grout in timber connections, particularly CLT connections, to increase initial stiffness and peak load capacities. Promising results were obtained through the use of bolted connectors embedded in grouted pockets (BCGP) during push-out tests, as compared to traditional dowel-type fasteners [28]. In addition to BCGP, research into both screw connectors in grouted pockets (SCGP) and grouted stud connectors (GSC) in timber-steel connections have also been conducted. Due to its higher stiffness, better ductility and increased peak load capacity research into the utilisation of grout in timber and STC connections is progressing rapidly.



**Figure 2.18:** Side perspective on push-out test samples of BCGP, SCGP and GSC (L-R) (Adapted from [34], [73] and [72])

#### Bolts connectors embedded in grout pockets

BCGP, as seen in Fig. 2.18(Left) has shown superior initial- and ultimate stiffness, increased load carrying capacity and a better ductility in push-out experiments when compared to traditional dowel-type fasteners [30] [33] due to higher elastic modulus and compressive/crushing strength of the grout when compared to CLT. It has been tested in full-size steel-CLT composite beam flexural tests and displayed its ability to increase initial beam stiffness and peak load capacity of the beam [31].



**Figure 2.19:** Load-Slip curves for STC connection specimen with changing diameters (Adapted from [28]) with (a) Coach screws, (b) Dog screws and (c) Bolt connectors in grouted pockets

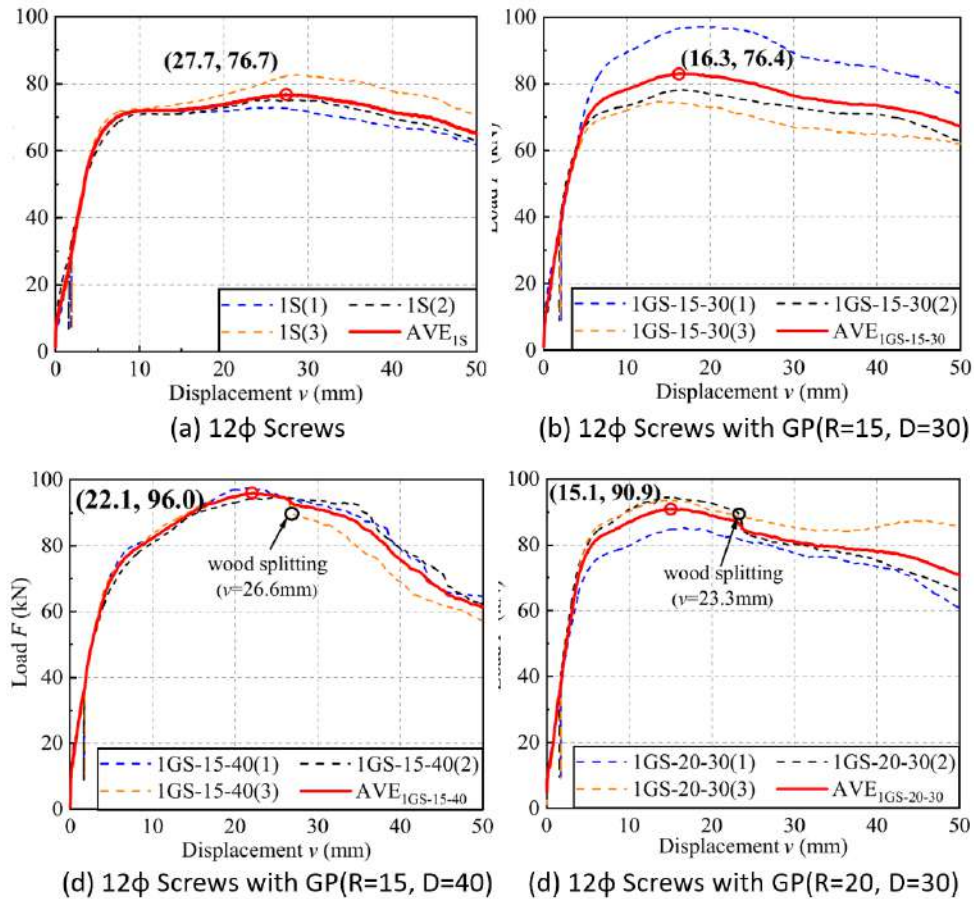
In Fig. 2.19 the load-slip curves of steel-CLT composite connection with (a) coach screws (4.6 steel grade), (b) dog screws (5.8 steel grade) and (c) bolt connectors in grouted pockets are depicted. The pre-peak stiffness and ultimate strength of steel-CLT shear connections with dog screws are slightly higher than with coach screws. The yield strength of the mechanical fastener has little effect on connections strength and stiffness as joint structural behaviour is largely governed by non-linear effects such as timber crushing [28].

Fig. 2.19 shows that BCGP steel-CLT composite connections have significantly higher stiffnesses, initial and pre-peak and a higher peak load capacity. Within a BCGP connection the size of the grouted pocket and yield strength of the bolts have little to no influence on pre-peak load-slip behaviour [28].

#### Screw connectors embedded in grout pockets

SCGP, as seen in Fig. 2.18(Middle) differ from BCGP due to the use of shallow grouted pockets, which do not reach the steel flange. In experiments, with a GLT panel, the screw was forced, by the use of the shallow grouted pocket, to behave according to failure mode E (Fig. 2.16) with two plastic hinges. When compared to grout-less similar connections the SCGP increased the peak load capacity, initial stiffness, ultimate stiffness and ductility by a maximum of 25.2%, 55.9%, 62.1% and 33.6%, respectively [73].





**Figure 2.20:** Load-Slip curves for STC connection specimen with screws in grouted pockets (Adapted from [73]) with (a) screws, (b) screw in grouted pocket, (c) SCGP with increased depth and lastly (d) SCGP in pocket with increased radius

Fig. 2.20 depicts the load-slip behaviour of steel-CLT connections with screw connectors in grouted pockets. There is an increase in stiffness with initial application of the grouted pocket. Increasing the radius and depth of the grouted pocket significantly increases the peak load, stiffnesses and ductility when compared to the common specimen with screws.

#### Grouted stud connectors

GSCs (grouted stud connectors), as depicted in Fig. 2.18 (Right), were investigated using finite element analysis [72]. The capacity, determined by design codes, was found to be underestimated compared to finite element results and other optimised calculation methods. GSCs show promise as an alternative for steel-timber composite constructions, but further experimental research is needed to bolster their viability.

#### 2.6.3. Comparison of experimentally tested steel-CLT connections

Table 2.1 displays the results from the existing experimental research done on steel-CLT composite connections in push-out tests. The table depicts the parameters of each experiment, such as the compressive stress parallel to the grain (as this was given for each study) in  $f_c$  and the layup and orientation of the CLT panel. Secondly for each experiment the abbreviation of the used composite connection is stated:

- DS: Dog screw
- CS: Coach screw
- BCGP: Bolt connector in grouted pocket

- B: Bolt
- SDS: Self drilling screw
- S: Screw (type unspecified)
- SCGP: Screw connector in grouted pocket

When no value of spacing is given an individual connector was tested instead of multiple connectors in a row. The results of the done experimental research which are displayed are the initial stiffness ( $k_{s,0.4}$ ), secondary stiffness ( $k_{s,0.6}$  or  $k_{s,0.7}$ ) and ultimate load capacity ( $P_u$ ).

**Table 2.1:** Comparison of existing experimental data on steel-CLT composite connections in push-out tests according to BS EN26891[21]

Study	$f_c$ (N/mm <sup>2</sup> )	Layup $t_i$ (mm)	Orien. (deg)	Connection Abbr. & ( $\phi$ )	s (mm)	$k_{s,0.4}$ (kN/mm)	$k_{s,0.6}$ (kN/mm)	$k_{s,0.7}$ (kN/mm)	$P_u$ (kN)				
[28]	24	A	B	DS16		29.65	11.66		54.4				
				DS19		17.16	6.23		68.6				
				CS12		18.69	9.52		35.8				
				CS16		22.23	8.21		49.9				
				CS20		10.37	6.11		67.5				
				BCGP12 <sup>bc</sup>		39.53	29.76		82.9				
				BCGP16 <sup>ad</sup>		58.68	45.26		103.4				
				BCGP16 <sup>bd</sup>		55.12	45.77		129.9				
				BCGP20 <sup>bc</sup>		64.57	53.68		153.3				
				BCGP20 <sup>bd</sup>		77.19	63.08		159.7				
							C	CS12		6.29	2.14		37.5
								CS16		6.81	6.11		53.6
								CS20		6.43	6.24		74.9
[68]	50.62	25,25	[0/0]	B6	100	12.47	13.43		43.13				
				B8	100	17.03	17.85		69.28				
				SDS5.5	100	36.51	27.92		39.55				
				B6	150	12.71	13.67		39.27				
				B6	200	12.85	13.23		37.63				
						15,15	[0/0]	B6	100	10.74	10.62		36.41
						20,20	[0/0]	B6	100	11.49	11.5		49.04
						30,30	[0/0]	B6	100	12.13	12.63		37.16
[73]	41.89	26,28,26	[0/0/0]	S12		12.45		10.06	76.33				
				SCGPr15d30*		15.69		11.5	76.41				
				SCGPr15d35		15.27		14.41	81.73				
				SCGPr15d40		16.33		15.49	91.03				
				SCGPr20d30		17.91		16.31	80.93				
				SCGPr20d35		19.41		14.69	85.43				
				SCGPr15d30	250	21.26		12.66	73.04				
				SCGPr15d30	200	22.27		17.01	78.58				
				SCGPr15d30	150	17.91		13.78	70.04				

\*: r for radius and d for depth of circular GP; A: 20,20,40,20,20; B: [0/90/0/90/0]; C: [90/0/90/0/90]; a: Fastener strength 4.6; b: Fastener strength 8.8; c: GP dimension 60x135; d: GP dimension 80x135

### 2.6.4. Spacing

Consequently to the finding mentioned in Section 2.6.1 that spacing is a leading factor in the achievement of satisfactory composite efficiency the question arises whether closer composite connection spacing could result in a higher composite efficiency. From experimental research [68][73] it is seen that in push-out tests the connector behaves more ambiguous than regulatory acceptance. [68] concluded that the ultimate load capacity is shown to be inversely proportional to the bolt spacing once the connectors are placed relatively closely together:

- An increase in bolt spacing decreases ultimate load capacity
- An increase in bolt spacing decreases ductility

This conclusion was reached with connectors at  $s = \{100, 150, 200\}mm$ . Contradictory, [73] tested the SCGP connection and showed a higher ultimate load capacity with increasing and decreasing connection spacing. The research found the ultimate load capacities with spacing  $s = 150mm$  and  $s = 250mm$  were higher than with the spacing of  $s = 200mm$ . This contradicts Eurocode 5 which clarifies the effective number of connectors  $n_{ef}$  in a composite beam as follows:

$$n_{ef} = \min \left\{ \begin{array}{l} n \\ n^{0.9} \sqrt[4]{\frac{a_1}{13d}} \end{array} \right. \quad (2.5)$$

With this equation the above mentioned case, according to the Eurocode would have the  $s = 200$  and  $s = 250$  not reduced in capacity whilst reducing the ultimate load capacity of  $s = 150mm$  by 5.6% as  $n_{ef} = 1.888$ . In regards to spacing it is clear that more composite connections results in higher composite efficiency. However with low spacing there complexity arises where a decrease and increase in spacing would change the ultimate load capacity of the connection and the result of a push-out test.

# 3

## Analytical analysis

A standard steel-CLT composite beam, as depicted in Fig. 1.5, can be analysed with Eurocode 5, Annex B [20]. In manual calculations the characterisation of the fastener is of importance, similarly to in finite element modelling. This is usually done by the slip modulus ( $K$ ) and spacing ( $s$ ) as seen in Section 2.1. However in manual calculation a linear response is assumed for the slip modulus and therefore the used connection will need to display linear behaviour pre-failure. In case of non-linearity in push-out test response the ultimate stiffness ( $k_{s,0.6}$ ) would be a more reliable slip modulus.

The following methodology is used to analytically calculate the effective bending stiffness of a steel-CLT composite beam with a CLT slab and a steel beam connected with a composite connection as seen in Fig. 3.1. In the exemplary cross-section depicted the CLT panel consists of 5 layers with the second and fourth layer being perpendicular to the grain. It approaches the composite connection with the above mentioned slip modulus and spacing of the connections.

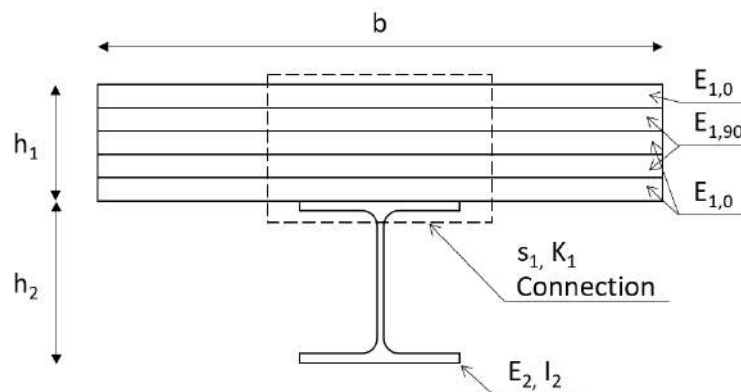


Figure 3.1: Cross-section of steel-CLT composite beam

### 3.1. Equivalent cross-section of the CLT panel

For the analytical approach firstly an equivalent cross-section of the CLT is necessary which leads to the homogenised MOE.

$$E_{h,CLT} \cdot I_h = EI_{eff} \quad (3.1)$$

where

$E_{h,CLT}$  is the homogenised MOE of the equivalent CLT cross-section

$I_h$  is the second moment of area of the CLT panel

$EI_{eff}$  is the effective bending stiffness of the CLT panel

The effective bending stiffness of the CLT cross-section ( $EI_{eff}$ ) can be calculated using the same Gamma-method which takes into consideration the relative stiffness between the different layers of the CLT panel. This methodology was initially proposed by [26] for cross-sections with 3- and 5-layer panels.

$$EI_{eff} = \sum_{i=1}^n (E_i I_i + \gamma_i E_i A_i a_i^2) \rightarrow E_{h,CLT} = \frac{\sum_{i=1}^n (E_i I_i + \gamma_i E_i A_i a_i^2)}{I_h} \quad (3.2)$$

where

$E_i$  is the MOE of layer i

$I_i$  is second moment of area of layer i

$A_i$  is the surface area of layer i

$a_i$  is distance between center of layer i and the cross-sectional center

$\gamma_i$  takes into consideration the relative stiffness between the different components of the cross section

The gamma factor,  $\gamma_i$ , for different layers in CLT differs for longitudinal layers and other layers in the direction of the bending of the beam. The gamma factor is calculated in the following way:

$$\gamma_i = \begin{cases} \frac{1}{1 + \frac{\pi^2 E_i h_i}{L^2} \cdot \frac{t_j}{G_{23,j}}} & \text{Longitudinal layers} \\ 1 & \text{Other layers} \end{cases} \quad (3.3)$$

where

$L$  is the length of the beam

$h_i$  is the height of layer i

$t_j$  is the thickness of the adjacent layer j

$G_{23,j}$  is the rolling shear stiffness of the adjacent layer j

The result of this analytical operation is a steel-CLT composite beam cross-section with an equivalent cross-section of the CLT as seen in Fig. 3.2

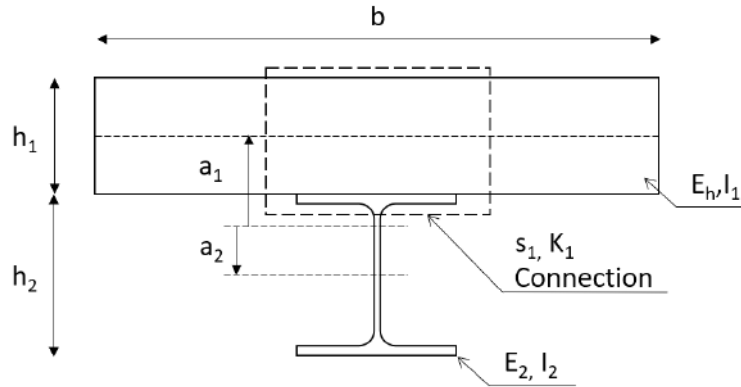


Figure 3.2: Cross-section of steel-CLT composite beam with equivalent CLT panel

### 3.2. Effective bending stiffness with full- and no-composite action

In the full-composite action scenario, when there is the assumption to no slip occurs between the CLT and the steel beam, the flexural bending stiffness for the full-composite T-section ( $EI_{\gamma=1}$ ) can be analytically determined from:

$$EI_{(\gamma=1)} = EI_1 + E_1 A_1 a_1^2 + EI_2 + E_2 I_2 a_2^2 \quad (3.4)$$

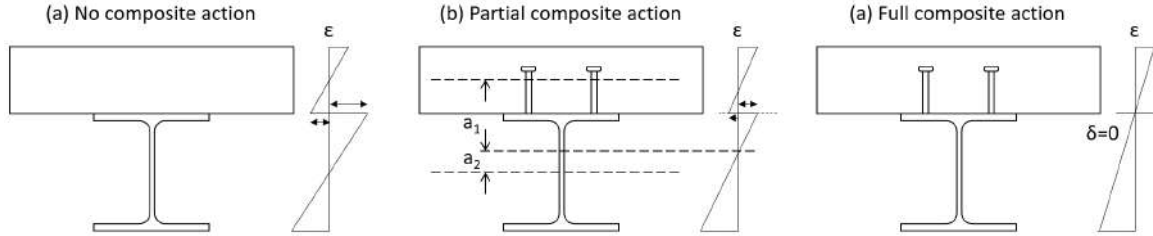
where

$$E_1 = E_{h,CLT}$$

$i = 1$  refers to the CLT panel equivalent

$i = 2$  refers to the steel beam

The distance from the neutral axis of each component to the cross-section neutral axis ( $a_1$  &  $a_2$ , respectively) are depicted in Fig. 3.3 (b).



**Figure 3.3:** Schematic illustration of the vertical strain distribution for cross-sections and the corresponding distances  $a_1$  &  $a_2$

In the case of no-composite action the horizontal shear force is not transferred at the material interface of the CLT and the steel flange. As a result the bending stiffness of the member ( $EI_{(\gamma=0)}$ ) can be determined from:

$$EI_{(\gamma=0)} = EI_1 + EI_2 \quad (3.5)$$

### 3.3. Mechanically jointed steel-CLT composite beam

After the CLT-equivalent slab is analysed, the analytical calculation of the mechanically jointed steel-CLT composite beam can be done following 1995-1-1 Annex B[19]. The position of the cross-sectional centroid has to be established which will result in the absolute distance to this centroid of the CLT panel and steel profile, respectively.

$$a_2 = \frac{\gamma_1 E_1 A_1 (h_1 + h_2)}{2 \sum_{i=1} (\gamma_i E_i A_i)} \quad (3.6)$$

In accordance with EN1995-1-1[19] Appendix B.2 the gamma-factor for mechanically jointed beams is the following for the steel-CLT composite beam where the CLT is mechanically jointed with the steel beam.

$$\gamma_1 = \frac{1}{1 + \frac{\pi^2 E_1 A_1 s_1}{K_1 L^2}} \quad (3.7)$$

where

$s_1$  is the spacing of the steel-CLT composite connections

$K_1$  is the slip modulus of the composite connection

This results in the calculation of the effective bending stiffness of the steel-CLT composite cross section ( $EI_{STC,eff}$ ) as:

$$EI_{STC,eff} = (E_{h,CLT} I_h + \gamma_1 E_{h,CLT} A_1 a_1^2) + (E_2 I_2 + \gamma_2 E_2 A_2 a_2^2) \quad (3.8)$$

where

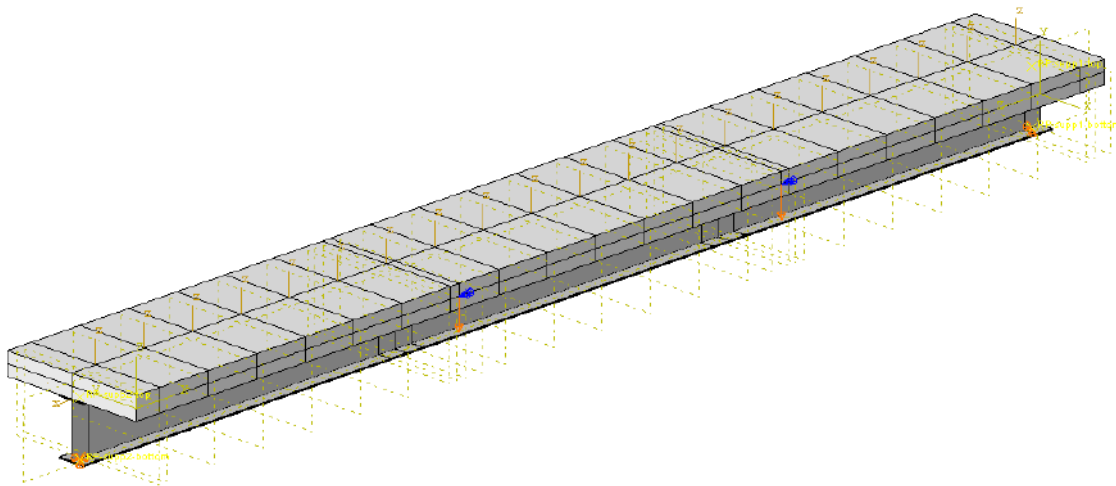
$$\gamma_2 = 1$$

# 4

## Finite element model

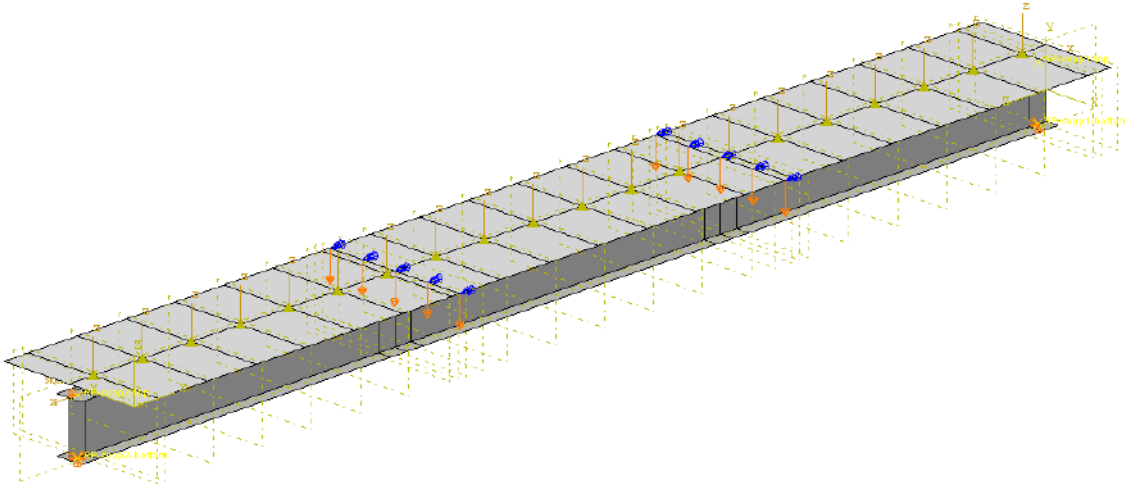
### 4.1. General

First off, It is important to keep in mind that a model is simply a tool, and its effectiveness relies heavily on the skills and knowledge of the user and generator. As the economist Kate Raworth puts it: "Every model can only ever be a model, a necessary simplification of the world, and one that should never be mistaken for the real thing."



**Figure 4.1:** Extruded 3D finite element model, used for validation, of simply supported steel-CLT composite beam

The 3D finite elements software ABAQUS [11] is used for the steel-CLT composite beam system shown in Fig. 4.1. The presented model was based on modeling approaches by [64] for SCC beams, which were adapted for the implementation of LVL by [57], in combination with characteristics from the 2D continuum-based finite element model from [31] to account for the use of cross-laminated timber. The model in this study is a numerical model of a steel-CLT composite beam in a four-point bending test, a flexural test in which the section between the points of loading are under a constant bending moment.

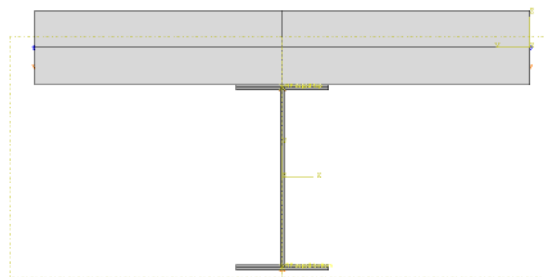


**Figure 4.2:** 3D finite element model, used for validation, of simply supported steel-CLT composite beam

The construction of the model was achieved by gradually increasing the complexity through a step-wise approach. Initially, the accuracy of the model was determined for a steel beam subjected to four-point bending. Subsequently, a CLT panel was added to the model, and the composite interaction between the two materials was modeled in both full and no interaction(friction) cases. Finally, to complete the model, the partial composite connection was introduced as the last level of complexity.

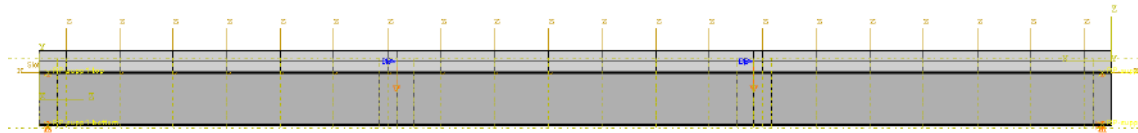
Fig.4.1 is the 3D depiction of the numerical used in the validation of the modelling against experimental data. In this figure the model is extruded to depict realistic dimension but it is actually modelled with shell elements. Shell elements with reduced integration are chosen as they capture the essential characteristics of the beam's cross-section, such as its thickness and curvature, while neglecting the finer details that may not significantly impact the overall behavior of the beam. Secondly, shell elements require fewer computational resources compared to solid elements. By using shell elements, the analysis time can be significantly reduced without compromising the accuracy of the results as they work great in elements in bending.

Fig. 4.2 depicts the non-extruded finite element model. In this figure the loading conditions are depicted clearly as the orange arrows with blue boundary conditions at  $L = 1/3 \cdot L$  and  $L = 2/3 \cdot L$  represent the vertical displacement that is prescribed during loading. Fig. 4.3 depicts the extruded cross-section of the numerical model whilst Fig. 4.4 displays the side perspective on the numerical model with extruded shell elements.



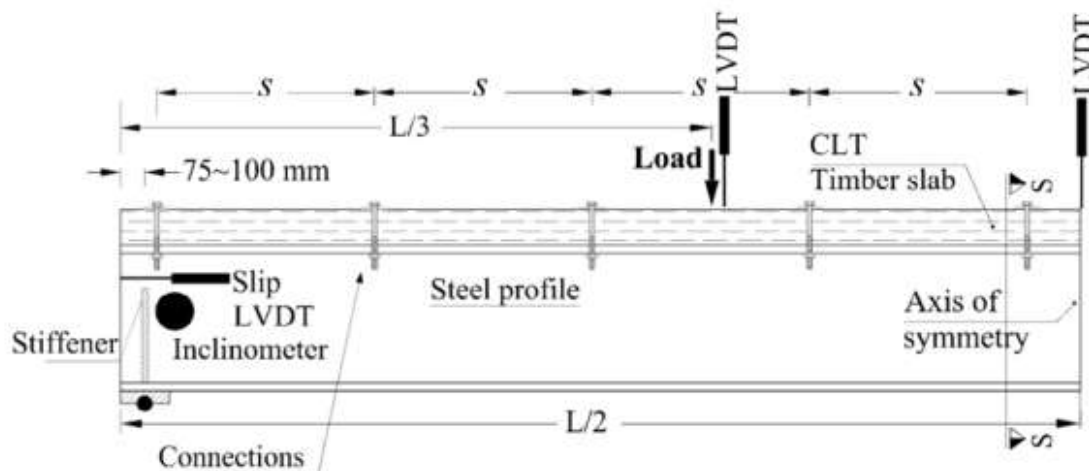
**Figure 4.3:** Finite element mode: Cross-section of simply supported steel-CLT composite beam used for validation





**Figure 4.4:** Finite element mode: Side view of simply supported steel-CLT composite beam used for validation

The initial validation of the numerical model was carried out by subjecting the modelled beam to a four-point bending test, which is commonly used to determine the flexural strength of a beam specimen. The aim of this was to establish reasonable level of preciseness in the scattering of the results by comparing the numerical results to experimental results obtained by [31] in which an identical steel-CLT composite beam was experimentally tested. The experimental test set-up used by [31] can be seen in Fig. 4.5.



**Figure 4.5:** Side view of 4-point bending tests on steel-CLT composite beam executed by (and figure adapted from:[31]) with instrumentation visual

In the subsections that describe the particular modelling steps and specifics, the parameters used for the validation of the model's scattering of results when compared to that of the experimental data.

## 4.2. Material properties and behaviour

### 4.2.1. Cross laminated timber slab

The timber slab is modelled as a composite of multiple lamellae with defined thickness and orientation. Orientation is in either parallel( $0^\circ$ ) or perpendicular( $90^\circ$ ) direction to the grain. The timber lamellae are modelled as orthotropic materials with the Hashin damage model to capture non-linearity in behaviour and failure of timber lamellae.

#### The Hashin damage model

is an approach for the modelling of timber that appropriately captures the failure and behaviour of the lamellae under bi-axial stress. The model predicts onset and propagation of damage, including cracking, splitting and other forms of degradation.

It is able to account for anisotropic nature of composite layers, such as timber lamellae, by correcting for mechanical properties in longitudinal, radial and tangential direction. Behavioural accuracy of the Hashin damage model for timber, under plane stress states was investigated by [41] and [63] and used in the numerical investigation of steel-CLT composite beams [31].

Fig. 4.6 explains the Hashin model as it shows the strengths accounted for in the model in stress-strain diagrams. Utilising those strengths the following Hashin criterion need to be applied:

- Tensile fiber failure

$$\left(\frac{\sigma_1}{\sigma_{t,1}}\right)^2 + \left(\frac{\sigma_{12}}{\sigma_{v,12}}\right)^2 = 1 \quad (\sigma_1 > 1) \quad (4.1)$$

- Compression fiber failure

$$\frac{|\sigma_1|}{\sigma_{c,1}} = 1 \quad (\sigma_1 < 1) \quad (4.2)$$

- Tensile matrix failure failure

$$\left(\frac{\sigma_2}{\sigma_{t,2}}\right)^2 + \left(\frac{\sigma_{12}}{\sigma_{v,12}}\right)^2 = 1 \quad (\sigma_2 > 1) \quad (4.3)$$

- Compression matrix failure failure

$$\left(\frac{\sigma_2}{2\sigma_{v,23}}\right)^2 + \left[\left(\frac{\sigma_{c,2}}{2\sigma_{v,23}}\right)^2 - 1\right] \frac{\sigma_2}{\sigma_{c,2}} + \left(\frac{\sigma_{12}}{\sigma_{v,12}}\right)^2 = 1 \quad (\sigma_2 < 1) \quad (4.4)$$

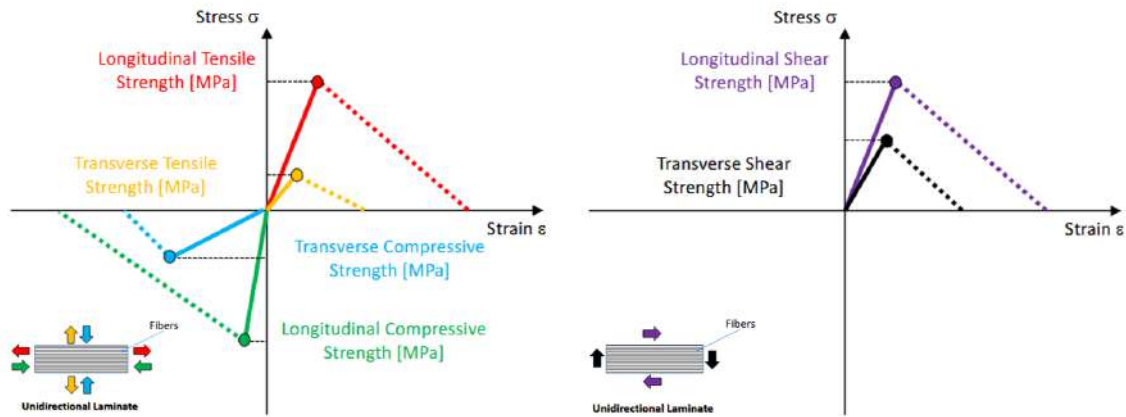


Figure 4.6: Stress-strain diagrams of the strengths in the Hashin damage model(Adapted from [65])

### Validation

of the model is done comparison with existing experimental data which was done with the mechanical, engineering, properties of the wood of the lamellae seen in Table 4.1 with the composite layup used, in the numerical model of the steel-CLT beam, was  $[0^\circ, 90^\circ, 0^\circ, 90^\circ, 0^\circ]$  with thickness per lamellae being respectively  $t = (20, 20, 40, 20, 20)$  mm.

The parameters of the Hashin damage model are given in Table 4.2.

Table 4.1: Mechanical properties of the timber lamellae adopted in the validation model

Young's Moduli			Poisson's Ratios			Shear Moduli		
$E_1$ (MPa)	$E_2$ (MPa)	$E_3$ (MPa)	$\nu_{12}$	$\nu_{13}$	$\nu_{23}$	$G_{12}$ (MPa)	$G_{13}$ (MPa)	$G_{23}$ (MPa)
11000	370	370	0.48	0.48	0.22	690	690	60

\* Direction 1 is parallel to the grain, direction 2 is perpendicular to the grain (over the width material) and direction 3 is perpendicular to the grain(over the height).

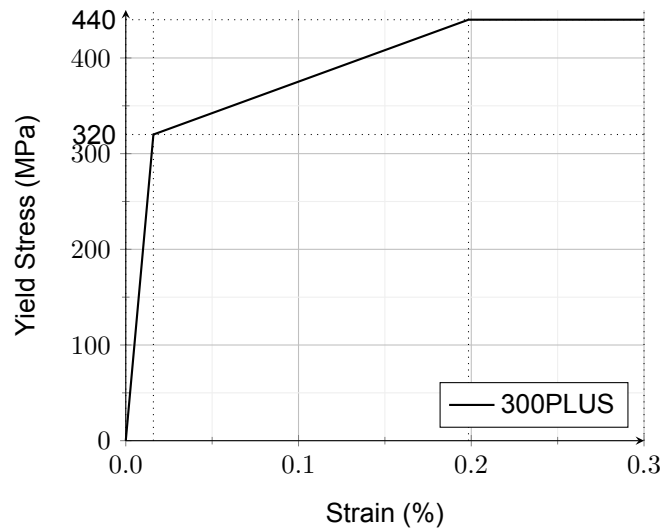
**Table 4.2:** Hashin damage model parameters adopted in the validation model

Longitudinal Strength		Transversal Strength		Longitudinal Shear Strength	
$\sigma_{c1}$ (MPa)	$\sigma_{t1}$ (MPa)	$\sigma_{c2}$ (MPa)	$\sigma_{t2}$ (MPa)	$\sigma_{v12}$ (MPa)	$\sigma_{v23}$ (MPa)
36	24	4.3	0.7	6.9	0.5

\* Direction 1 is parallel to the grain, direction 2 is perpendicular to the grain (over the width material) and direction 3 is perpendicular to the grain(over the height). Longitudinal- and Transversal strength are shown in tension and compression.

#### 4.2.2. Steel beam

The material model for steel is uni-axially modelled as elastic-isotropic with plastic hardening. The corresponding stress-strain relationship, as implemented, is displayed in Fig. 4.7.

**Figure 4.7:** Uniaxial stress-strain relationship for the steel beam

#### Validation

of the model is done comparison with existing experimental data was done with the steel grade 300PLUS, an Australian standard grade, with a nominal yield strength ( $f_{y,s}$ ) of 320 MPa and an ultimate strength ( $f_{u,s}$ ) of 440 MPa. The elasticity modulus ( $E_s$ ) is 200,000 MPa with a Poisson's ratio ( $\nu$ ) as 0.3. The profile in the validation model is a 310UB 32. The material properties can be in seen in Table 4.3.

**Table 4.3:** Properties of the 310UB32 profile

Section depth	Flange width	Flange thickness	Web thickness	Yield strength	Ultimate strength	Elastic modulus	Poisson's ratio
$d$	$b_f$	$t_f$	$t_w$	$f_y$	$f_u$	$E_s$	$\nu$
298 mm	149 mm	8.0 mm	5.5 mm	320 MPa	440 MPa	200,000 MPa	0.3

\* 310UB32 is a profile commonly used in Australia and New Zealand

### 4.3. Shear connection

The interaction between the CLT panel and the steel beam was simulated using various methods. The model was progressively made more complex, starting from a basic scenario of a steel beam undergoing 4-point bending. In the first stage, a CLT panel was added on top with the interaction between the components limited only to the friction coefficient. This scenario is referred to as "no

composite action” and is defined in Section 2.6. Next, a full composite action (as defined in Section 2.6) was achieved by completely bonding the surfaces. Before moving on to a partial composite connection, a rigid composite connection was simulated to set an upper bound.

#### 4.3.1. No composite action

For the model used in this research ‘no’ composite action was achieved having friction as the only interaction property between the two components. The contact interface of the components, the slab and the beam, was modelled by mechanical interaction properties: tangential behaviour characterised by a friction coefficient of 0.45[1] and normal behaviour described as “Hard” contact.

“Hard” contact implies that any two surfaces that interact in the normal direction will resist penetration and bear against each other.

It is important to note that the friction is excluded from the partial composite connection models since friction is already included in the load-slip behaviour of a push-out test. Secondly, although in this research this is mentioned as ‘no composite action’, due to the modelling of friction between the CLT and the steel flange, some slip is resisted.

#### 4.3.2. Full composite action

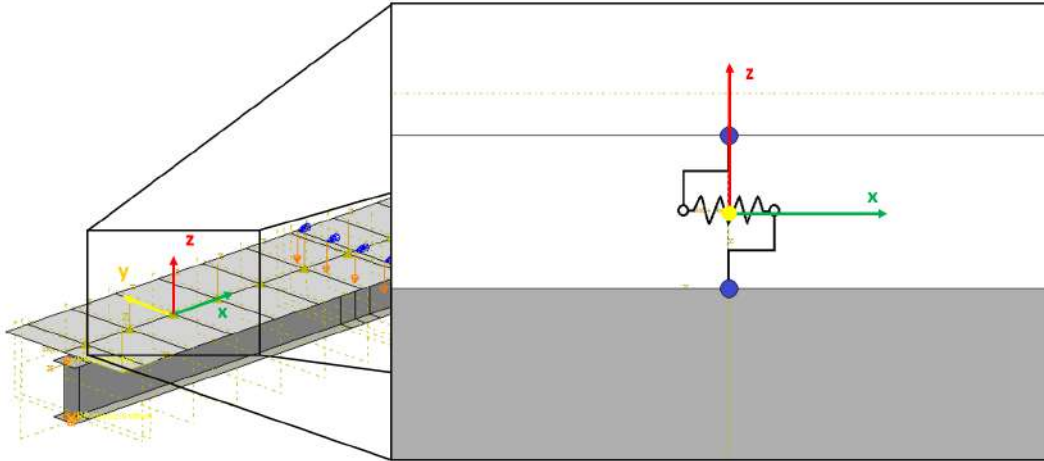
Full composite action, also known as rigid shear interaction as shown in Fig. 2.1, is achieved when the two components of a composite floor system work together as a single entity. To achieve this, all nodes on the surface of the beam are tied to their respective counterparts on the CLT. This ensures that the beam and CLT act together as one unit, resulting in superior, theoretical, stiffness and strength of the composite floor system. In the model in this study a tie constraint is used which ties two surfaces, and its nodes, together to constraint relative motion.

#### 4.3.3. Rigid composite connection

A composite connection with infinite stiffness, a rigid composite connection, was modelled by the use of multi-points constraints (MPCs), specifically the MPC type ‘Beam’. Such constraints allow constraints to be imposed between different degrees of freedom of the model [11]. The MPC type ‘Beam’ constraints the displacement and rotation of one node to a second node by providing a rigid beam in between creating a rigid link at specified positions.

#### 4.3.4. Partial composite connection

The model used in this study involved partial composite action between the CLT slab and the steel beam. This partial composite action was activated by modelling the elastic resistance of a particular composite connection in longitudinal direction with a zero-length spring, Fig. 4.8, that connects the elements.



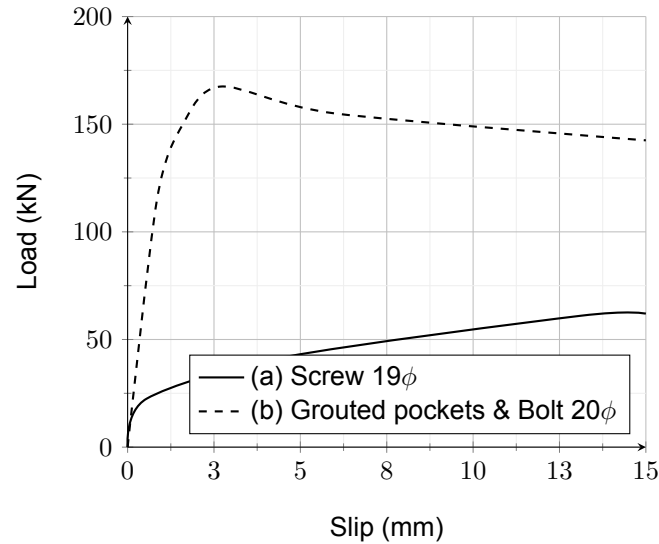
**Figure 4.8:** Zero-length spring, modelling with connector element 'Translator' that connects node of CLT panel with node of top flange of steel beam with a local axis system

To model this zero-length spring a 'wire' which connects two nodes was given a sectional properties. This connector section, which dictates the behaviour of the wire, had the properties of translational behaviour of the type "slot" and rotational behaviour of the "align" type. This combination is also known as a translator and can be seen in Fig. 4.9. This translator section allows displacement in a single direction while constraining the others, thereby enabling longitudinal displacement along the interface of the CLT slab and the steel flange. This simplistic approach could provide reasonable accuracy as long as a sufficient number of connectors were placed along the composite member.



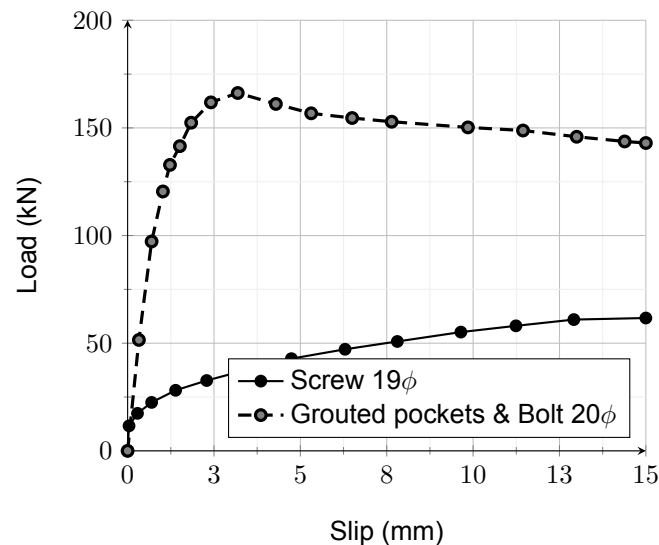
**Figure 4.9:** Connection type TRANSLATOR imposes kinematic constraints and uses local orientation definitions equivalent to combining connection types SLOT and ALIGN [11]

The mechanical behaviour of the connectors, thus the translator, was characterized with experimental push-out test data (Fig. 4.10). This curve was used to define the elastic characteristics of the translator (Fig. 4.9). However for implementation in the numerical model the experimental load slip data (Fig. 4.10) has to be transformed into a piece-wise linear load slip curve, thus dissecting the experimental push-out test data in pieces of linear curves as seen in Fig. 4.11. To summarise, experimental load-slip data from a composite connection can be implemented in the numerical model by characterising the translator with a piece-wise linear load-slip curve.



**Figure 4.10:** Load-slip curve of two composite connections used in validation of the finite element model with data from [31]

Thus, the translator with elasticity represents a zero-length spring element with definable resistance. This zero-length spring connects a node of the CLT panel with a node of the steel top flange with elastic resistance in longitudinal direction as seen in Fig. 4.8. The accuracy of this model is heavily dependent on the load-slip data, of experiments, to appropriately capture the partial composite action of the steel-CLT beam with that particular composite connection.



**Figure 4.11:** Piece-wise linear load-slip curve of two composite connections used in validation of the finite element model

#### Validation

of the finite element model was done by implementing the load-slip data obtained from push-out tests, seen in Fig. 4.10, of both 19mm dog screws and 80 by 135 mm grouted pockets containing 20mm diameter bolts(BCGP)[31] seen in Fig. 2.18 on the left.

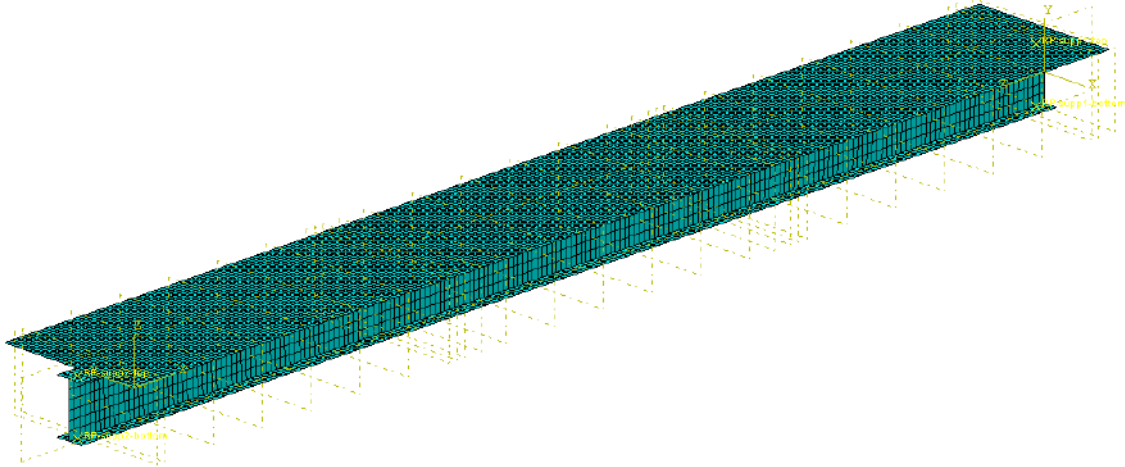
In the implemented push-out test data identical CLT panel as specified for the beam model used for validation (Section 4.2.1) is used as it is an important parameter for the load-slip behaviour as clarified in Section 2.6. These connectors were spaced 300mm apart in the experimental beam test and thus

implemented as such in the numerical model.

## 4.4. Meshing

### 4.4.1. Elements

The timber slab is modelled with four-node shell elements with reduced integration (S4R). Such a shell element lends itself to the modelling of thin-walled structures such as the web and flanges of a beam or a slab.



**Figure 4.12:** 3D perspective on FEM with displayed mesh

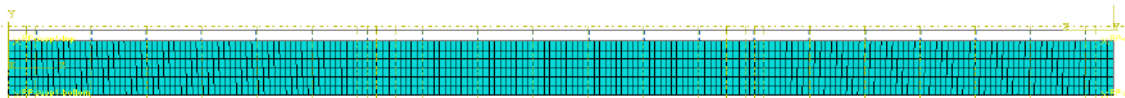
It allows for bending and twisting of the shell without shear locking, which is caused when an element cannot accurately capture the shear deformation.

The S4R element has two degrees of freedom per node. Both degrees of freedom are in displacement and respectively in x- and y-direction.

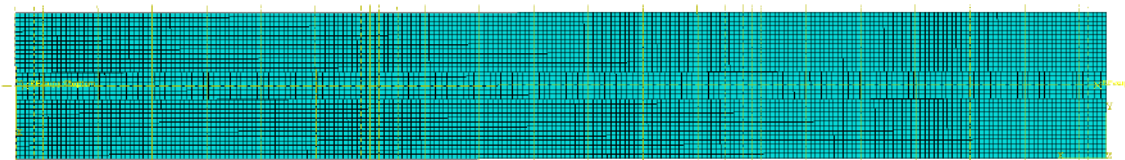
Reduced integration results in less number of integration points to calculate in the element stiffness matrix. Elements can then be calculated more efficiently and can avoid numerical instabilities. It should be used in caution as it can cause a loss in accuracy of the model.

### 4.4.2. Mesh

The maximum size of the S4R elements are limited to 25 mm for the steel beam and the CLT panel. An outline of the mesh used in the validating model can be seen in Fig. 4.14.



**Figure 4.13:** Side perspective on FEM with displayed mesh



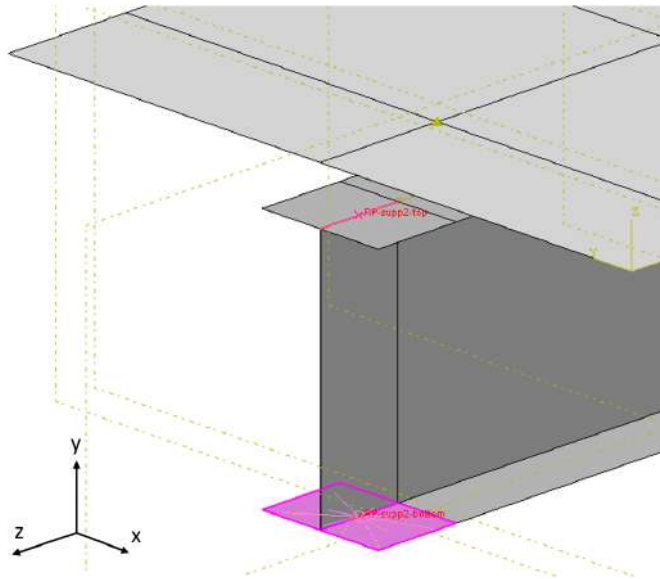
**Figure 4.14:** Top perspective on FEM with displayed mesh of the CLT panel

## 4.5. Analysis and boundary conditions

### 4.5.1. Supports

Supports were modelled by coupling two 100mm wide sections of the bottom flange (depicted in Fig. 4.15), constraining all degrees of freedom, to two reference points, respectively. These reference points are then simply supported. This represents the experimental situation depicted in Fig. 4.5.

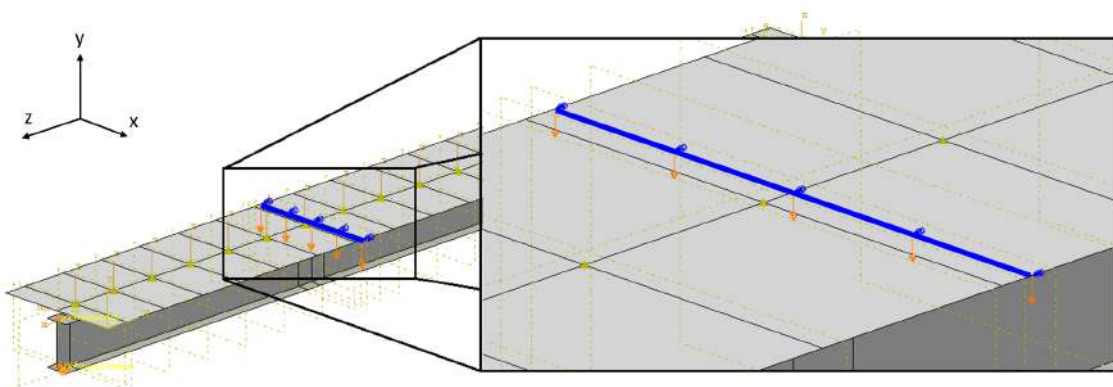
Secondly, the central vertices at the supports of 100mm in length, of the top flanges (depicted in Fig. 4.15) were coupled to their respective reference points which in their turn were laterally restrained ( $U_x = 0$ ), by restraining movement of the beam out-of-plane. The reference points, at the bottom, were then supported as a simple ( $U_x = 0$ ,  $U_y = 0$  and  $U_z = 0$ ) and a roller support ( $U_x = 0$  and  $U_y = 0$ ) to create a statically determinate beam.



**Figure 4.15:** Modelled support with the bottom section simply supported and central vertice laterally restrained

### 4.5.2. Loading conditions

The model is analysed with displacement controlled loading on central line of the CLT panel at  $L/3$  and at  $2L/3$  to accurately depict a four-point bending test. This loading condition is depicted in Fig. 4.16. The entire highlighted line of nodes on the CLT panel can only move vertically.



**Figure 4.16:** Loading conditions of the finite element model zoomed in on position  $z = 2L/3$

In displacement controlled loading, a node, or a group of nodes in the presented model, is given



a prescribed displacement ( $U_y$ ) at each loading step. This displacement results in stresses. The corresponding vertical load of this prescribed displacement can be analysed in the vertical force in the supports. Displacement control more accurately depicts the behaviour of a beam in a bending test and can also capture the decrease in force.

### 4.5.3. Iterative scheme

The iterative scheme employed in the finite element analysis is the full Newton-Raphson method to solve the nonlinear problems. It solves the equilibrium equations for the system iteratively until convergence is reached. Important is the fact that at every iteration the stiffness matrix is updated making it more accurate but also more computationally intensive than the modified Newton-Raphson or arc-length method.

## 4.6. Validation of Numerical model

The numerical model (Section 4.1) has to be validated against experimental data. The experimental data used to validate is from the experiment depicted in Fig. 4.5 in which two different partial composite connection were used (Fig. 4.10) with the material properties described in Section 4.2. The experiment loaded the steel-CLT beams of 6 meters in length according to BO EN-26891 requirements[21]. The specimen were loaded up to 40% of the estimated failure capacity after which they were unloaded to 10% and reloaded until failure[31].

The first results, Fig. 4.17, show the results of the numerical model in 5 different scenarios:

- A **Steel beam** which functions as a lower bound
- The steel beam with the 5-layered CLT panel on top connected purely with **Friction** as described in Section 4.3.1
- An upper bound to the load-deflection results as a result of '**Full composite action**' (Section 4.3.2). The steel beam and CLT panel work as one entity in bending.
- a partial composite connection (Section 4.3.4) with **20 $\phi$  Bolts in grouted pockets (BCGP)** of 80 by 135 mm spaced 300 mm apart
- a partial composite connection (Section 4.3.4) with **19 $\phi$  Screws** spaced 300 mm apart

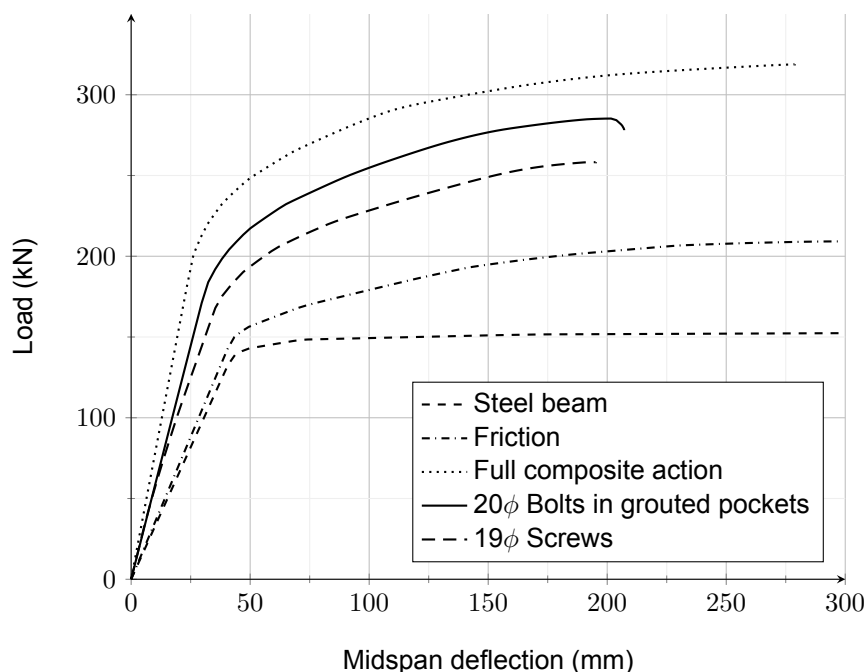
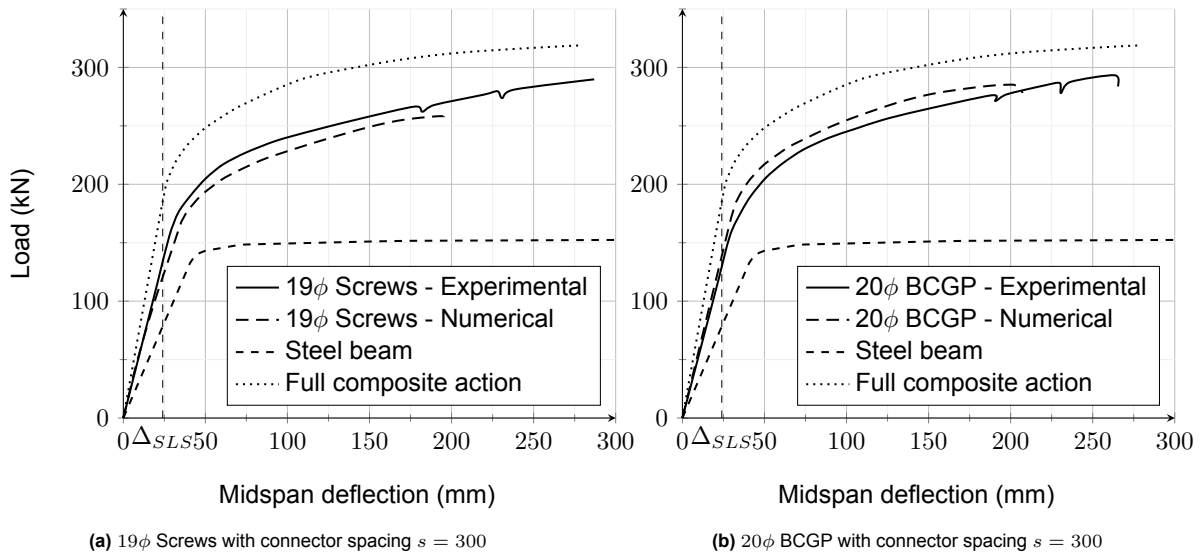


Figure 4.17: Numerical Results: Load-midspan deflection curve

To validate the above mentioned results of the partial composite connection they are compared against the experimental data from [31] depicted in Fig. 4.5. The numerical model of the 6 meter long steel-CLT composite beam with the partial composite connection with 19 $\phi$  screws spaced 300 mm apart is compared against its respective experimental data in Fig. 4.18a and the numerical model is compared against the experimental test with 20 $\phi$  Bolts in grouted pockets (BCGP) shear connectors in Fig. 4.18b.

By utilising linear interpolation on the data points, the scattering of the results of the numerical model was assessed by calculating the mean squared error (MSE) as a percentage relative to the corresponding experimental data. The results demonstrate that the numerical model relatively precisely predicts the load corresponding to a specific deflection level within a tolerance of 5% in the scattering of the results. Specifically, in Fig. 4.18a, the scattering of the results is determined to be 4.9%, while in Fig. 4.18b, the scattering of the results is measured at 4.8%. These findings indicate the reliability and effectiveness of the numerical model in simulating the experimental outcomes.



**Figure 4.18:** Load-Midspan deflection of experimental tests and numerical model (Experimental data from [31])

The initial beam stiffness is measured over the first 5 loading steps, which corresponds to reaching 10% of the serviceability deflection or 2.4 mm at midspan. The initial beam stiffness ( $K_{b,ini}$ ) of the numerical model with the 19  $\phi$  screws with connector spacing of 300 mm is 5.94 kN/mm and that of the numerical model with the 20  $\phi$  BCGP connection with identical spacing is 5.82 kN/mm. The experimental initial beam stiffness are 5.92 kN/mm and 5.66 kN/mm respectively.

In Table 4.4, a comparison is presented among the experimental data from [31], the numerical finite element model (Section 4), and the analytical analysis (Section 3). This comparison highlights the close scattering of the results of the numerical model in the elastic range when compared to the experimental data. The model demonstrates precise levels of scattering of results in both initial beam stiffness and bending stiffness within the elastic range when compared to the experimental data. Furthermore, the analytical bending stiffness is calculated to be  $20.41 \cdot 10^{12}$ , Nmm<sup>2</sup> for the steel-CLT composite beam with 19 $\phi$  screws, and  $24.82 \cdot 10^{12}$ , Nmm<sup>2</sup> for the steel-CLT composite beam with 20 $\phi$  BCGP (Section 2.6.2).

The bending stiffness is calculated from the deflection of the beam at midspan in relation to the force applied under two point loads at one third and two thirds of the length; the initial beam stiffness:

$$EI = \frac{23L^3}{1296} \cdot K_{b,ini} = \frac{23L^3}{1296} \cdot \frac{P}{\Delta} \quad (4.5)$$

**Table 4.4:** Comparison beam behaviour of the numerical model, experimental test data, and analytical results

	$K_{b,ini}$ (kN/mm)		$EI_{ini}$ ( $\cdot 10^{12}$ Nmm <sup>2</sup> )				$P_{SLS}$ (kN)			
	Exp.	Num.	Exp.	Num.	(%)*	Ana.	(%)*	Exp.	Num.	(%)*
Screws	5.92	5.94	22.79	22.69	0.4	20.41	11.7	137.3	138.8	1.1
BCGP	5.66	5.82	22.33	21.70	2.9	24.82	10.0	128.4	120.7	6.3

\* The procentual difference of the analysis with the experimental data from [31]

The assessment of numerical data against experimental measurements demonstrates that the numerical model can achieve a relatively precise level of scatter whilst looking at the global deflection of the beam at 5% (Fig. 4.18 & b) but is even more accurate in the elastic phase. Specifically, when the beam is in the elastic regime, the numerical model achieves a scattering of a high degree of precision, and it can effectively capture the initial stiffness of the beam as shown in Table 4.4.

However, when the composite beam transitions into the partially plastic regime, the performance of the numerical model begins to diverge from the actual behaviour of the beam. Secondly, as the maximum capacity of the timber is reached in either tension or compression, the numerical model cannot capture behaviour past that point due to convergence problems. Thus, as the damage becomes increasingly severe, the numerical model ultimately fails to capture the ultimate load capacity of the beam as seen in Fig. 4.18 where the experimental test until failure has a much higher deflection.

# 5

## Numerical study

This thesis aims to investigate the factors that influence the behaviour of steel-CLT composite beams and how their design can be optimised for maximum structural benefit. To achieve this goal, a parametric study is conducted about geometry-related parameters and design-related parameters. The former investigates the effect of various geometric parameters, such as slab width, span length, spacing under identical circumstances on the structural response. The latter focuses on the influence of the characteristics of a composite connection, and thus the push-out test results, on the beam's behaviour.

This division is necessary because an essential input parameter for the numerical model used in this study is the load-slip data, which is generated through push-out experiments. Both the type of composite connection and the properties of the CLT panels can significantly impact the load-slip results of the push-out test. Therefore, dividing the parametric study into these parts allows for a comprehensive understanding of the behaviour of steel-CLT composite beams.

During push-out tests, the CLT layup, thickness, and properties have a substantial influence on the load-slip behaviour of the composite connection. As a result, isolating a single parameter for investigation in the proposed numerical model is not feasible. By considering both the geometric parameters and the push-out test results, this study aims to capture the complex interactions and provide a more accurate representation of the behaviour of steel-CLT composite beams.

### 5.1. Parametric Study

#### 5.1.1. Configurations

Table 5.1 provides a summary of the steel-CLT composite beam configuration studies conducted in the geometry-related parametric study. The changes in this table focus solely on the effects of parameters related to geometry, such as span length, beam height, and steel beam spacing, while keeping the parameters that influence a push-out test unchanged.

Connection types A and B were performed with identical CLT parameters, allowing for a direct comparison of their impact on the global beam behaviour. The connection type is linked to the CLT parameters, which were obtained from the push-out test experiment and thus remain unchanged. In this part, only geometry-related parameters are varied, while the input parameters related to push-out tests are kept constant for comparability, as previously mentioned. Table 5.2 presents the properties of the composite connections that were subjected to push-out tests under identical circumstances in terms of the CLT properties.

The purpose of this parametric study is to gain insight into how various factors impact the structural performance of the composite beam. By analysing the results of each configuration, it becomes possi-

**Table 5.1:** Configurations of steel-CLT composite beams

No. #	Length (m)	Profile	Steel grade	Slab width (m)	Spacing (s) (mm)	Connection type*
1	6	IPE 300	S275	0.8	300	A
2	3	IPE 300	S275	0.8	300	A
3	12	IPE 300	S275	0.8	300	A
4	6	IPE 300	S275	1.2	300	A
5	6	IPE 300	S275	1.6	300	A
6	6	IPE 300	S275	0.8	400	A
7	6	IPE 300	S275	0.8	500	A
8	6	IPE 200	S275	0.8	300	A
9	6	IPE 400	S275	0.8	300	A
10	6	IPE 300	S275	0.8	300	B
11	6	IPE 300	S275	0.8	400	B
12	6	IPE 300	S275	0.8	500	B

\* The connection type is elaborated upon in Table 5.2.

**Table 5.2:** Properties of the composite connection

No. #	Timber grade	Slab layup & thickness (mm)	Lamella Orient. (°)	Type of connector	Diameter (mm)	Pocket size (mm)	Strength grade
A	C24	(20,20,40,20,20)	[0,90,0,90,0]	Dog screws	19		5.8
B	C24	(20,20,40,20,20)	[0,90,0,90,0]	BCGP	20	80x135	8.8

\* A,B,C push-out test results are tested by [31]

ble to identify the most influential parameters and determine the optimal values that provide maximum structural benefit.

### 5.1.2. Material properties

The steel grade selected for this study is S275, in accordance with European standards. The properties of S275 steel are defined in Table 5.3. The modulus of elasticity (Young's modulus) for structural steel is specified in the design standard EN 1993-1-1 Section 3.2.6[17]. Additionally, based on the same design standard, the Poisson's ratio in the elastic range is determined to be 0.3.

The material model used for steel is elastic-isotropic with plastic hardening, representing a uniaxial behaviour. The corresponding stress-strain relationship, as implemented, is displayed in Fig. 5.1.

**Table 5.3:** Properties of the S275 steel grade

Yield strength ( $f_y$ )	Ultimate strength ( $f_u$ )	Elastic modulus ( $E_s$ )	Poisson's ratio ( $\nu$ )
275 MPa	430 MPa	210,000 MPa	0.3

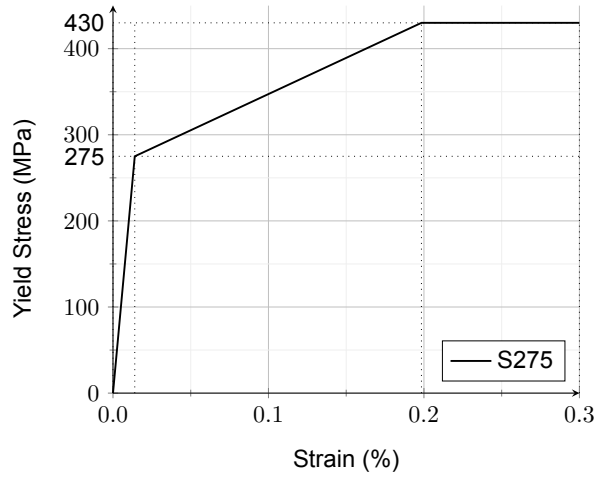


Figure 5.1: Uniaxial stress-strain relationship of S275 as defined by EN1993-1-1 §3.2.6 [17]

## 5.2. Results

### 5.2.1. Overview of beam behaviour

In the results, it is important to consider the reference load levels associated with the data. The numerically simulated four-point bending test involved incrementally loading the beam with a prescribed displacement underneath the concentrated loads, reaching a final displacement of 250 mm. The cutoff of results occurs due to the termination of the finite element analysis. Table 5.4 provides an overview of the load levels referenced in the analysis.

Table 5.4: Load level and Prescribed displacement

Load level		1	2	3	4	5
Prescribed displacement	(mm)	50	100	150	200	250

Fig. 5.2 illustrates the displacement of a simply supported beam with two concentrated loads, showing the load levels beneath the loading points and their corresponding displacements.

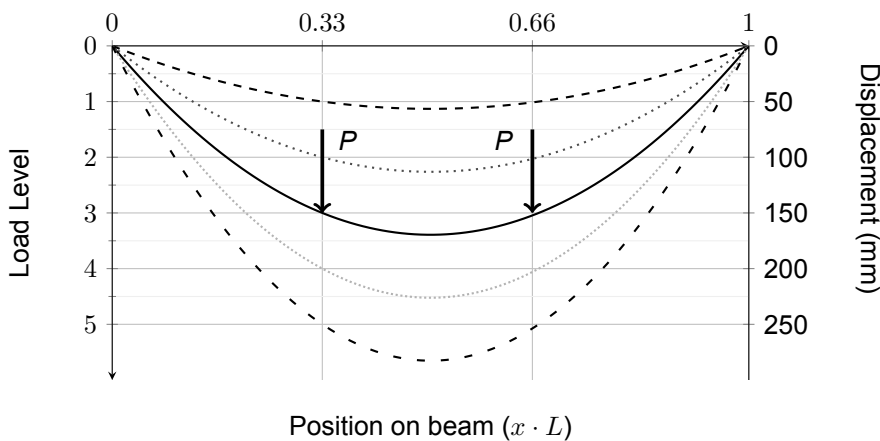
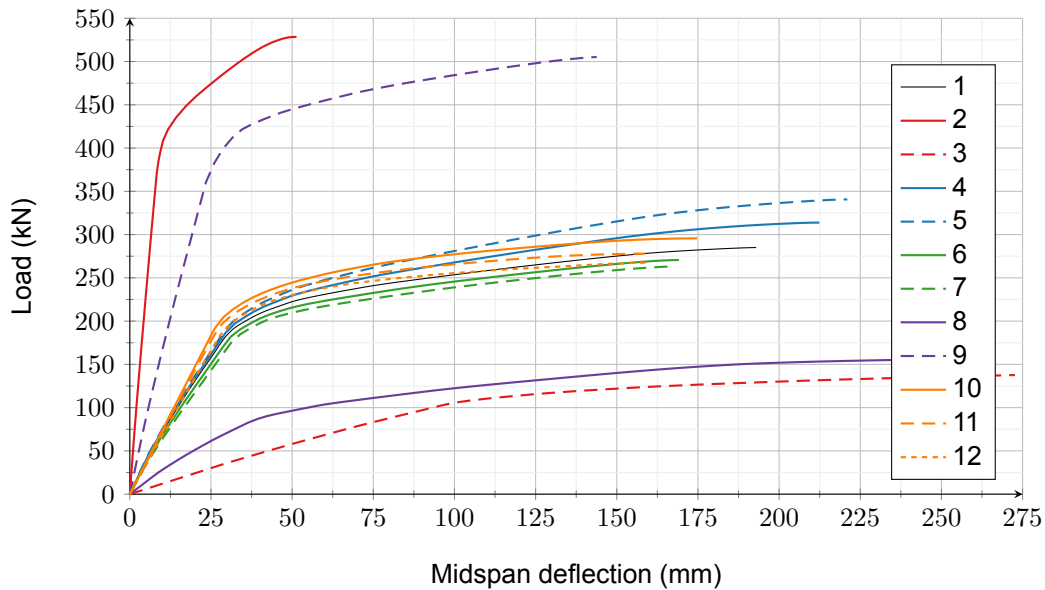


Figure 5.2: Deflection of simply supported beam at different load levels in four-point flexural bending test numerically tested (I.E. force ( $P$ ) and deflection (solid black line) at load level 3 in the figure)

Fig. 5.3 presents an overview of the behaviour of the steel-CLT composite beam configurations analysed numerically, as mentioned in Table 5.1.



**Figure 5.3:** Load-Midspan deflection of all configuration specified in Table 5.1 with parametric changes in length(red), slab width(blue), spacing(green), profile(purple) and connection type(orange)

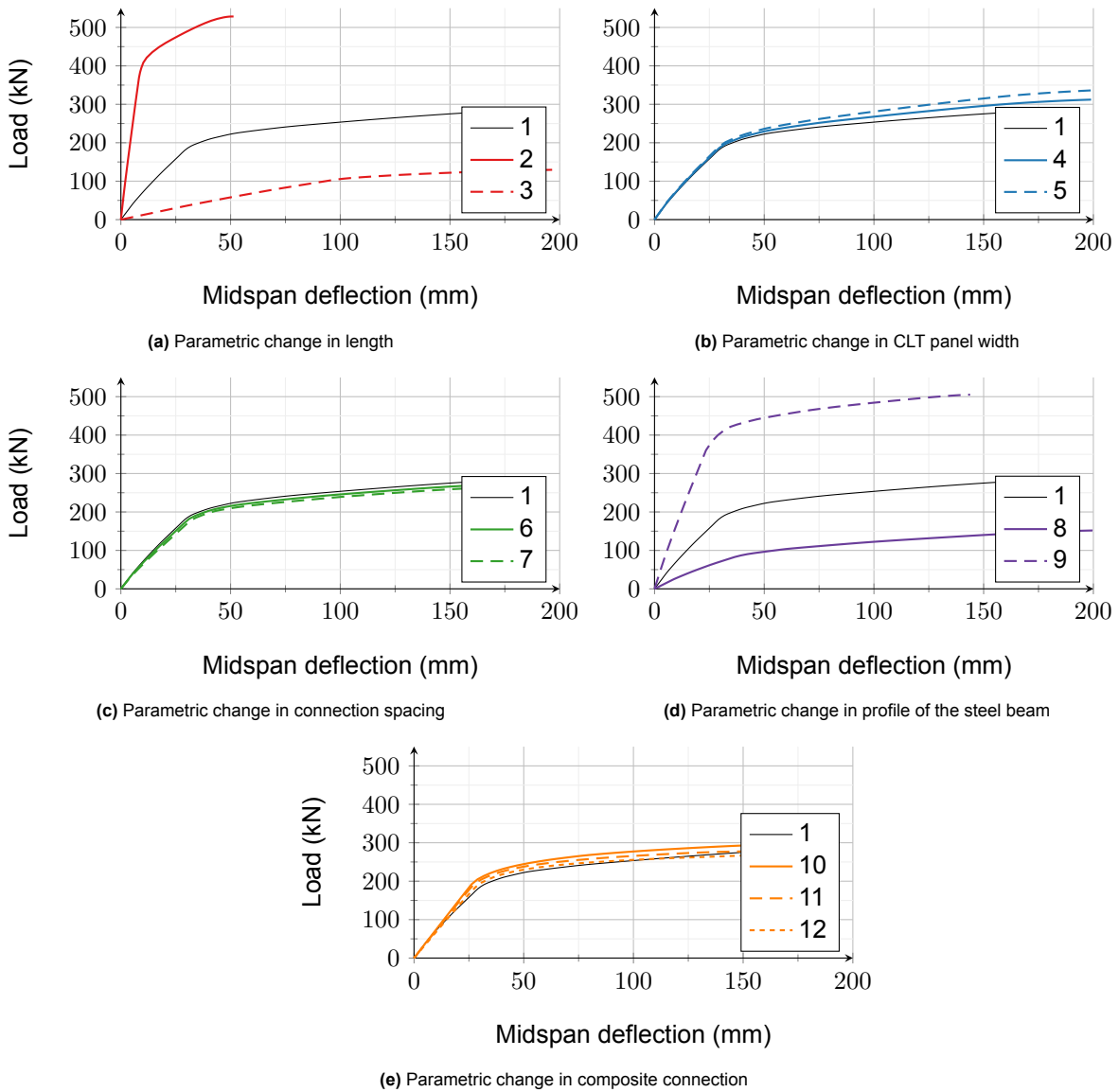
Due to the parameter changes in beam length (Numerical models No. 2 & 3) and the parameter changes in profile (Numerical models No. 8 & 9) the results vary significantly. A varying parameter can be identified by colour as clarified in Table 5.1 and specifically displayed in Fig. 5.4:

- **Length** - Red
- **CLT panel width** - Blue
- **Spacing of composite connection A** - Green
- **Profile of the steel beam** - Purple
- **Spacing of composite connection B** - Orange

The presented figure(Fig. 5.3) showcases the initial benchmark configuration (Configuration 1), which serves as the foundation for all subsequent variants. The plot illustrates the elastic behaviour of the system, exhibiting linear response until reaching an approximate displacement of 30 mm. At this point, a cumulative load of 175 kN is applied to the steel-CLT composite beam.

In Fig. 5.4a, the load-midspan deflection of Configurations 2 and 3 is presented in red. These configurations differ from configuration 1 in terms of their length, with configuration 2 having a length of 3 meters and configuration 3 being 12 meters long. Configuration 2 exhibits a 6.7 times higher initial stiffness, a load increase at SLS of 178%, and minimal displacement, which can be attributed to the change in length. Conversely, configuration 3, being twice the length of configuration 1, demonstrates contrasting characteristics for the same reason, including decrease in initial stiffness of 85%, a decreased force at SLS of 69%, and larger displacements.

In Fig. 5.4d, the purple variants, Configuration 8 and 9, represent the outcomes of a parametric change in the steel beam profile. The initial configuration utilises an IPE300 profile, while Configuration 8 and 9 employ an IPE200 and IPE400 profile, respectively. The response of the steel-CLT composite beam varies significantly when the steel profile is altered, as a larger profile substantially increases the beam's resistance at SLS, as evident in the results with an increase of 137%. To account for the diverse range of results attributed to the length and profile parameters, a detailed perspective



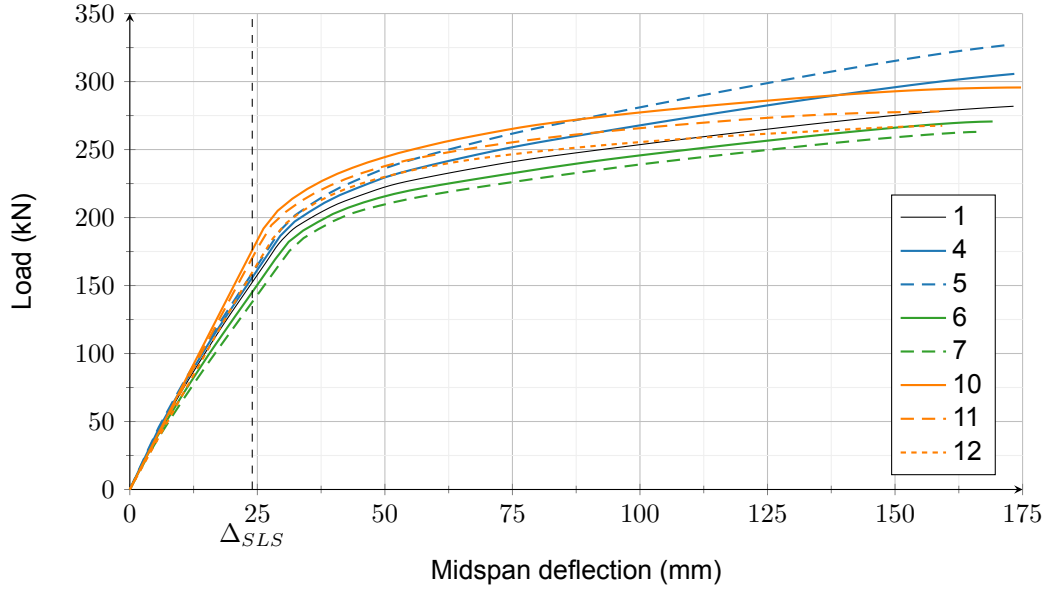
**Figure 5.4:** Load-Midspan deflection of all configuration specified in Table 5.1 with parametric changes

is provided in Fig. 5.4.

Fig. 5.4b, Fig. 5.4c and Fig. 5.4e illustrates the observed behaviour resulting from parametric variations in slab width, spacing, and composite connection. The latter, the use of a stiffer composite connection, achieved through the utilisation of bolted connectors in grouted pockets, is associated with improved initial stiffness, as indicated by the steeper slope of the three orange lines (configurations 10, 11 & 12). These three configurations have a differing spacing of the connection from 300mm to 500mm. The further the connections are spaced apart the less composite action is achieved and the less load the configuration resists. This depicted by the load resisted at serviceability limit state which decreases by 7% and 11.5% as the spacing increases from 300mm to 400 and 500mm.

All configurations shown in Fig. 5.5 have the same length of 6 meters the allowed deflection in serviceability limit state ( $\Delta_{SLS}$ ) is 24 mm. The vertical line at this displacement shows the relative ability of the steel-CLT composite beam to perform in serviceability.





**Figure 5.5:** Load-Midspan deflection of all configuration specified in Table 5.1 with parametric changes in slab width (blue), spacing (green) and connection type (orange)

An increase in slab width, as observed in configurations 4 and 5 (shown in blue), leads to an 8.2% increase in initial stiffness as CLT panel width is doubled. Secondly, the load resisted at serviceability also increases by 5.6%. This can be attributed to the increased capacity of the top flange in compression, resulting in enhanced resistance to bending.

**Table 5.5:** Overview of configurations' beam behaviour

Conf.	Analytical	Difference	Numerical			$\Delta_{SLS}$	Load level	
	$EI_a$ ( $\times 10^{12}$ , Nmm <sup>2</sup> )	$\Delta_{EI}$ %	$EI_n$ ( $\times 10^{12}$ , Nmm <sup>2</sup> )	$K_{b,ini}$ (kN/mm)	$k$ (N/mm <sup>2</sup> )	$P_{SLS}$ (kN)	$P_1$ (kN)	$P_2$ (kN)
1	25.73	10.9%	28.98	7.56	25.20	151.9	227.6	260.8
2	20.87	13.7%	24.29	50.70	169.00	421.6	528.5	-
3	32.05	8.6%	37.11	1.21	4.03	46.9	64.9	111.6
4	27.08	11.8%	30.44	7.94	26.47	156.7	235.8	277
5	28.13	9.2%	31.36	8.18	27.27	160.4	243.4	292
6	24.47	14.5%	28.18	7.35	18.38	141.7	219.9	252.2
7	23.56	12.4%	26.72	6.97	13.94	135.3	213.8	245.6
8	8.91	22.4%	10.96	2.86	9.53	62.2	101.7	128.4
9	60.82	12.9%	68.62	17.90	59.67	360.6	447.8	491.6
10	31.20	14.1%	28.37	7.40	24.67	173.3	250.2	282.8
11	29.81	8.7%	27.52	7.18	17.95	161.7	241.9	270.1
12	28.69	9.8%	25.95	6.77	13.54	153.4	233.7	259.1

Note: SLS = Serviceability Limit State with midspan deflection at  $\Delta = \frac{L}{250}$ . Load levels clarified in Fig. 5.2

Lastly, in green (configurations 6 and 7) displays steel-CLT composite beam behaviour change due to a change in spacing with the same connection as configuration 1. Similarly to the behaviour under change of spacing as configurations 10, 11 and 12 an increased spacing does lead to less resistance. With this composite connection the increase in spacing from 300mm to 400 and 500mm leads to a decrease in load resisted at serviceability limit state of 6.7% and 11%, respectively.

A tabulated interpretation of Fig. 5.3 is presented in Table 5.5. In this table, the analytical bending

stiffness ( $EI_a$ ) (Section 3) is compared to the numerical bending stiffness ( $EI_n$ ) (Section 4.6) for each configuration. It can be observed that the analytical initial bending stiffness is of the same order of magnitude as the numerical estimation of the bending stiffness. However, as mentioned in Section 4.6, the analytical estimation underestimates the bending stiffness when the connection type A (screws) is used, while it overestimates the bending stiffness when connection type B (bolted connectors in grouted pockets) is employed. Table 5.5 also depicts the percentile variation when comparing the analytical determination of the bending stiffness against the numerical bending stiffness. The average variation between the numerical estimation and analytical bending stiffness is 12.42 %.

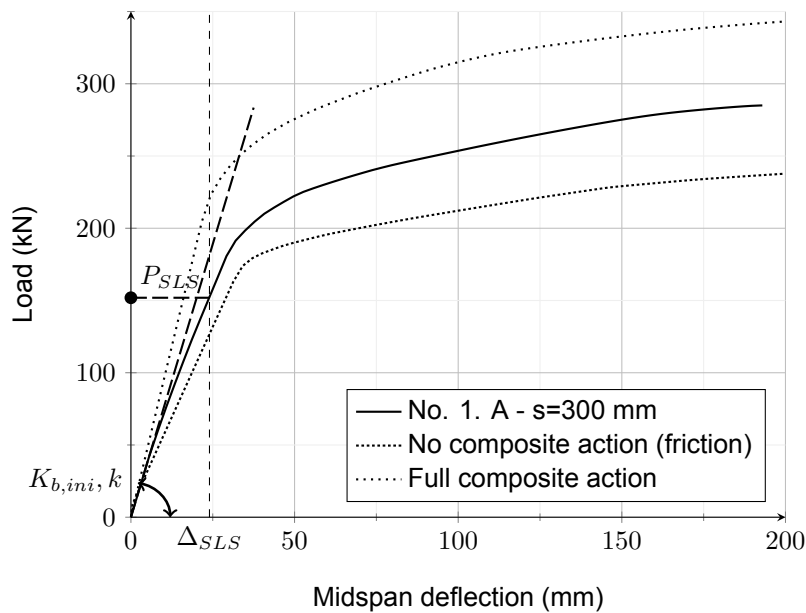
$$K_{b,ini} = \frac{P_{ini}}{\Delta_{ini}} \quad (5.1)$$

$$k = \frac{K_{b,ini}}{s} \quad (5.2)$$

where

$P_{ini}$  &  $\Delta_{ini}$  are the initial force and corresponding displacement  
 $s$  is the spacing of the composite connection

Secondly, in Table 5.5 the initial beam stiffness ( $K_{b,ini}$ ) and the stiffness per unit length ( $k$ ) of each steel-CLT beam is displayed. Both values are extracted from the numerical analysis. The initial beam stiffness is derived from the load-midspan displacement graph and is the slope of the initial deflection as depicted in Fig. 5.6 whilst the stiffness per unit length divides that quantity by the spacing of the composite connections.



**Figure 5.6:** Load-midspan deflection of configuration 1 with force at serviceability limit state ( $P_{SLS}$ ) and angle of initial beam stiffness ( $K_{b,ini}$ ) and stiffness per unit length ( $k$ )

Fig. 5.6 is a visual representation of a single load-deflection curve at midspan of configuration 1. The initial beam stiffness ( $K_{b,ini}$ ) and the stiffness per unit length ( $k$ ) of each steel-CLT beam are displayed as an angle whilst the force resisted at serviceability limit state ( $P_{SLS}$ ) is marked on the y-axis. The force at the point of yielding ( $P_y$ ) is unable to be accurately predicted as it is often approached with

angle( $K_{b,ini}$ ) and the ultimate load capacity ( $P_u$ ). The ultimate load capacity is not determinable with the proposed numerical model and thus the yield force ( $P_y$ ) can only be visually estimated.

As the displacement increases beyond the elastic resistance of the steel-CLT composite beam, the additional load resisted by the beam decreases. Fig. 5.7 illustrates the cumulative force resisted at each load level by each configuration.

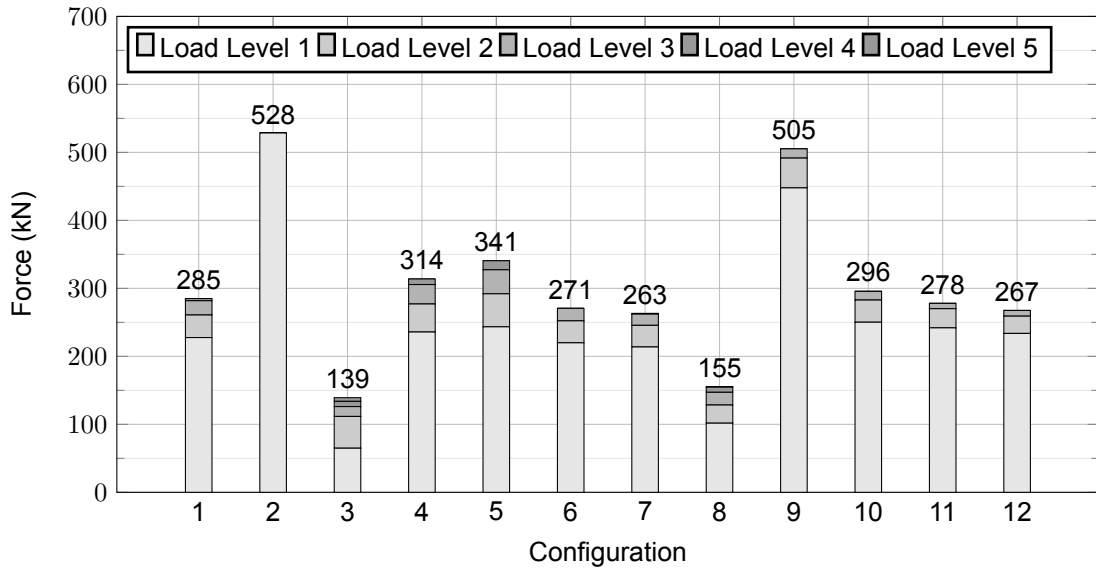
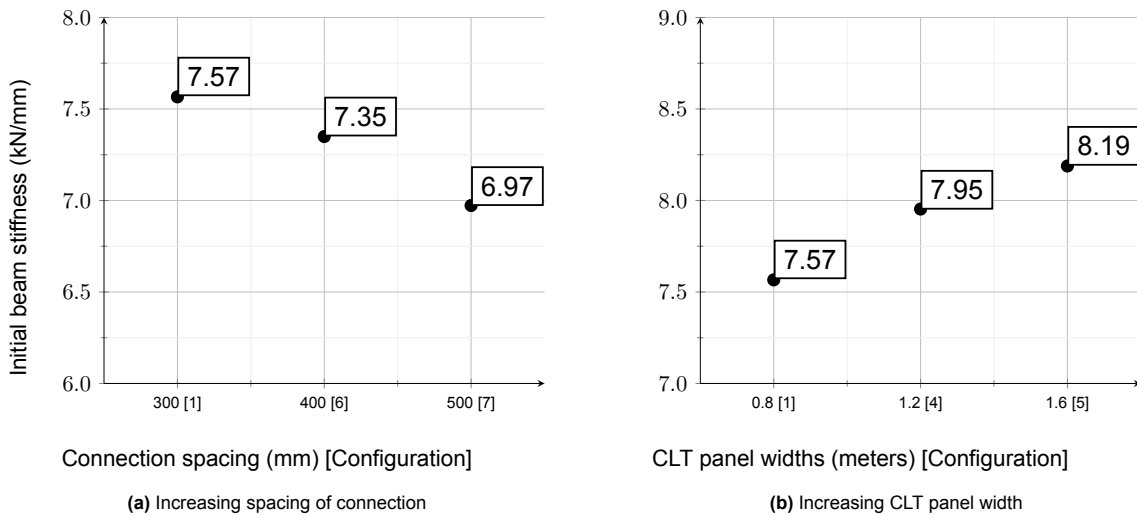


Figure 5.7: Cumulative maximum force at given displacement (load level) for the tested configurations

### 5.2.2. Initial beam stiffness

The initial stiffness of the beam, as validated in Section 4.6, provides the most accurate result from the numerical model. Table 5.7 offers a comprehensive perspective of the beams and their load-displacement behaviour in relation to their initial beam stiffness.

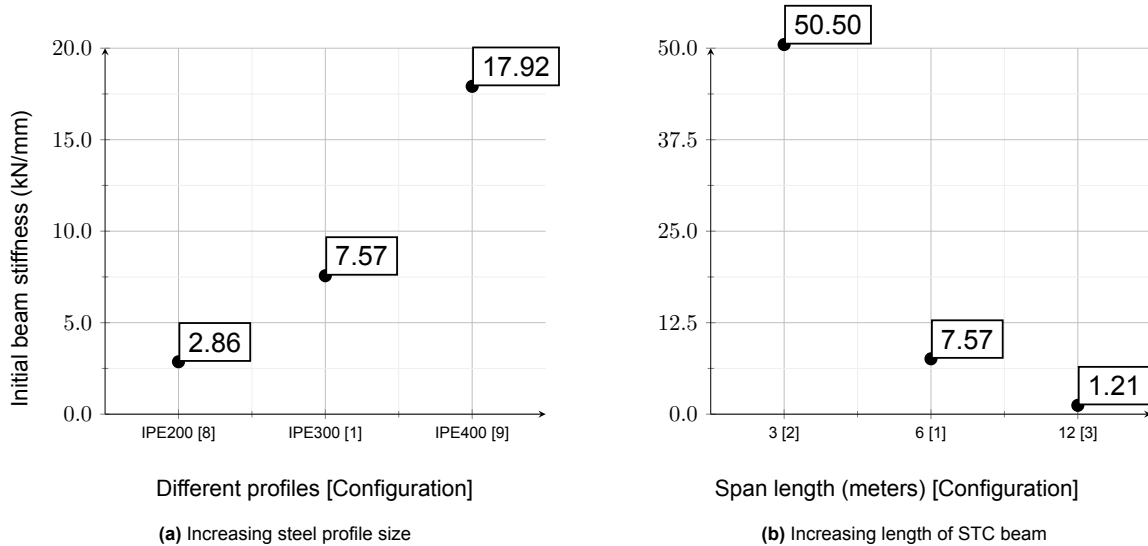


(a) Increasing spacing of connection

(b) Increasing CLT panel width

Figure 5.8: Initial beam stiffness of different configurations in numerical four-point bending test

The following figures depict the parametric changes and the corresponding changes in initial stiffness. Fig. 5.8 illustrates the different configurations with connector spacing of type 'A' (left) and the different configurations with different CLT panel widths (right). It can be observed that a closer connector spacing leads to a higher initial stiffness, while a wider panel also results in a higher initial stiffness of the steel-CLT beam.



**Figure 5.9:** Initial beam stiffness of different configurations in numerical four-point bending test

Fig. 5.9 illustrates the change in initial beam stiffness with different profiles (left) and different beam spans (right). These parameters have a significant influence on the initial beam stiffness.

### 5.2.3. Slip

Section 2.1 clarified that the behaviour and performance of a composite beam depend on the composite connection's ability to resist slip. In addition to friction, this resistance is influenced by the elastic behaviour of the composite connection and the spacing of the connections (S).

Fig. 5.10 displays the slip over the longitudinal length of the steel-CLT composite beam configuration 2, which has a length (L) of 3 meters. Each marker represents a composite connection of type A (Table 5.2) in configuration 3. The y-axis represents the slip of each connection, showing its movement along the longitudinal axis relative to its starting position when no slip occurs. The x-axis indicates the position on the beam in the longitudinal direction.

Figures 5.11a to 5.11d display the slip of configurations 1, 6, 7, and 10. Configurations 6 and 7 differ from configuration 1 by having increased spacing of 400 mm and 500 mm, respectively. Configuration 10 has the same spacing as configuration 1 but utilises connection type B instead of A (Table 5.2). This connection is much stiffer in its load-displacement behaviour and employs bolted connectors in grouted pockets (BCGP) (Section 2.6.2) instead of regular screws used in configuration 1.

Fig. 5.11a, Fig. 5.11b, Fig. 5.11c, and Fig. 5.11d clearly demonstrate the difference in absolute slip among different configurations. It can be observed that configurations with fewer composite connections exhibit higher levels of slip, with maximum slip values of 3.07 mm, 4.43 mm, and 5.29 mm for configurations 1, 6, and 7, respectively.

Another notable observation is the impact of a stiffer connection on slip behaviour. Configuration 10 (Fig. 5.11d), which utilises a more rigid connection type B, reaches a maximum slip of 1.60 mm. This

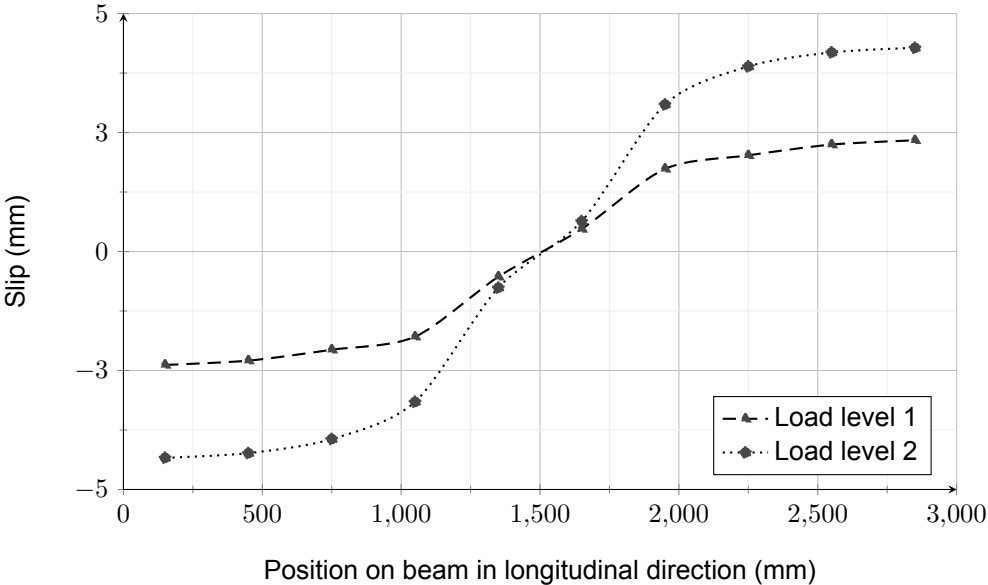


Figure 5.10: Configuration 2: The slip at material interface over the length of the beam

highlights the influence of the number of connections and the elastic stiffness of the connection on slip resistance. As discussed in Section 2.1, slip resistance is closely linked to increased beam capacity and stiffness. This parametric influence is also evident in Fig. 5.3, where configuration 10 exhibits the highest initial beam stiffness and load capacity compared to configurations 1, 6, and 7.

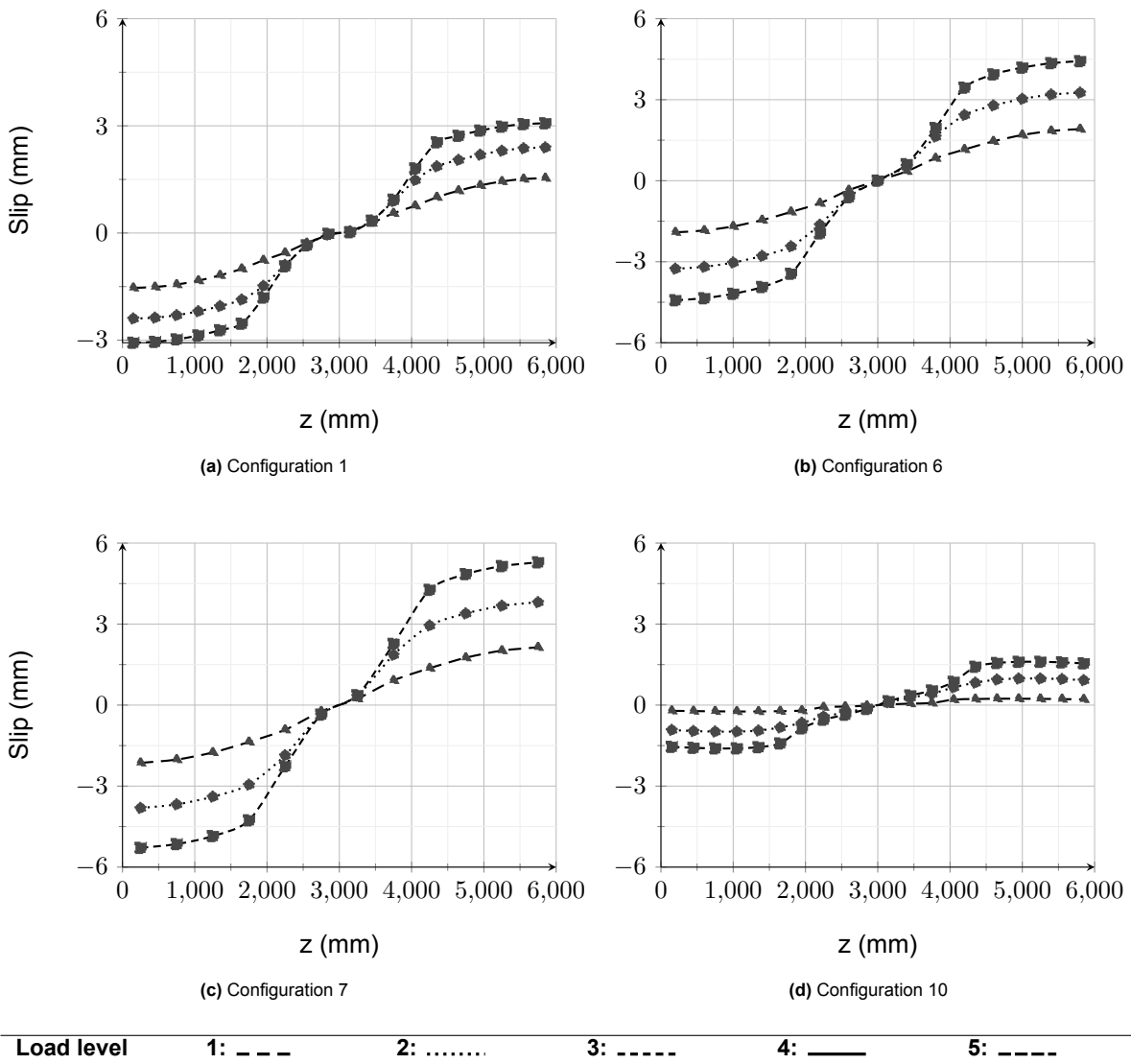
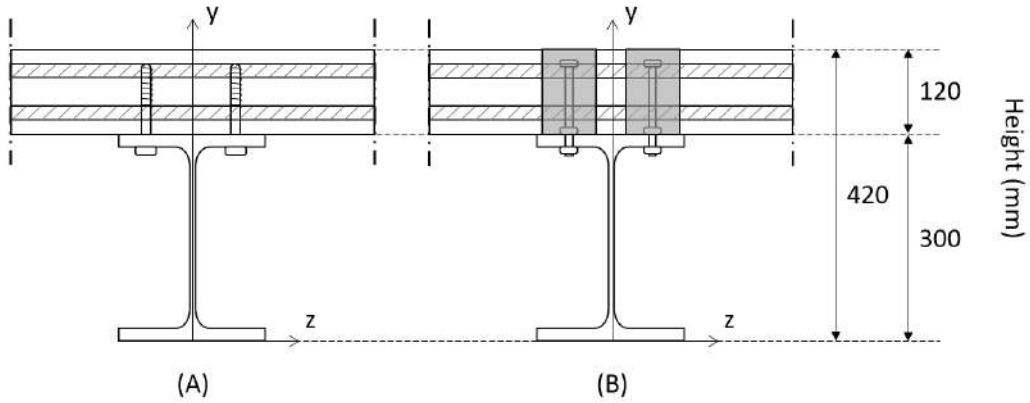


Figure 5.11: The slip at the material interface over the length of beam configurations

### 5.2.4. Stress over cross-section height at midspan

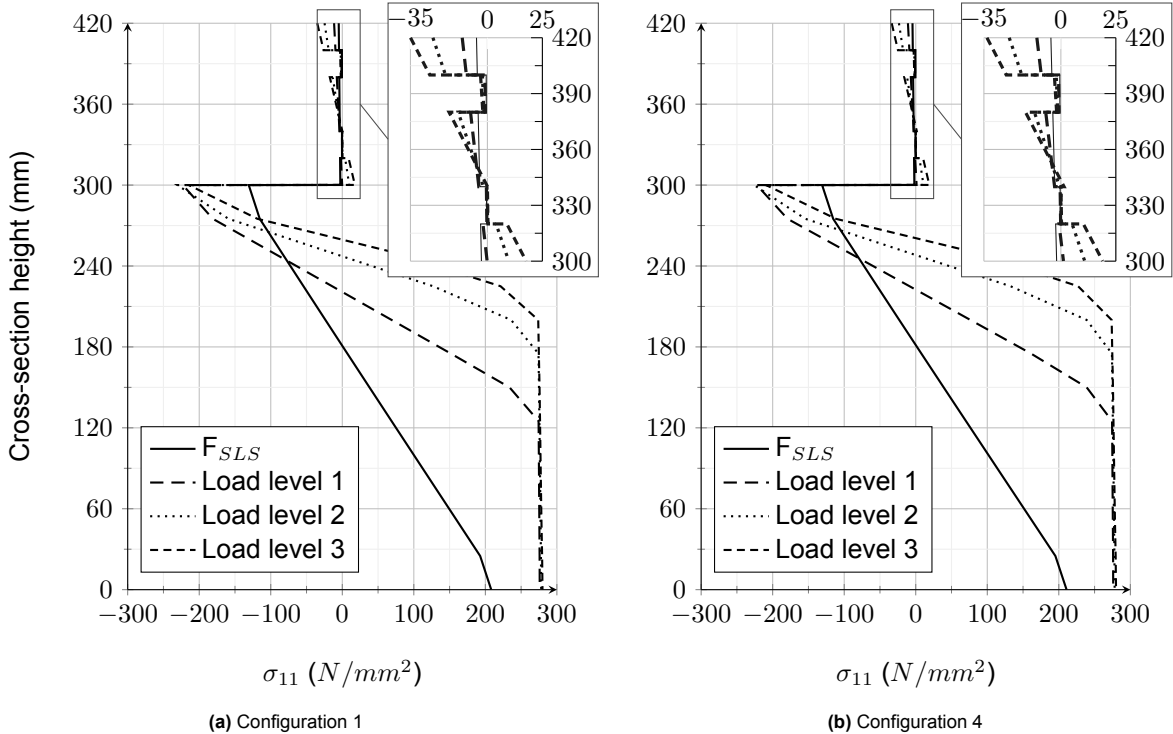
This section examines the development of longitudinal stress in the cross-section as the load increases along the cross-sectional height at midspan, specifically at the axis of transversal symmetry. The stress state at the serviceability limit state is initially presented for each configuration, followed by the stress levels at load levels 1, 2, and 3.

Figure 5.12 provides a schematic view of the cross-sections analysed in the parametric study, along with their corresponding reference heights. In Figure 5.12(a), the cross-sections of configurations 1 to 9 are depicted, while Figure 5.12(b) shows the cross-sections of configurations 10, 11, and 12. The width dimensions of the panel vary depending on the configuration (as explained in Table 2.1), and the specific details of the composite connections and CLT panel can be found in Table 5.2.



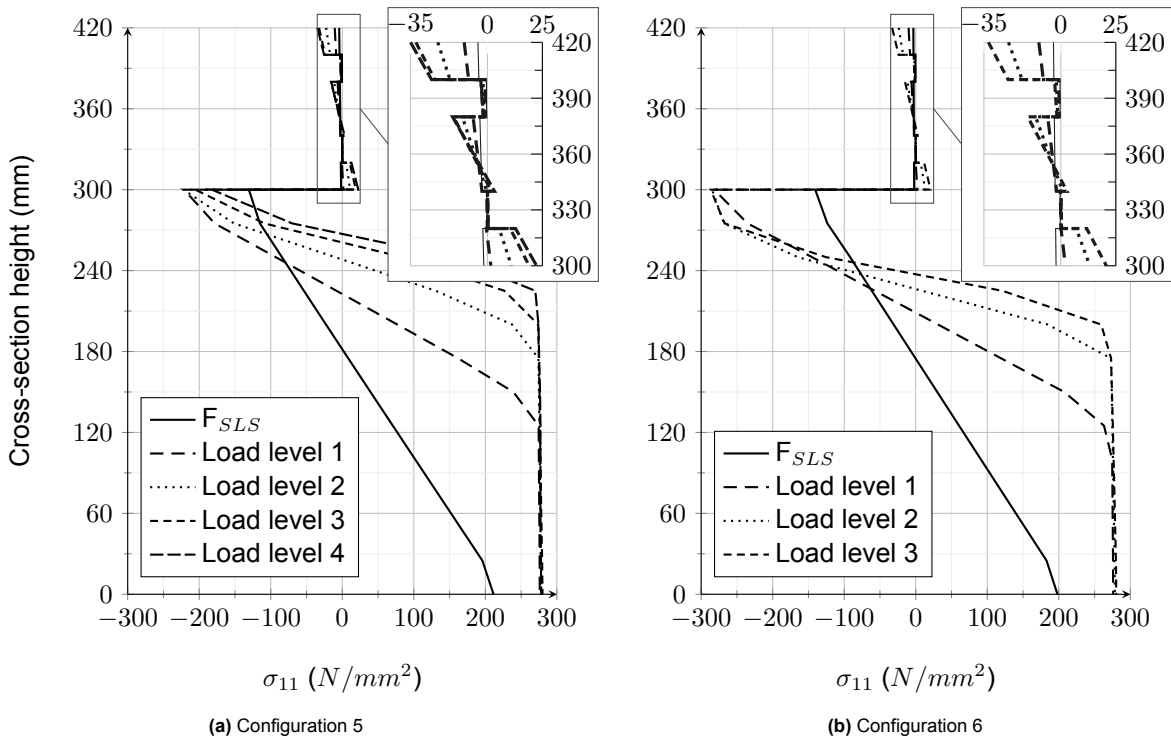
**Figure 5.12:** Side perspective of steel-CLT composite beam cross section of the numerical study with the connections: (a) dog screws and (b) BCGP (Further specified in Table 5.2)

Fig. 5.13, 5.14, 5.15 and 5.16 depict the development of stress over the height of their respective steel-CLT beam cross-section under changing load at the intersection of two axes of symmetry; at midspan. The figures also highlight the stress in the CLT panel with a zoomed-in perspective of the top 120 mm of the cross-section as depicted at the top right. In Fig. 5.13a the stress of configuration 1 is depicted. At serviceability limit state the stress in the steel profile is depicted at bottom and top flange of 208 and  $-131 \text{ N/mm}^2$ , respectively. As load increases the yield strength of the steel is already reached at Load level 1 (as explained in Figure 4.16) until about 125 mm in cross-sectional height. Furthermore, the maximum stress level in the top flange does not exceed  $-231 \text{ N/mm}^2$ . Lastly, the stress at the bottom of the CLT panel is in tension up to  $17.6 \text{ N/mm}^2$  at Load level 3 as not enough composite action is achieved for it to be fully in compression.



**Figure 5.13:** Longitudinal stress ( $\sigma_{11}$ ) distribution at midspan over longitudinal axis of symmetry over the height of the cross-section

Fig 5.13b visualises the stress development over the cross-section at midspan for configuration 4. At the serviceability limit state, the figure indicates stresses in the steel profile at the bottom and top flanges of 211 and 131  $N/mm^2$ , respectively. As the load increases, the yield strength of the steel is already reached at Load level 1 until approximately 125 mm in cross-sectional height. Additionally, the maximum stress level in the top flange does not exceed -226  $N/mm^2$ . Moreover, the stress at the bottom of the CLT panel experiences tension up to 19  $N/mm^2$  at Load level 3, indicating that sufficient composite action is not achieved for it to be fully in compression. Overall, the stresses appear relatively comparable to configuration 1, despite the increase in slab width from 800 mm to 1200 mm.



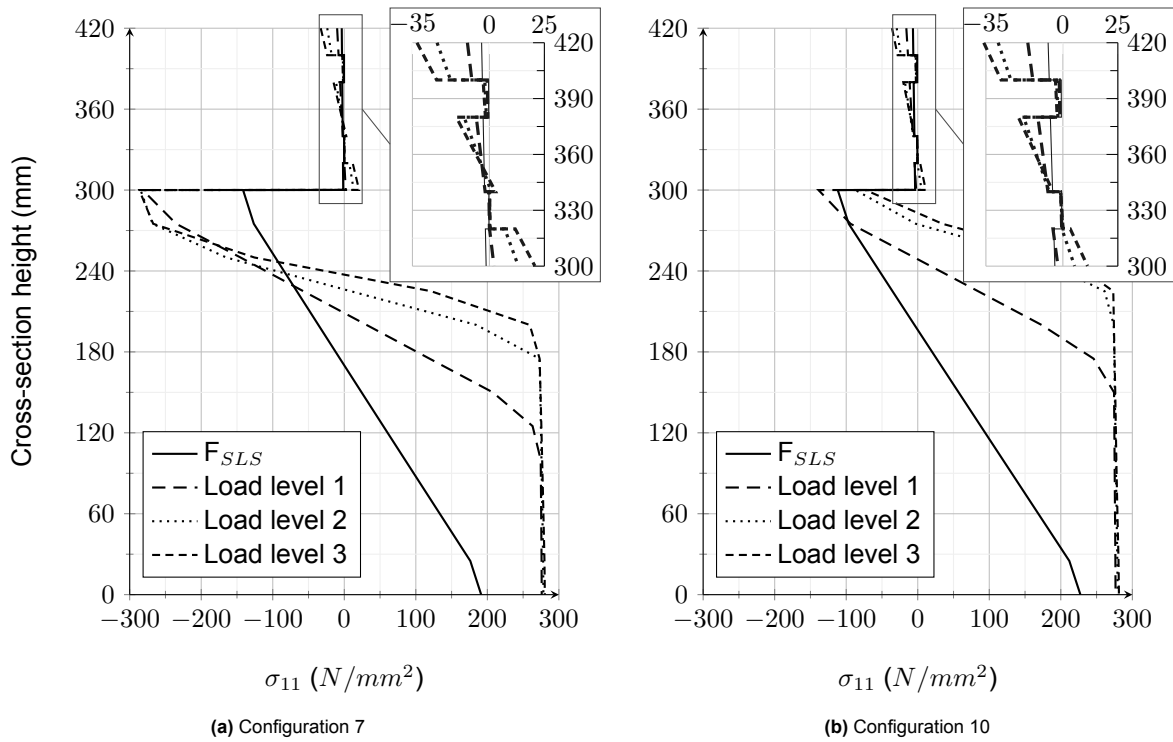
**Figure 5.14:** Longitudinal stress( $\sigma_{11}$ ) distribution at midspan over longitudinal axis of symmetry over the height of the cross-section

In Fig. 5.14a the stress distribution of configuration 5, which differs from the benchmark configuration with double the slab width, is depicted. When compared to configuration 1 and 4 little has changed as the figure indicates stresses in the steel profile at the bottom and top flanges of 211 and -131  $N/mm^2$ .

When pivoting to Fig. 5.14b a difference is noticeable. Configuration 6 has, compared to configuration 1 ( $s = 300$  mm), an increase in connector spacing ( $s = 400$  mm). This should in theory, decrease the amount of composite action. In Fig. 5.14b, at serviceability limit state, the stress in the steel profile is depicted at bottom and top flange of 191 and -141  $N/mm^2$ , respectively. As load increases the yield strength of the steel is exceeded at Load level 1 until about 100 mm in cross-sectional height. Furthermore, the maximum stress level in the top flange does not exceed -287  $N/mm^2$ . Which is significantly higher than previously seen. A more significant difference between stresses at material interface would indicate less composite action. Lastly, the stress at the bottom of the CLT panel is also greater, with tension up to 21  $N/mm^2$  at Load level 3.

Fig. 5.15a provides additional insights to the aforementioned perspective, as the spacing is further reduced to  $s = 500$  mm. At the serviceability limit state (SLS), the stress in the bottom flange is 191  $N/mm^2$  in tension, while the top flange of the steel beam experiences compression with a stress of -141  $N/mm^2$ .

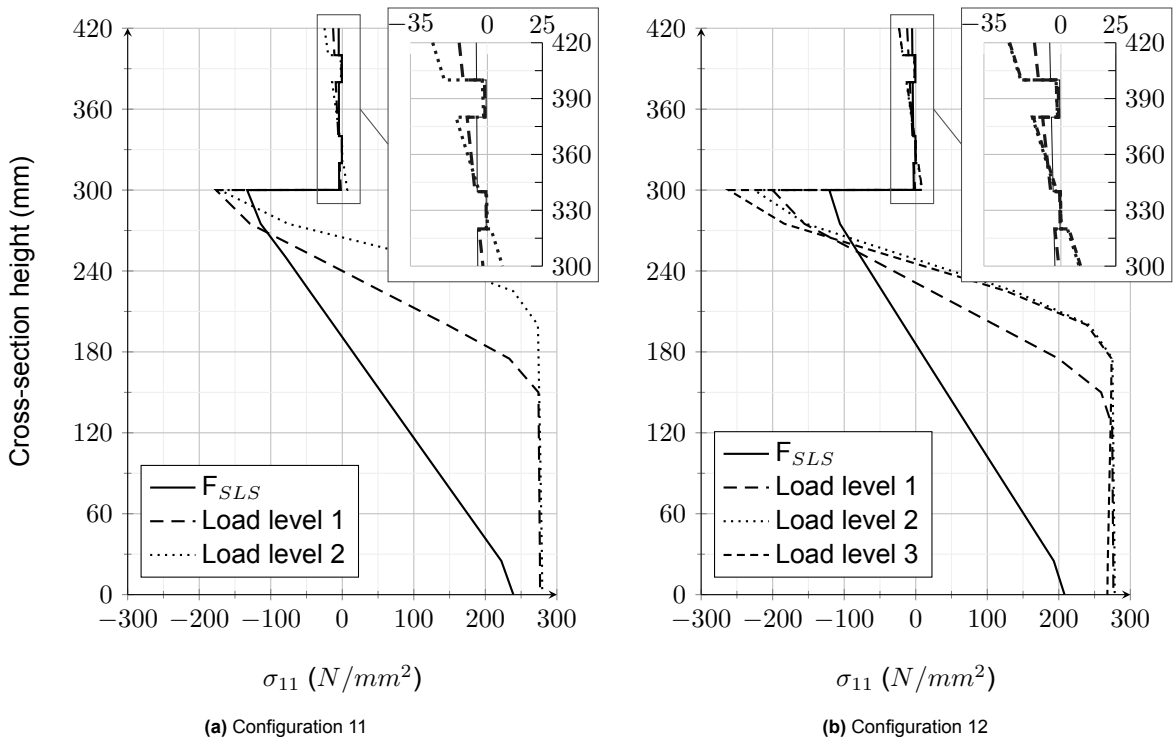




**Figure 5.15:** Longitudinal stress( $\sigma_{11}$ ) distribution at midspan over longitudinal axis of symmetry over the height of the cross-section

In contrast, Fig. 5.15b illustrates the stress distribution across the cross-section of configuration 10, which features a different and stiffer composite connection. At SLS, the stress values in the top and bottom flanges differ from the previously shown results. The stress in the bottom flange is  $227 \text{ N/mm}^2$  in tension, while the top flange of the steel beam is under compression with a stress of  $-111 \text{ N/mm}^2$ . More composite action is evident, as the difference in stress at the material interface is significantly reduced, with a maximum stress of  $-138 \text{ N/mm}^2$  in the top flange of the steel beam. The web of the steel beam reaches plasticity earlier, with the cross-section experiencing a stress of  $275 \text{ N/mm}^2$  at Load level 1, extending up to a height of 150 mm. Figures 5.13a, 5.13b, 5.14a, 5.14b, and 5.15a all depict the CLT panel being fully in compression at the serviceability limit state. on the contrary, configuration 10, represented by Fig. 5.15b, the CLT is shown to be completely in compression even at Load level 1.

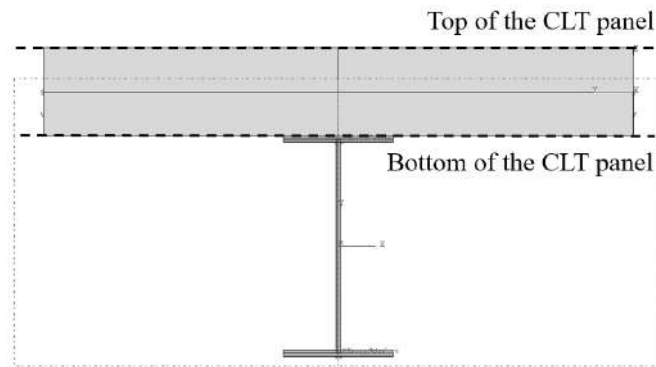
Lastly, in 5.16 the stress over cross-sectional height of configuration 11 and 12 is shown, which differ from configuration 10 by a similarly increasing spacing as seen in configuration 1,6 and 7. Thus, the composite action decreases which is seen by the stress development at the material interface as the maximum stress of configuration 11, in Fig. 5.16a, is  $-177 \text{ N/mm}^2$  and the maximum stress of configuration 12, in Fig. 5.16b, is  $-261 \text{ N/mm}^2$ .



**Figure 5.16:** Longitudinal stress( $\sigma_{11}$ ) distribution at midspan over longitudinal axis of symmetry over the height of the cross-section

### 5.2.5. Stress over width of CLT panel

The stress distribution in the CLT panel is of interest in understanding the load development within the composite beam. Figure 5.17 provides an example of the cross-section of a steel-CLT composite beam used in the numerical analysis. It shows the top and bottom layers of the CLT panel, which are subjected to stress during loading. By analysing the stress distribution in the CLT panel, valuable insights can be gained into the behaviour and performance of the composite beam.



**Figure 5.17:** Example of cross-section of steel-CLT composite beam used in numerical analysis

Configurations 1, 4, and 5 have one varying parameter: CLT panel width. In the following 6 figures (Fig. 5.18 - Fig. 5.25), the longitudinal stress development over increasing prescribed displacement is shown for both the top and bottom of the CLT panel at midspan.

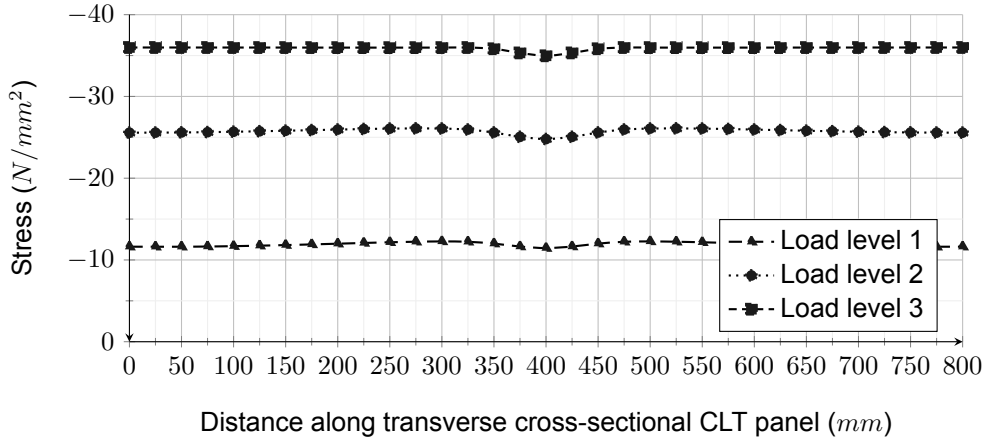


Figure 5.18: Stress development in compression at midspan at the top of the CLT panel of configuration 1

In Fig. 5.18, the development of the compressive stress in the top of the CLT panel at midspan in configuration 1 is displayed. Configuration 1 differs from configurations 4 and 5 due to its width of the CLT slab, which is 800 mm. In progressive development, the compressive stress increases until it approaches the longitudinal compressive strength ( $\sigma_{c1}$ ) of 36 MPa. Secondly, there is a noticeable local change in stress near the center where stress is transferred to the steel beam (Section 2.4).

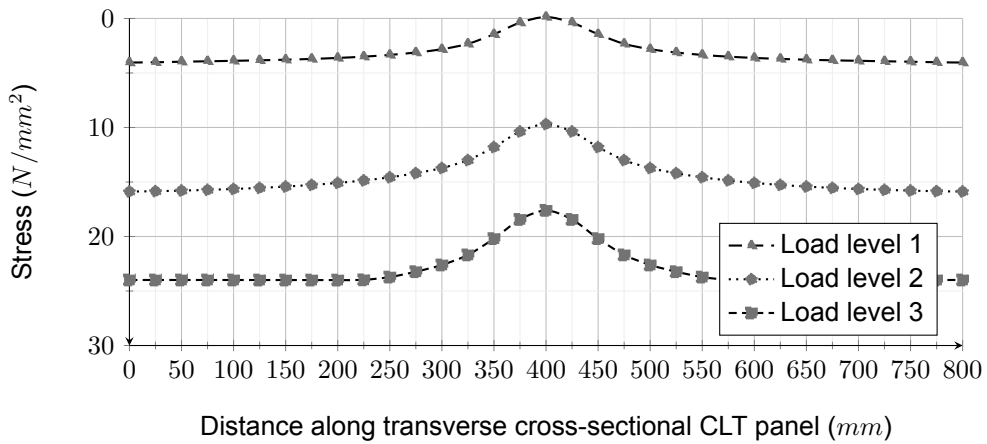
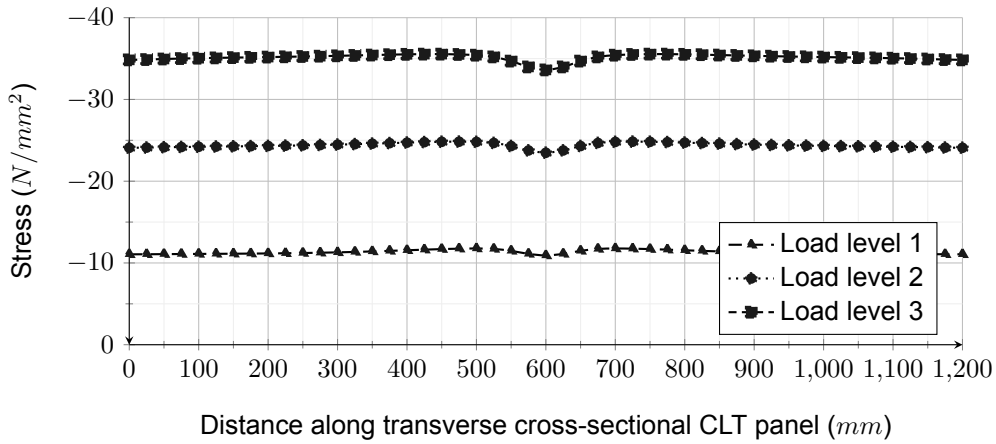


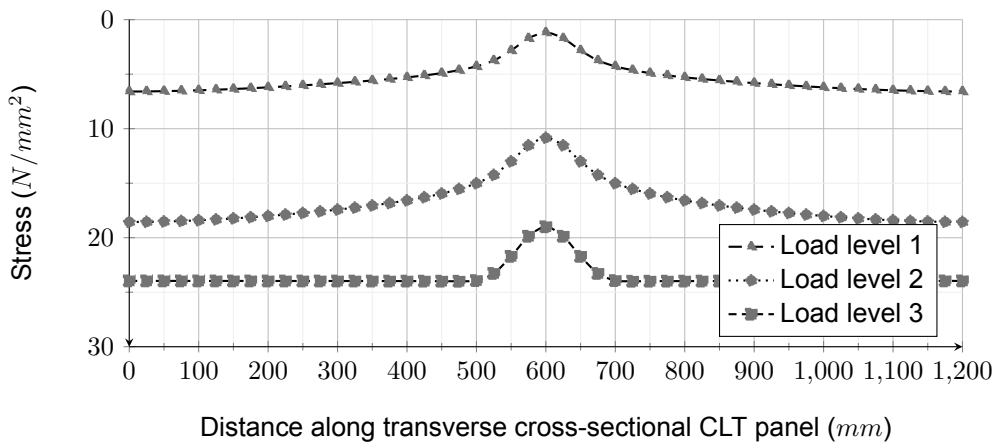
Figure 5.19: Stress development in tension at midspan at the bottom of the CLT panel of configuration 1

Fig. 5.19 displays the progressive loading and response of the bottom of the CLT panel at midspan of configuration 1. Noticeable, in comparison to the top part of the CLT panel, is the significant change in stress near the center, at the position of the steel beam. Secondly, visualised is the width of the deviation in stress decrease as more load is applied; and more capacity is utilised of the CLT panel. As load is incrementally increased the maximum longitudinal tensile strength ( $\sigma_{t1}$ ) of 24 MPa is reached near the boundaries of the panel.



**Figure 5.20:** Stress development in compression at midspan at the top of the CLT panel of configuration 4

With an increased width of the CLT panel(1200 mm) in configuration 4 this configuration also has more load bearing resistance as initially displayed in Fig. 5.3. There is little difference in comparison to the top of the CLT panel of configuration 1(5.18).



**Figure 5.21:** Stress development in tension at midspan at the bottom of the CLT panel of configuration 4

In Fig. 5.21 it shows that the local stress transfer to the steel beam still has the same absolute width. The local stress transfer is not impacted by the increase in CLT panel width when compared to Fig. 5.19. What is noticeable is the significant increase in CLT panel utilisation as load increases. At load level 3 most of the CLT panel at the bottom is under stress at its maximum longitudinal tensile strength ( $\sigma_{t1}$ ) of 24 MPa.

In configuration 5 the panel width is increased to 1600mm in width. With increased capacity of steel-CLT composite beam (Fig. 5.3) the top flange also has increasing levels of stress until it approaches the longitudinal compressive strength ( $\sigma_{c1}$ ) of 36 MPa.

Fig. 5.25 shows the development of stress is the bottom of the CLT panel in configuration 5. When comparing this figure with the stress development in the bottom of configuration 1 and 4 some things are noticeable. Firstly, the local change in stress as a result of the bottom flange connecting to the steel is much more pronounced at load level 1 with a wider CLT panel. Secondly, what is consistent over all the figures regarding the bottom of the CLT panel is that stress is distributed more evenly once more load is applied and more capacity is utilised.

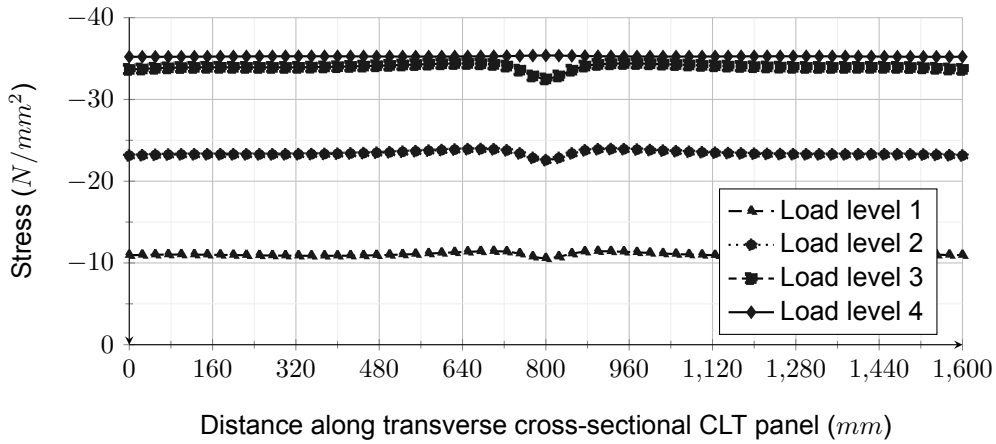


Figure 5.22: Stress development in compression at midspan at the top of the CLT panel of configuration 5

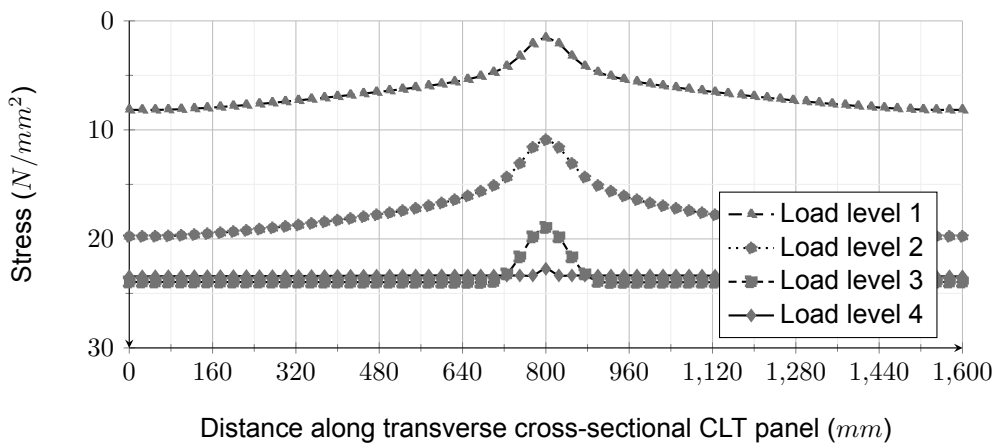


Figure 5.23: Stress development in tension at midspan at the bottom of the CLT panel of configuration 5

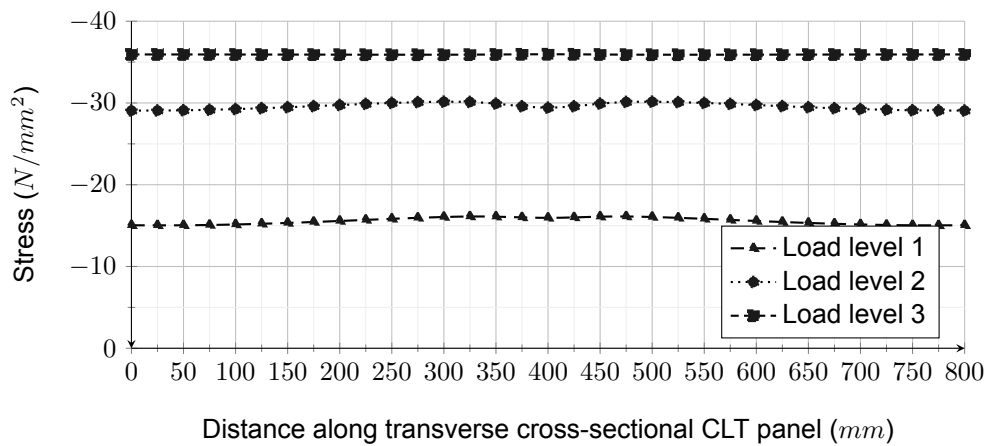
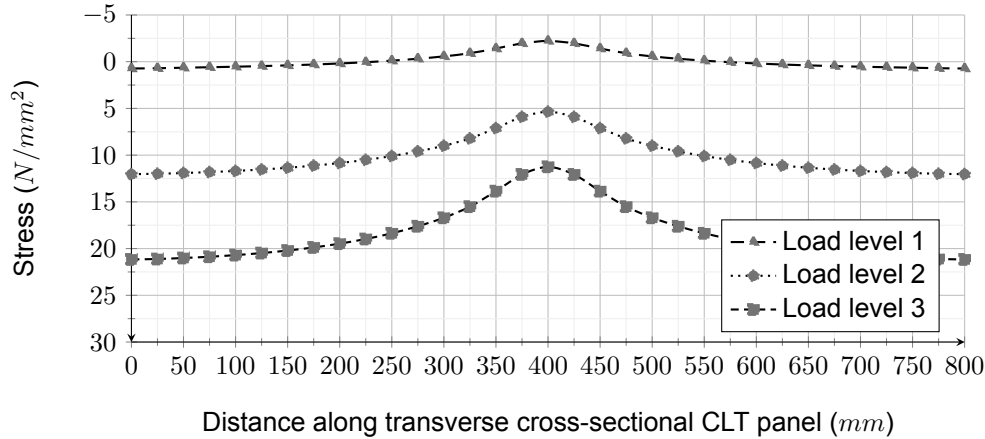


Figure 5.24: Stress development in compression at midspan at the top of the CLT panel of configuration 10

Lastly, for contrast, the stress development over the width of the CLT panel of configuration 10 is displayed as it has a different composite connection, which has a higher ultimate load capacity and

stiffness. In comparison to configuration 1, there is less stress deviation near the centre at the top of the CLT panel and similar stress at several Load levels near the bottom.



**Figure 5.25:** Stress development mostly in tension at midspan at the bottom of the CLT panel of configuration 10

The biggest difference between configuration 10 and 1 in relation to the stress distribution over the width of the CLT panel is that, while the absolute value of stress change is similar, the width of the local effect is much wider for with a more stiff composite connection.

### 5.2.6. Composite efficiency

A measurement of the effectiveness in a composite beam achieving full composite action is composite efficiency ( $C$ ). Composite efficiency is calculated, as a percentage, with a load-deflection response, from experimental or numerical analysis with the following formula:

$$C = \frac{\Delta_{\text{Partial-composite}} - \Delta_{\text{Non-composite}}}{\Delta_{\text{Full-composite}} - \Delta_{\text{Non-composite}}} \times 100 \quad (5.3)$$

where the following parameters are the mid-span deflections of the STC beams at different percentages of the peak load capacity

$\Delta_{\text{Partial-composite}}$  at different load levels

$\Delta_{\text{Non-composite}}$  at different load levels

$\Delta_{\text{Full-composite}}$  at different load levels

This composite efficiency shows the relative effectiveness of a configuration of a composite beam in respect to full composite action ( $C = 100\%$ ) where the components act as one unified material and no composite action ( $C = 0\%$ ) in which only the friction contributes to the resistance of slip.

Table 5.6 depicts the composite efficiency of all configurations and the difference at differing load levels. The composite efficiency highlights a configuration's relative performance when compared to that configuration purely utilising friction (No-composite action or non-composite) and being a unified single element (full-composite action).

The benchmark scenario, configuration 1, demonstrates moderate levels of composite efficiency that slightly improve as the load level increases. This increase in composite efficiency is attributed to the consistent absolute position of the configuration relative to the full- and non-composite deflections as the beam responds beyond the elastic state. Fig. 5.29a illustrates this behaviour, where the solid black line represents the actual deflection, and the closely-spaced dashed black line and dotted black line represent the boundaries set by the deflection with no composite action and full composite action,

**Table 5.6:** Composite efficiency of configurations

Load level	Composite efficiency (%) of configuration											
	1	2	3	4	5	6	7	8	9	10	11	12
1 (50 mm)	37.0	-*	72.9	34.2	32.7	28.1	21.1	44.2	27.7	62.7	53.3	43.9
2 (100 mm)	40.3	-*	70,3	36.7	34.9	32.0	25.7	45.7	34.4	61.6	49.3	38.3
3 (150 mm)	45.3	-*	-**	41.4	38.8	34.6	26.6	52.2	-**	58.5	39.5	-***

\* The composite efficiency of configuration 2 cannot be calculated as the full-composite variant does not reach load level 1

\*\* The composite efficiency at load level 3 of configuration 3 and 9 cannot be calculated as the configuration does not reach load level 3 without composite action

\*\*\* The composite efficiency at load level 3 of configuration 12 cannot be calculated as the configuration does not reach load level 3

respectively. Additionally, a decrease in composite efficiency with increasing load would mean a downwards change in absolute deflection of a configuration relative to its respective full- and non-composite boundaries. This trend can be observed in configurations 3, 10, 11, and 12.

Configurations 10, 11 and 12 utilise composite connection B (Table 5.2). This connection is initially, at low levels of displacements much more stiff than connection type A while additionally having a much higher load carrying capacity. Fig. 4.11 shows the behaviour of both connections in push-out tests in a load-displacement curve.

A more stiff composite connection results in earlier utilisation of the complete cross section as seen in Fig. 5.13a and Fig. 5.15b. Therefore less load resistance is developed after the elastic behaviour of the beam resulting in decreasing composite efficiency as deflection increases.

Configuration 3, which varies from the benchmark configuration with double the length, achieves high level of composite efficiency at the first two load levels at 72.9% and 70.3%, respectively. Both load levels at which the composite efficiency is calculated are within the elastic range of the beam behaviour (depicted in Fig. 5.3).

Configurations 4 and 5, which have an increased CLT panel slab width compared to configuration 1, exhibit a moderate level of composite efficiency. In configuration 1, the composite efficiency at load levels 1, 2, and 3 is 37%, 40.3%, and 45.3%, respectively. With an increased slab width in configuration 4, the composite efficiency is reduced to 34.2%, 36.7%, and 41.4% at their respective load levels. This same trend is observed in configuration 5, where the composite efficiency is 32.7%, 34.9%, and 38.8% at increasing load levels. This perspective reveals that, at every load level, an increase in slab panel width leads to a decrease in composite efficiency. Therefore, increasing the slab width, without any other parametric changes, results in a slightly less effective partial composite beam.

Table 5.2.6 highlights a significant decrease in composite efficiency when the spacing of connections is reduced. This trend is observed in configurations 1, 6, and 7, where the composite efficiency drops from 37% to 28.1% and 21.1%, respectively, at load level 1. A similar decrease is observed at higher load levels. The spacing of connections appears to have a notable influence on achieving higher composite efficiency. This observation is further supported by the composite efficiency of configurations 10, 11, and 12. With a different, stiffer composite connection, the same trend of decreased composite efficiency is observed with increased spacing under different load levels. With composite connection B (Table 5.2) at load level 1 the composite efficiency is high at 62.7% with a spacing (S) of 300 mm. This decreases to 53.3% and 43.9% with a spacing of 400 mm and 500 mm, respectively.

### 5.3. Shear connection location optimisation study

Shear connections are most effective when located near the supports of a simply supported beam, where the shear force is higher. In the subsequent section, we investigate the impact of a non-uniform distribution of composite shear connections along the length of the beam in order to optimise force

transfer and enhance the behavior of the steel-CLT composite beam.

As the previously studied configuration all had uniform shear connection distributions, 4 additional configurations will be studied which are variations with differently positioned shear connectors. The shear connections will be concentrated near the supports and vertical deformation will need to be prevented with shear connectors over the entire beam.

The previously presented configurations (Table 5.5) featured uniform distributions of shear connectors with varying spacing. In this study, two optimised configurations will be examined, as illustrated in Fig. 5.26. The figure shows, from top to bottom, the previously evaluated uniform distribution seen in configurations 1 and 10, which had a total of 20 shear connections. Additionally, configurations 7 and 12, which include 12 shear connections, as well as the newly introduced configurations  $7_{O,1}$ ,  $7_{O,2}$ ,  $12_{O,1}$ , and  $12_{O,2}$ , which will include 12 connections concentrated near the supports, are depicted.

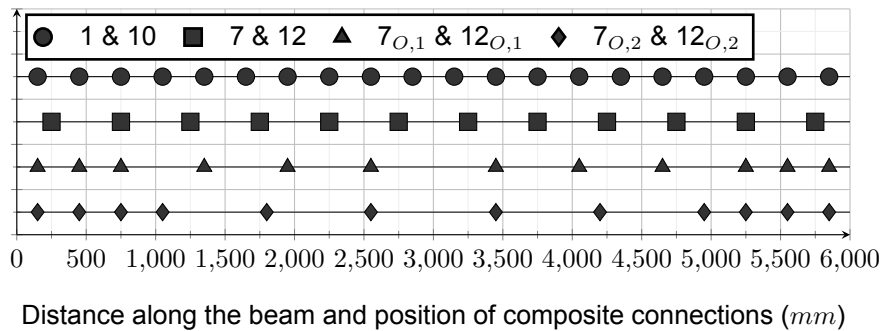


Figure 5.26: Additional configurations ( $7_{O,1}$ ,  $12_{O,1}$ ,  $7_{O,2}$ ,  $12_{O,2}$ ) with different positions of shear connections in comparison to configurations 1,7,10 and 12

Fig. 5.27 presents the load-midspan deflection of the additional configurations depicted in Fig. 5.26. Specifically, Fig. 5.27a compares the performance of configuration 1 with uniformly spaced 300 mm screw composite connections, configuration 7 with uniformly spaced 500 mm connections, and the optimised configurations  $7_{O,1}$  and  $7_{O,2}$  with screw composite connections. Similarly, Fig. 5.27b compares the performance of configuration 10 with uniformly spaced 300 mm screw composite connections, configuration 12 with uniformly spaced 500 mm connections, and the optimised configurations  $12_{O,1}$  and  $12_{O,2}$  with screw composite connections.

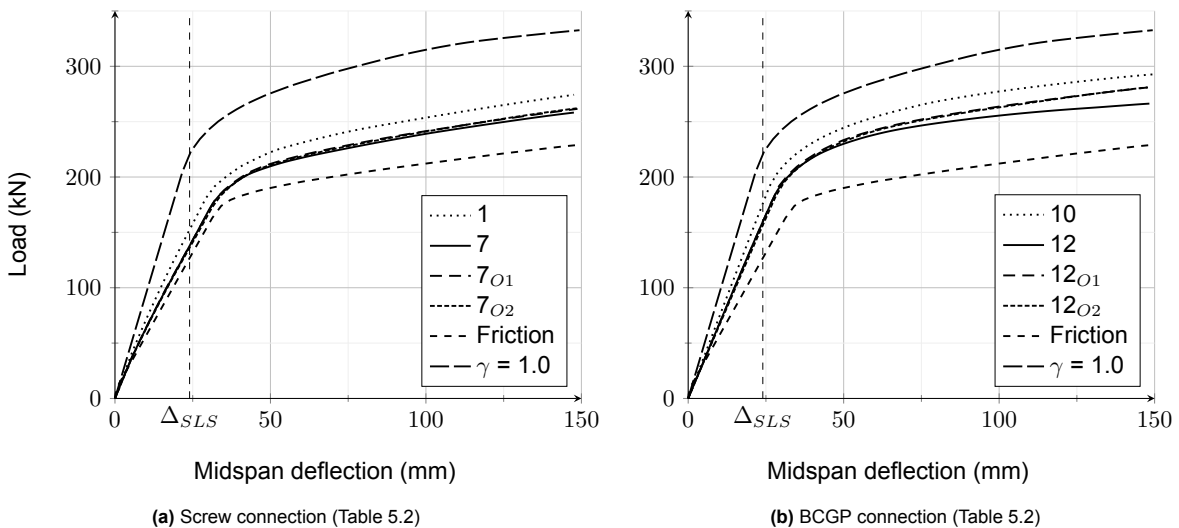
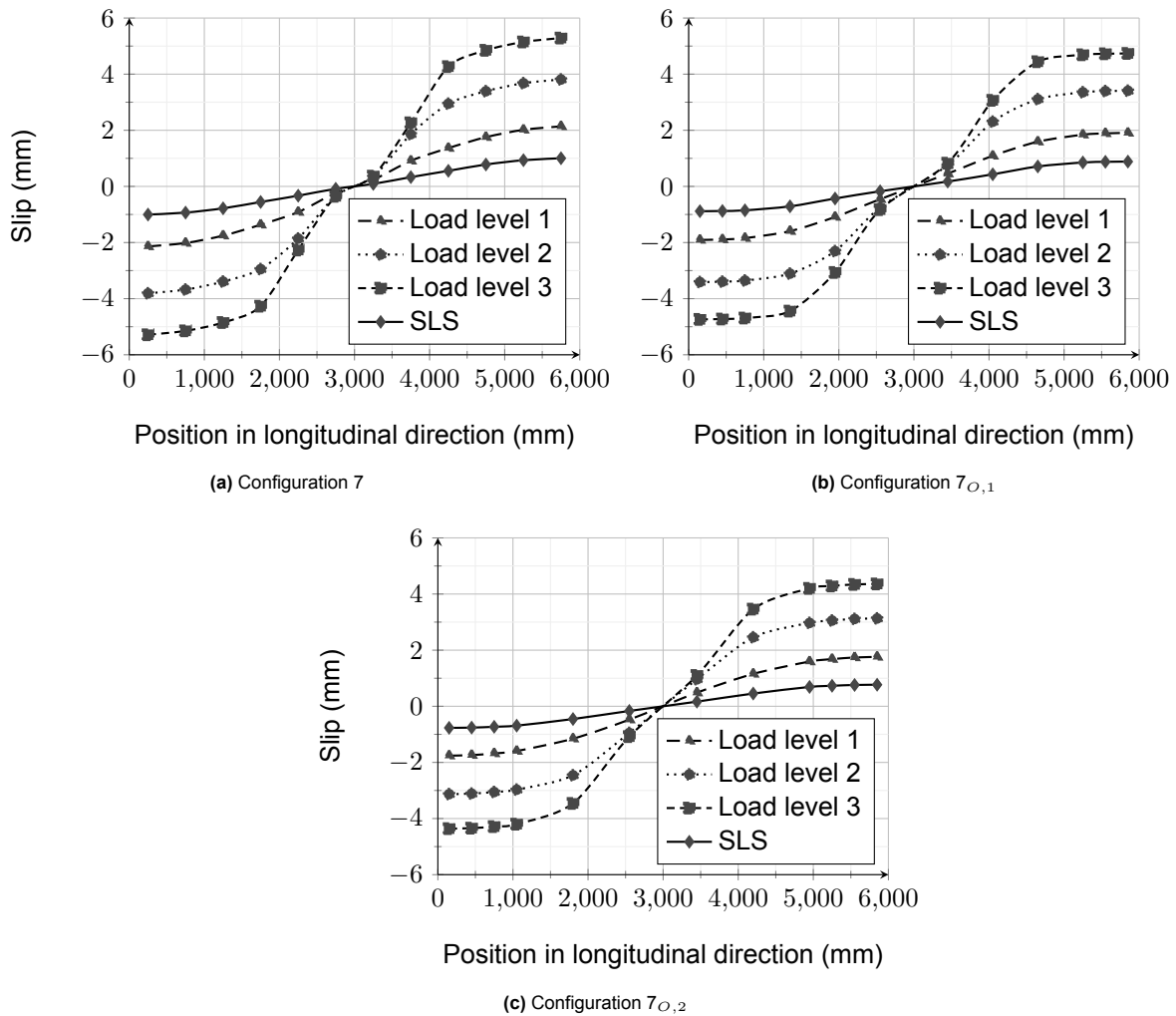


Figure 5.27: Load-Midspan deflection of configurations with non-uniform en uniform shear connection distribution



Notably, there is a very insignificant difference in both situations, whether using screws or BCGP connections, during the elastic phase. The load resisted, initial bending stiffness, and load deflection path are identical, regardless of whether shear connection location optimization is applied or not. Optimizing the shear connection location does not compensate for the use of fewer shear connections in configurations 7,  $7_{O,1}$ ,  $7_{O,2}$ , 12,  $12_{O,1}$ , and  $12_{O,2}$ , which only utilise 12 connections compared to the 20 connections in configurations 1 and 10. After the onset of plasticity the optimisation of the shear connection position does slightly impact the load-deflection behaviour, in both scenarios, as more shear force accumulates near the supports. For further insight Fig. 5.28 displays the change in slip over the length of the beam, due to location optimisation with configurations 7,  $7_{O,1}$  and  $7_{O,2}$ .



**Figure 5.28:** The slip at the material interface over the length of the beam

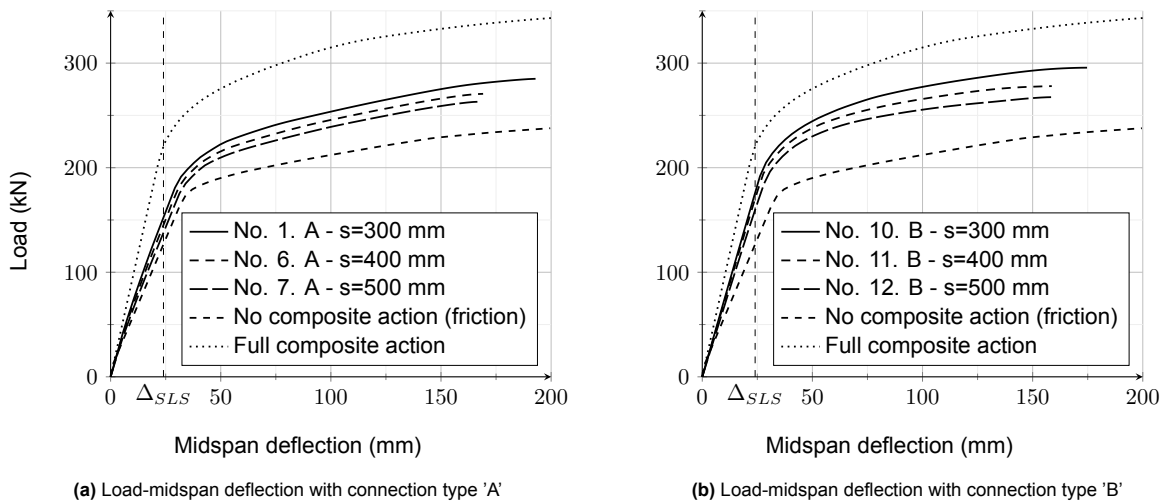
Fig. 5.28 displays that a slight difference in slip is visible at the outer ends of the beam as location optimisation is employed. However, this becomes, in absolute terms, higher as load increases and once the beam is already far past the elastic phase. At serviceability limit state the slip of configurations 7,  $7_{O,1}$  and  $7_{O,2}$  in slip at the outer point is 1.00 mm, 0.88 mm and 0.77 mm, respectively, and at load level 3 this has increased to 5.29 mm, 4.74 mm and 4.36 mm, respectively.

## 5.4. Conclusions from numerical study

### 5.4.1. Spacing of composite connections

As clarified in Section 2.6.1, the spacing ( $s$ ) is a key parameter in achieving high composite beam efficiency. However, the behaviour of closely placed composite connectors to achieve this high composite efficiency has not been tested in composite beams.

Figure 5.29 displays the midspan displacement of a 6-meter-long beam in a numerical four-point bending test with increasing spacing of the composite connections. The composite connections are of type 'A' and 'B' (Table 5.2).



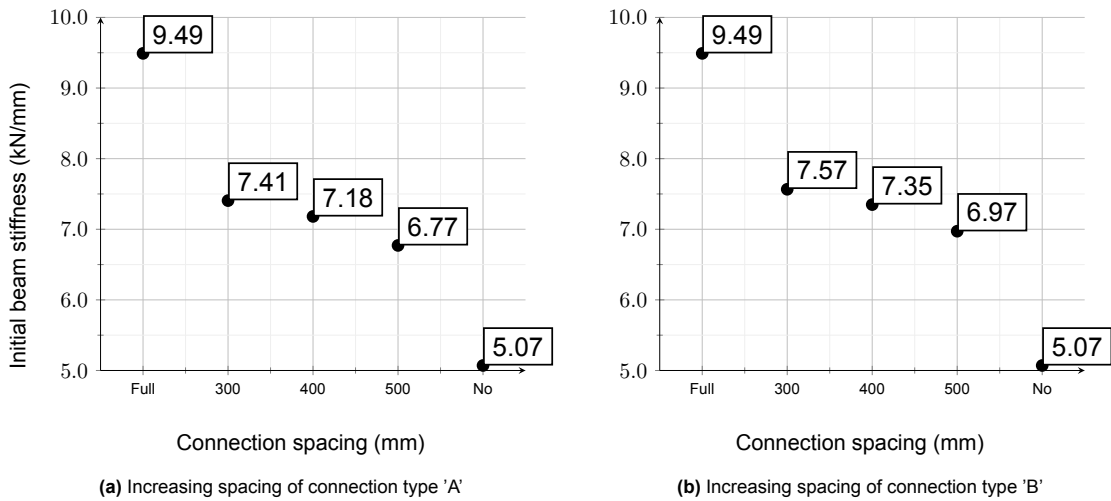
**Figure 5.29:** Load-midspan deflection of configurations with a changing spacing ( $s$ ) of composite connections type 'A' (left) and type 'B' (right) (Connection types clarified in Fig. 5.2)

Decreasing the spacing allows the steel-CLT composite beam to resist deflection at a significantly higher rate. A relatively stiff composite connection of type B (as clarified in Section 4.3.4) is much closer to the behaviour of a fully composite steel-CLT beam, as seen in Figure 5.29. In a fully composite beam, all nodes of the surface of the CLT panel and the steel flange are tied together, allowing the composite beam to act as a single element.

Regarding the slip of the connectors, a comparable perspective from Figures 5.11a, 5.11b, and 5.11c shows the change, with slip increasing as fewer shear connectors are used (the effect of increasing the spacing). This aligns with the information gathered from the stress distribution along the cross-section of the same configurations in Figures 5.13a, 5.14b, and 5.15a, where the absolute change in stress level at the material interface increases as the spacing increases, depicting the decrease in composite action.

The initial beam stiffness of the steel-CLT composite beam was shown to be the most accurate result when comparing the numerical model against the experimental data (Section 4.6). Figure 5.30 displays the increase in beam stiffness with a decrease in spacing.

As shown by the above-mentioned results and the concept of composite efficiency in Section 5.2.6, not only does the initial beam stiffness increase with a decrease in connector spacing, but the overall composite efficiency also improves. This is achieved by having more composite connections and tighter integration between the steel and CLT components.



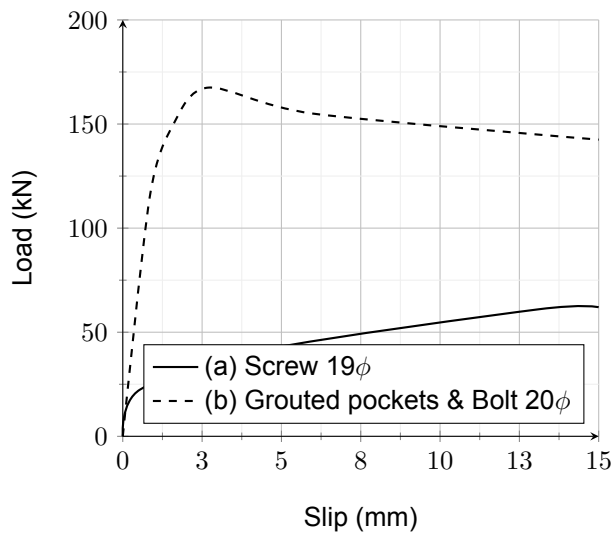
**Figure 5.30:** Initial beam stiffness of configuration 1,6 & 7 with composite connection A (left) and configuration 10,11 & 12 with composite connection B (right) with initial beam stiffness at full- and no-composite action

Decreasing the spacing further impacts the characteristics of shear connectors and the load-slip curve, which would require more detailed push-out testing [68][73]. In short, it is clear that closely spacing composite connections results in greater composite action due to higher composite efficiency, initial beam stiffness, and initial bending stiffness in the steel-CLT beam.

Lastly, in conclusion, the optimisation of shear connection location does not provide significant behavioural benefits in the design of steel-CLT composite beams, as observed in Fig. 5.27. It is however observed that the amount of slip at the extremities of the beam decreases as seen in Fig. 5.28.

### 5.4.2. Characteristics of the composite connection

In this parametric study, two composite connections have been tested as described in Table 5.2: a bolt connector in grouted pockets (defined as connection type B) and screws (defined as connection type A). The load-slip behaviour of the two connectors in experimental push-out tests has been displayed in Fig. 5.31.



**Figure 5.31:** Load-slip curve of two composite connections used in validation of the finite element model [31]

Fig. 5.29 clearly demonstrates the effect of the characteristics of the composite connection on the numerical model. The load resistance is higher with a stiffer composite connection in the post-elastic phase. However, at the beginning of the elastic regime, the initial beam stiffness seems to be only slightly impacted, as displayed in Figure 5.30, where the difference in initial beam stiffness due to a change in connection, over the three variations of connection spacing, is only 0.18, kN/mm on average. But, in the elastic phase, we see significant difference in load capacity at serviceability limit state as displayed in Table 5.5. For three different configurations of spacing using the superior connection increases the load capacity at serviceability limit state from 151.9 kN, 141.7 kN and 135.3 kN to 173.3 kN, 161.7 kN and 153.4 kN, respectively. Initially, as no slip has occurred both connections perform similar, as displayed in Fig. 5.31, but this quickly changes as depicted by the increased load capacity in SLS.

When comparing the slip due to a change in the composite connection, Fig. 5.11a and Fig. 5.11d show that the composite connection with significantly higher stiffness and ultimate capacity almost halves the maximum slip from 3 mm to 1.5 mm. This indicates a significant change in composite action, which is supported by Fig. 5.13a and Fig. 5.15b, where the absolute level of stress difference at the material interface also significantly decreases for configuration 10, the stiffer composite connection.

In terms of composite efficiency, both configurations, 1 and 10, behave differently as the load increases: the composite efficiency increases for configuration 1, while it decreases for configuration 10. However, it is clear that a higher-performance composite connection has a very positive impact on composite efficiency. Configuration 1, employing screws, has composite efficiencies of 37%, 40.3%, and 45.3% at load levels 1, 2, and 3, respectively. On the other hand, configuration 10, with BCGP, has composite efficiencies of 62.7%, 61.6%, and 58.5% at load levels 1, 2, and 3, respectively, which is much higher.

In summary, these results indicate that the characteristics of the composite connections, such as stiffness and ultimate capacity, significantly affect the behaviour and performance of the steel-CLT composite beam. A stiffer composite connection leads to higher load resistance, reduced slip, and increased composite efficiency. These findings highlight the effect of selecting and designing of the composite connections in order to optimise the performance of steel-CLT composite beams for greater composite action.

### 5.4.3. Width of the CLT panel

The effect of the width of the CLT panel on the behaviour of the steel-CLT composite beam can be assessed by comparing configurations 1, 4, and 5, where the CLT panel deviates at 800 mm, 1200 mm, and 1600 mm, respectively. The impact of this variation is initially observed in Table 5.5, where the initial numerical bending stiffness increases from  $28.98 \times 10^{12}$  Nmm<sup>2</sup> at an 800 mm width to  $30.44 \times 10^{12}$  Nmm<sup>2</sup> and  $31.36 \times 10^{12}$  Nmm<sup>2</sup> at 1200 mm and 1600 mm panel widths. Simultaneously, this leads to an increase in the load at the serviceability limit state from 151.9 kN to 156.7 kN and 160.4 kN. Therefore, doubling the width of the CLT panel results in a small increase of 8.2% in bending stiffness and a 5.6% increase in  $P_{SLS}$ . This is supported by the slight increase in initial bending stiffness seen in Fig. 5.8b.

When examining Fig. 5.13 and 5.14a, it can be seen that the stress at  $P_{SLS}$  remains the same for all three configurations. This implies that the increased force resistance at the serviceability limit state is enabled by the additional width.

And regarding the stress over the width of the panel little change is seen when increasing panel width as seen in Section 5.2.5. Notable is the fact that the local deviation around the flange of the steel beam stays the same in absolute width as the panel width increases.

Lastly, as the composite efficiency (Section 5.2.6) is viewed it can be seen that at every load level, an increase in slab panel width leads to a decrease in composite efficiency.

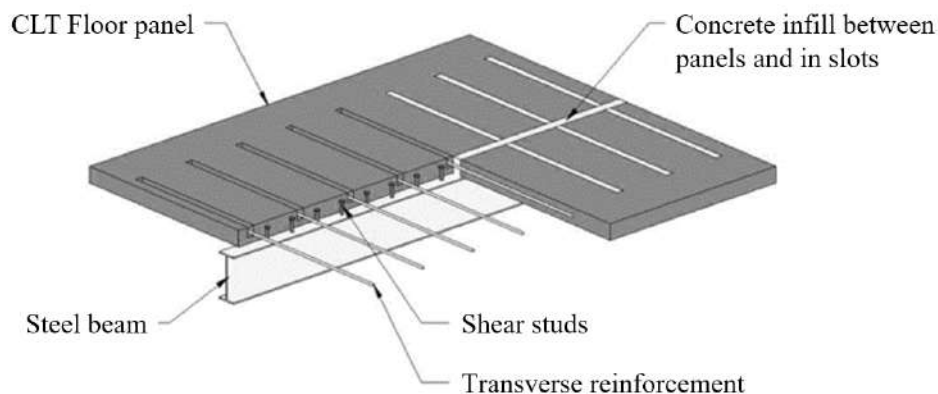
# 6

## Floor System Evaluation

This chapter aims to conduct a numerical evaluation of the floor systems discussed in Section 2.5. The floor system presented in Section 2.5.1 will be assessed using the connections described in Table 5.2, along with the specified CLT layup. On the other hand, the system introduced in Section 2.5.2 will be evaluated after predicting the performance of the specific connection in terms of stiffness and strength.

### 6.1. Floor system with transverse reinforced concrete slots with welded studs

Based on the conducted analysis, it is possible to make predictions about the behavior of the steel-CLT composite floor system mentioned earlier (Section 2.5.2 and depicted in Fig. 6.1). This system utilises transverse concrete infill with transverse and welded studs as composite connections whilst the CLT panel spans two steel beams. By examining other push-out test results, particularly the load-slip curve and the underlying mechanical mechanisms, it becomes feasible to make predictions with a reasonably defined confidence interval.



**Figure 6.1:** The design for the composite connection from WSP

If we review above mentioned system, displayed in Fig. 6.1, we see striking similarities to the grouted stud connectors in steel-CLT composite connections displayed in Fig. 2.18(right):

- Both utilise a welded stud
- Stud loaded in shear
- Presumed to use C25/30

- Similar grout-width to stud ratio
- Undefined stud strength and size

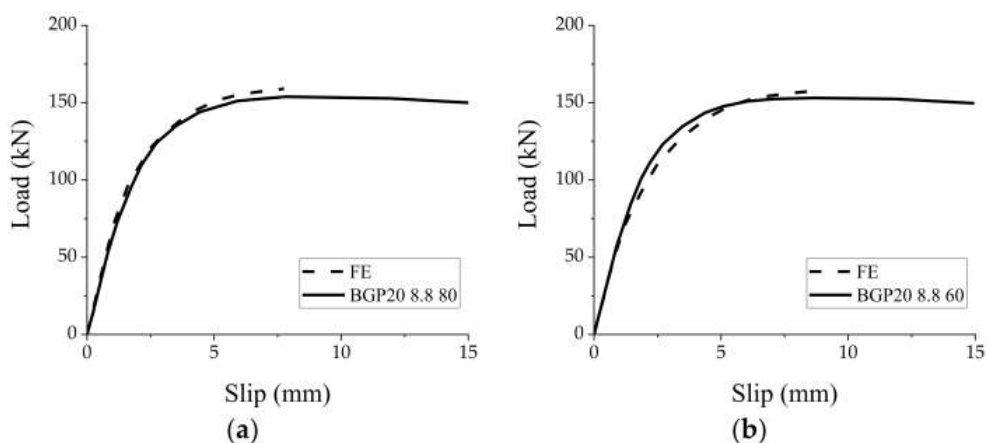
With these similarities in mind it would be interesting to know the failure mechanisms and forces at play in such a connection. For this evaluation, the start is referring to the research conducted by [28] on bolted connections in grouted pockets. In the study, the load-slip behavior of these connections reveals a distinct post-peak softening branch attributed to the crushing of grout within the grouted pockets. The ultimate load capacity of the connection is influenced by the strength of the bolt, while the stiffness remains unaffected. On the other hand, the size of the grouted pocket has minimal influence, slightly flattening the post-peak softening branch. It is evident from these findings that the strength and stiffness of a bolted connection in grouted pockets are primarily determined by the mechanical properties of the cementitious grout.

In terms of failure modes and mechanical mechanisms, [28] found that the  $20\phi$  bolts in the bolted connections exhibited no damage or excessive deformation, while the  $16\phi$  and  $12\phi$  bolts underwent plastic deformation. Moreover, as the bolt size decreased, the crushing zone in the concrete became smaller, resulting in crushing of the concrete. These results emphasize the significant role of bolt size in influencing these failure modes and the presence of the main two failure modes, if transfer of the force from concrete to CLT is enabled with large enough CLT surface area:

- Shear failure of the welded stud
- Concrete crushing

Building upon these insights, we turn our attention to the research by [72], which focuses on the numerical study of the shear performance of grouted stud connectors (GSC) in steel-CLT composite beams. This particular connection type, similar to the design proposed by WSP (Section 2.5.2), involves two welded studs encased in grout instead of one. It does have a similar grout-to-width ratio. As BCGP connections and GSC connections vary little in mechanical behaviour as both have a steel shaft and head encased in grout (as seen in Fig. 2.6.2) the hypothesis is made that the GSC connection will also be subject to identical leading failure modes.

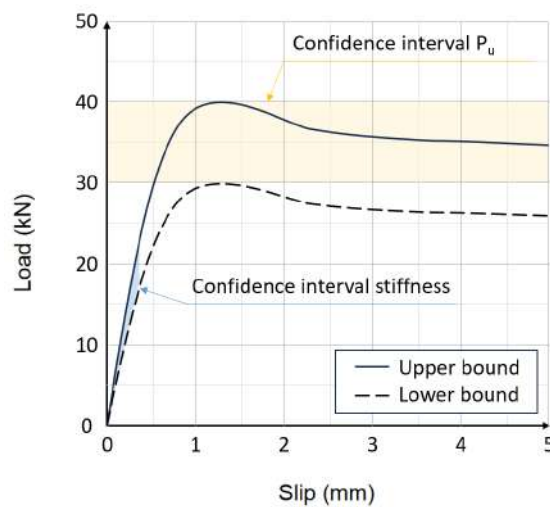
Secondly, the study [72] proposes a finite element model with solid elements able to capture localised behaviour and verified this model against the previously mentioned BCGP results of [28]. The difference in ultimate load capacity between the experimental data and finite element model was less than 7.5% whilst the prediction of stiffnesses varied significantly more as seen in Fig. 6.2. With this displayed accuracy [72] proposes guidance for the calculation of the initial stiffness ( $k_{s,0.4}$ ), secondary stiffness ( $k_{s,0.6}$ ) and ultimate load capacity ( $P_u$ ) for GSC connections.



**Figure 6.2:** Comparison (by [72]) between simulated results and test curves from literature [32] and finite element data from [72]. (a) BGP12 8.8 60; (b) BGP16 8.8 80

Based on the hypothesis that failure modes in the GSC connection would be similar to that of the BCGP connection and the striking similarity between the GSC connection and the composite connection with transverse reinforced concrete slots with welded studs, the guidance for GSC ([72]) is applied to the composite connection with transverse reinforced concrete slots with welded studs to give an indication of the initial stiffness ( $k_{s,0.4}$ ), secondary stiffness ( $k_{s,0.6}$ ) and ultimate load capacity ( $P_u$ ).

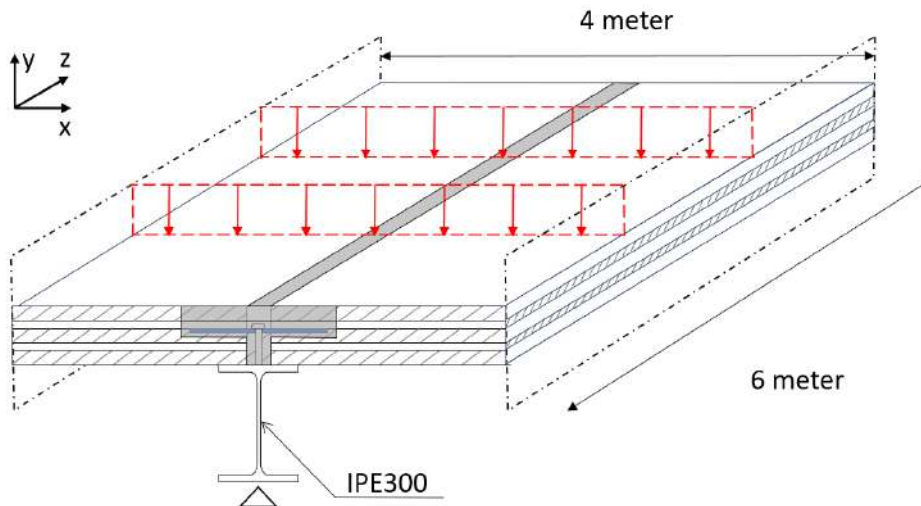
The research conducted by [72] provides relations between stud diameter, strength, CLT panel, and connection strength and stiffness. In combination with the above stated analysis which compared failure modes of BCGP and GSC connections, a conservative prediction is made for the composite connection with transverse reinforced concrete slots with welded studs. The ultimate load capacity might range from 30 kN to 40 kN, depending on the size and strength of the studs, which are currently undefined. Furthermore, the initial stiffness ( $k_{s,0.4}$ ) is estimated to be between 86 kN/mm and 94 kN/mm, while the secondary stiffness ( $k_{s,0.6}$ ) is predicted to be between 52 kN/mm and 72 kN/mm. This prognosis is displayed in Fig. 6.3 in which a load-slip is created based on the above mentioned capacity and stiffness.



**Figure 6.3:** Estimation of the load-slip behaviour of the composite connection with transverse reinforced concrete slots with welded studs displayed in Fig. 6.1

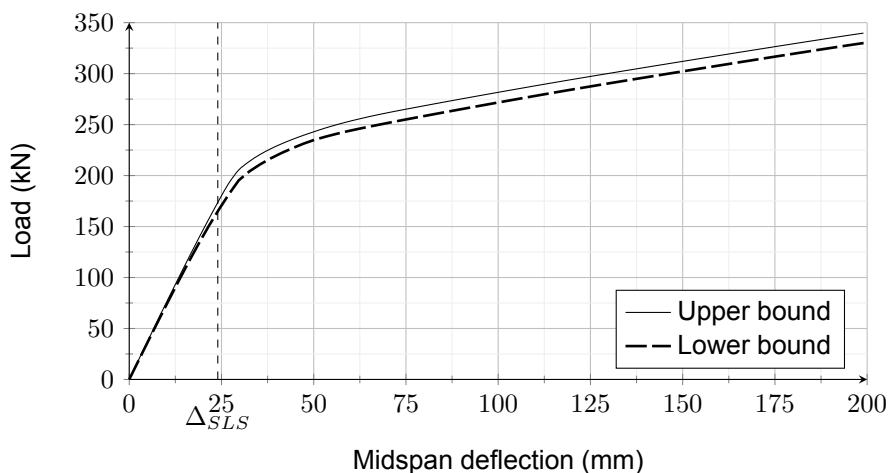
To support this prediction, the failure of welded studs is verified according to EN1994-1-1 [18], which specifically addresses steel-concrete composite construction. Following the guidance provided, the ultimate load capacity for shear failure of the stud is expected to range from 29.0 kN to 51.5 kN, depending on the size and strength of the studs, while the ultimate load for crushing of the concrete is estimated to be between 29.4 kN and 52.3 kN. This guideline does not take into account the fact that in steel-CLT composite connection which utilise grout sufficient area is needed between the grout and CLT to transfer the force. This is enabled in the design (Section 2.5.2) by the transverse slots with reinforcement that distribute the force. The above failure capacities, support the conservative prediction for the failure and behaviour, depicted in Fig. 6.3, of the connection with transverse reinforced concrete slots with welded studs as the ultimate load capacity is in the same range.

With this behavioural load-slip prediction an analysis of the steel-CLT composite beam and the floor system can be done based on the numerical analysis described in Section 4. A repetitively divided part of the floor system will be subject to a four-point bending test as depicted in Fig. 6.4. The CLT is configured with 5 layers ( $t = (40, 20, 40, 20, 40)$  mm) with a mainly transversal orientation ( $[90^\circ, 0^\circ, 90^\circ, 0^\circ, 90^\circ]$ ) enables a 4 meter transversal span between steel beams while remaining loadbearing after a 120 minute fire. Secondly the composite connection is uniformly spaced every 300 mm whilst the steel profile is an IPE300.



**Figure 6.4:** Floor system segment from Section 2.5.2 with transverse reinforced concrete slots with welded studs numerically tested in four-point bending test

Fig. 6.5 displays the load-deflection behaviour of the depicted floor segment in Fig. 6.4 and secondarily shows the deflection of the secondary beam at serviceability limit state at 24 mm. The impact of the confidence interval of the behaviour is visualised through the upper- and lower bound.



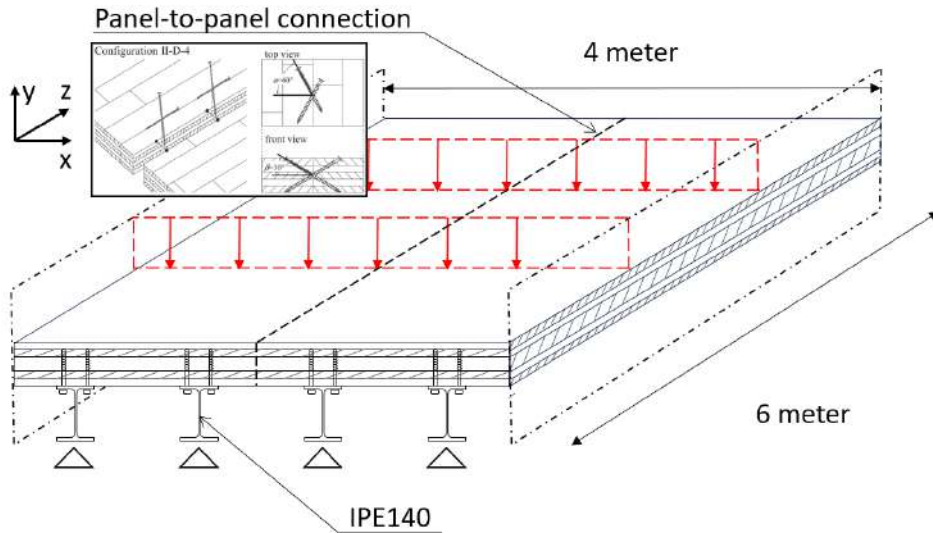
**Figure 6.5:** Upper- and lower bound of the load-midspan deflection of the floor segment with transverse reinforced concrete slots and welded studs

## 6.2. Floor system with continuous CLT panel

Secondly, a comparative analysis will be conducted for the floor system discussed in Section 2.5.1, which was researched by [44]. This system features a continuous CLT slab on top of a steel section and utilises a panel-to-panel connection to ensure continuity between 2-meter wide prefabricated elements, as depicted in Fig. 6.6..

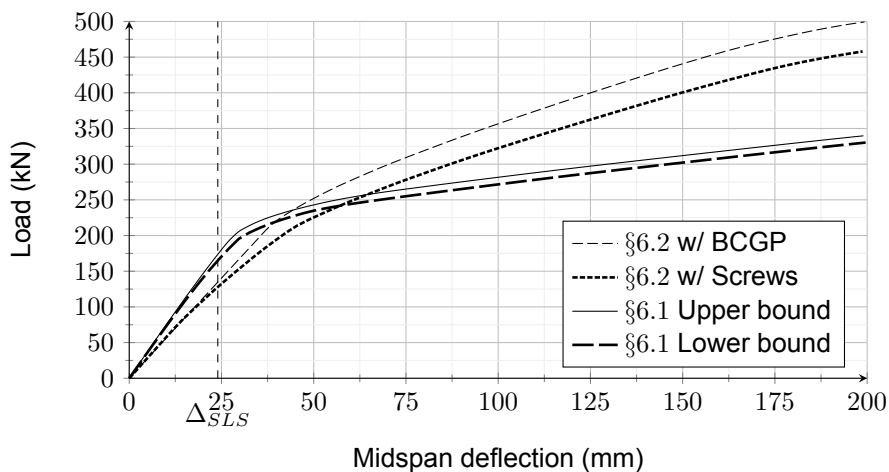
In contrast to the system depicted in Fig. 6.4, this system has most of its CLT in the longitudinal direction, contributing to the composite action. As a result, it requires more closely spaced beams since the CLT can span a shorter distance. The CLT consists of 5 layers ( $t = (20, 20, 40, 20, 20)$  mm) with a predominantly longitudinal orientation ( $[0^\circ, 90^\circ, 0^\circ, 90^\circ, 0^\circ]$ ).





**Figure 6.6:** Floor system segment from Section 2.5.1 with screws (or BCGP) and panel-to-panel connection from [45]

Secondly, the composite connection is uniformly spaced every 300 mm, and the steel profile used is an IPE300. This analysis will numerically study this floor system with the previously used BCGP and screws as composite shear connections (Table 5.2).



**Figure 6.7:** Load-midspan deflection of the floor segment with transverse reinforced concrete slots and welded studs and the segment with continuous CLT panel

Fig. 6.7 illustrates the additional load-deflection behavior of the continuous CLT slab system, providing a contrast to the system discussed in Section 6.1. Utilising the currently selected profile, IPE140, the system exhibits a lower initial stiffness, as evident from the less steep angle in the figure. However, as the deflection increases, it significantly resists more load.

This difference in composite action can be attributed to the number of shear connections. The system in Fig. 6.4 is equipped with 20 shear connections, whereas the system in Fig. 6.6 has 80 shear connections.

## 6.3. Evaluation

Both systems demonstrate feasibility in construction, showcasing their ability to resist load and deflection, although they differ significantly in design. A comparison can be made based on the chosen steel profiles in the floor system, and an evaluation of both presented options is displayed in Table 6.1.

**Table 6.1:** Evaluation

Floor system		Weight		Performance			Sustainability	
		CLT (kg)	Steel (kg)	$P_{SLS}$ (kN)	$q_{SLS,net}^*$ (kN/m <sup>2</sup> )	$EI_{n,ini}$ ( $\cdot 10^{12}$ Nmm <sup>2</sup> )	LCA (A1, A3) (kg CO <sub>2</sub> -eq)	Biogenic carb. (kg CO <sub>2</sub> -eq)
§6.1	Upper bound	1882	253	173.6	6.4	29.03	786.9	-3086
	Lower bound			164.9	6.0	28.13		
§6.2	BCGP	1411	310	134.7	4.9	21.58	739.8	-2314
	Screws			127.9	4.6	22.05		

\*net refers to the fact that the self-weight is subtracted

\*\*A1 & A3 Life cycle assessment takes into account Raw Material Acquisition, Manufacturing and Assembly

For each evaluated floor system, Table 6.1 presents the weight of both the CLT and the steel used in the supporting secondary beams. The system with transverse reinforced concrete slots and welded studs (Section 6.1) exhibits a 33% higher CLT weight due to the increase in thickness of the outer lamellae. Conversely, the steel weight of the system in Section 6.1 is 18% lower due to the utilisation of a single IPE300 beam instead of four IPE140 beams of similar length.

In addition to the weight comparison, Table 6.1 provides an assessment of the corresponding performance in three parameters: the force resisted at serviceability, the remaining distributed force after subtracting the self-weight, and the initial bending stiffness (as defined in Section 4.6), which is measured over the first 5 loading steps. These loading steps correspond to reaching 10% of the serviceability deflection or 2.4 mm at midspan.

**Table 6.2:** Load categories and resulting design value of action

Load categories	NEN-EN 1991-1-1+C1+C11/NB[52] $q_k$ (kN/m <sup>2</sup> )	EN 1991-1-1[16] $q_k$ (kN/m <sup>2</sup> )	EN 1990[15] $\gamma_{Q,1}$	$q_{E,d}$ (kN/m <sup>2</sup> )
Class A (Residential)	1.75	1.5 to 2.0	1.50	2.63
Class B (Office)	2.5	2.0 to 3.0		3.75

Table 6.2 depicts various load categories that can be applicable to the discussed floor systems. The acting load is determined based on the Eurocodes [16] and National Annex [52], and then multiplied by the gamma-value for leading variable action [15] to obtain the design value of the action.

**Table 6.3:** Design value of resistance of floor systems compared to design value of action

Floor system		Load capacity	EN1995-1-1[19]	Comparison	
		$q_{SLS,net}$ (kN/m <sup>2</sup> )	$\gamma_{M,CLT}$	$q_{R,d}$ (kN/m <sup>2</sup> )	$q_{E,d,max}$ (kN/m <sup>2</sup> )
§6.1	Upper bound	6.4	1.25	5.12	> 3.75
	Lower bound	6		4.8	> 3.75
§6.2	BCGP	4.9		3.92	> 3.75
	Screws	4.6		3.68	< 3.75

In Table 6.3 the maximum design value of the action ( $q_{R,d,max}$ ) for the office floor is compared against the design value of the resistance ( $q_{R,d}$ ) achieved by reducing the load capacity at the serviceability limit state using the partial material factor of CLT [19]. While the floor system is a steel-CLT

composite floor system, reducing the entire system by the CLT partial material factor is a conservative assumption. The resulting design values of the resistance are all greater than the maximum design value of action, except for the floor system of Section 6.2 when employing screws as the composite connection. However, as the assumption is conservative and the design value of action is nearly similar to that of the resistance, it can be concluded that both systems, in their currently designed configuration (including secondary beams), are capable of fulfilling applicable functionalities for office and residential use, as the ultimate limit state satisfies whilst the deflection requirements of the serviceability limit state are sufficient.

Lastly, Table 6.1 provides insights into the sustainability of the respective systems by comparing a brief Life Cycle Assessment (LCA) that evaluates stages A1 and A3, concerning raw material acquisition and manufacturing/assembly, respectively, of both systems. It reveals a slight disparity in the environmental impact between the two options in terms of carbon dioxide equivalent ( $kgCO_2 - eq$ ), with the system of Section 6.1 emitting 6.4% more. Secondly, it depicts the biogenic carbon of both systems. Timber sequesters carbon during its growth phase, as trees absorb carbon-dioxide through photosynthesis and store the carbon in their structure, resulting in a net reduction in carbon-dioxide emissions when utilising the steel-CLT composite system. This sequestered carbon is greater for the system of Section 6.1 as it uses more CLT.

# 7

## Conclusions

This section presents the conclusions, which are the culmination of the research objectives aimed at addressing the four research questions related to the assessment of steel-CLT composite floor systems. It not only provides the answers to these questions but also, briefly, outlines the methodology employed to obtain them.

The research aimed to answer the following research questions:

- i. How can a steel-CLT composite floor system be effectively constructed, considering the unique orthotropic properties of the CLT slab in contrast to traditional concrete?
- ii. What are the different types of steel-CLT composite connections, their characteristics and their influence?
- iii. How do geometry and strength-related parameters influence the behaviour and performance of steel-CLT composite beams?
- iv. How can the behaviour of steel-CLT composite beams be predicted analytically and numerically?

### Conclusions

- i. In regard to the feasibility of a steel-CLT composite floor system, it can be concluded that such a system can be successfully constructed, offering environmental benefits, reduced structural weight, and comparable structural performance to traditional floor systems.

Several designs for steel-CLT composite floor systems have been assessed in the literature (Section 2.5), and a potential prospective design has been identified. Appropriate layering of the CLT panel enables the desired load dispersion even though the CLT is unique due to its orthotropic properties.

The use of steel-CLT composite beams in these systems offers environmental benefits (Section 1.1.4), as it results in lower carbon dioxide equivalent emissions during raw material acquisition, manufacturing, and assembly compared to steel-concrete composite beams. Additionally, timber's life cycle enables it to store biogenic carbon through its growth, extracting it from the atmosphere.

Additionally, the numerical analysis (Section 5) revealed that a single steel-CLT composite beam can be designed to remain in the elastic phase within the serviceability limit state which enables the implementation of steel-CLT composite beams in floor systems.

Lastly, this feasibility was confirmed in Section 6 where two floor systems were compared in terms of weight, performance, and sustainability. It was demonstrated that the studied floor systems were feasible for application in a residential or office usage scenario.

- ii. In terms of steel-CLT composite shear connections it can be concluded that a connection with better performance, such as higher initial- and secondary stiffness and ultimate load capacity,

can be achieved with the implementation of grout. Secondly, such improved shear connector behaviour in strength and stiffness results in significant increase in composite action for steel-CLT composite beams.

When comparing the existing body of research on steel-CLT composite connections (Section 2.6), it is evident that only a limited number of shear connections have been studied. Apart from standard dowel-type connections (Section 2.6.1), the implementation of grout in steel-CLT composite connections has demonstrated improvements in initial stiffness, secondary stiffness, and ultimate capacity (Section 2.6.3), as displayed by bolted connectors in grouted pockets (BCGP) and screw connectors in grouted pockets (SCGP).

Various sizes of dog screws and coach screws, tested in push-out tests, did not exceed an initial stiffness of 29.65 kN/mm, a secondary stiffness of 11.66 kN/mm, and an ultimate load capacity of 54.4 kN. In contrast, the weakest and least stiff BCGP exhibited an initial stiffness of 39.65 kN/mm, a secondary stiffness of 29.76 kN/mm, and an ultimate load capacity of 82.9 kN [28]. Increasing the dimensions of the bolt and the grouted pocket nearly doubled these performance metrics even further as seen in Table 2.1.

In a different experimental set-up[73] a  $12\phi$  screw-tip was encased in grout to force a particular failure mode and to increase its strength and stiffness. Without the use of grout the screw, in a push-out test, the initial stiffness, secondary stiffness and ultimate load capacity were 12.45 kN/mm, 10.06 kN/mm and 76.33 kN, respectively. Employing grout in a cylinder around the screw tip could increase the initial-, secondary stiffness and ultimate load by 56%, 46% and 12%, respectively (Table 2.1).

In terms of sustainability, the primary influence of the composite connection is its contribution to circularity and demountability within the implemented steel-CLT composite floor system. This contribution is affected by the demountability of the connection, which is notably restricted by the use of grout. However, it should be noted that the sole use of dowel-type connectors as steel-CLT composite connections, in current connection designs, does not guarantee full demountability, as the drilling of screws and the preloading of bolts can cause permanent damage to the timber. Secondly, the significant performance increase, as elaborated upon in the subsequent conclusions, observed in connections utilising grout, as demonstrated in this research, could potentially support the argument for grout use while considering a trade-off with demountability to improve material efficiency.

The impact of the characteristics of the composite shear connection on a steel-CLT composite beam was studied by implementing two significantly different connections in terms of load-slip behavior, as shown in Fig. 5.31 in a numerical analysis of a four-point bending test (Section 4). Comparing the two composite shear connections, the difference is quantitatively evident as the  $19\phi$  screws had lower initial stiffness, secondary stiffness, and ultimate load capacity compared to the  $20\phi$  bolts in a 60 by 135 mm grouted pocket, with the latter being 175%, 762%, and 123% higher, respectively (also depicted in Table 2.1).

In the numerical flexural beam test, where both connections were employed, the increased connector performance led to an average increase of load carried at serviceability limit state, over 3 different distances of connector spacing, of 13.8% (as displayed in Table 5.5). Notable is the fact that their initial bending stiffness and stiffness per unit length were similar, due to nearly identical slope of load-slip figures when little to no slip has occurred. This significant increase in SLS load carrying capacity depicts the a higher level of composite action which is supported by a significant increase in composite efficiency, less slip and less stress deviation between the materials at the interaction interface.

It can conclusively be said that a connection with higher strength and stiffness leads significantly improved load-deflection behaviour and composite action supported by above mentioned details and insights from Section 5.4.2.

Lastly, a prediction of load-slip behaviour of the composite connection with transverse reinforced concrete slots (from Section 2.5.2) was done based on available literature and own analysis. The ultimate load capacity is likely to range from 30 kN to 40 kN, depending on the size and strength of the studs, which are currently undefined in the design. Furthermore, the initial stiffness ( $k_s, 0.4$ ) is estimated to be between 86 kN/mm and 94 kN/mm, while the secondary stiffness ( $k_s, 0.6$ ) is predicted to

be between 52 kN/mm and 72 kN/mm.

- iii. In relation to optimal parametric design considerations, it can be concluded that uniformly and closely spacing connectors significantly improves load-deflection performance and the composite action of the beam. However, there is an optimum point where further decreasing the spacing reduces connection effectiveness. For instance [73] determined this optimal spacing to be 200 mm for SCGP connections (see Table 2.1).

Furthermore, panel width has impact on the total resistable force in serviceability as it increases 5.6% when the panel width is doubled. However doubling the panel width has significant influence on the design scenario. Therefore, the design should meet the requirements of the chosen floor system, including considerations for transverse load dispersion and span instead of maximising behavioural performance through panel width.

As highlighted in Section 5.4.1, the composite action significantly increases as the uniform connector spacing decreases from 500 mm to 300 mm. This decrease results in an increase in the force at serviceability from 135.3 kN to 151.9 kN when using screws as shear connectors. Consequently, the numerical bending stiffness also increases from  $26.72 \times 10^{12}$  Nmm<sup>2</sup> to  $28.98 \times 10^{12}$  Nmm<sup>2</sup>.

With a stiffer composite connection, the force further increases from 153.4 kN to 173.3 kN as the spacing decreases from 500 mm to 300 mm. This corresponds to a bending stiffness increase from  $28.69 \times 10^{12}$  Nmm<sup>2</sup> to  $31.2 \times 10^{12}$  Nmm<sup>2</sup>. These improvements in flexural performance are supported by a reduction of maximum slip at the material interface by half (Fig. 5.11) and a more optimal stress distribution (Section 5.2.4)

In terms of non-uniform connector spacing the location optimisation study in Section 5.3 revealed that the optimised configurations, which concentrate shear connectors near the supports, where shear is highest, hardly influences the steel-CLT composite beam behaviour in the elastic phase as force resisted at serviceability limit state was practically identical for configurations 7,  $7_{O,1}$  and  $7_{O,2}$  as for configuration 12,  $12_{O,1}$  and  $12_{O,2}$ . It can be concluded that in the post-elastic phase the contribution of optimised shear connection location does contribute to less deflection (Fig. 5.27) as the slip is less (Fig. 5.28).

As a design consideration, it can be concluded, based on the aforementioned details, that closely spacing the connectors is desirable for achieving high composite action. However, it should be noted that the numerical analysis did not consider connector spacing closer than 300 mm, as it relied on experimental push-out test data.

The literature study, on the other hand, highlights an important boundary regarding connector spacing. Research [73] has demonstrated that there exists an optimum spacing for a single connection in terms of initial stiffness, secondary stiffness, and ultimate load capacity (Table 2.1). Beyond this optimum spacing, decreasing the spacing further would result in a diminishing performance per composite connection. This counteracts the potential increase in composite efficiency due to additional connectors placed per length. Such optimum is likely to be different per connection type as they interact different locally with the CLT panel.

As mentioned, the force resisted at serviceability increases from 151.9 kN to 156.7 kN and 160.4 kN when widening the CLT panel width from 800 mm to 1200 mm and 1600 mm, respectively, in the numerical study. This increase is significant. However, as discussed in Section 2.5, the design of the floor system is likely the determining factor for the panel width. Therefore, in terms of steel-CLT composite beam performance optimisation, the focus should be directed towards other aspects.

Lastly, the steel profile and beam length have a logical impact on the performance of steel-CLT composite beams, as illustrated in Figure 5.3. With increasing beam length, a higher level of composite efficiency is attained. Similarly, a smaller steel beam profile results in higher composite efficiency. This implies that as the load-carrying capacity of the base scenario, represented by a steel beam alone, decreases, the contribution of the composite interaction with the CLT panel becomes more significant.

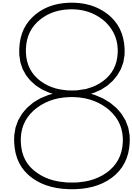
---

In short, when aiming to achieve greater steel-CLT composite beam action, several design considerations should be taken into account. The focus-points include closely spacing stiff and strong composite connections and selecting a panel width that meets the requirements of the floor system in question.

- iv. It can be concluded that the proposed numerical model relatively precisely captures steel-CLT composite beam behaviour in the initial elastic phase whilst the analytical model can over- or underestimate the bending stiffness by more than 10%, dependent on composite connection characteristics. Once the yield strength of the steel-CLT composite beam has been exceeded the scattering of the numerical model decreases to no more than 5% and the proposed numerical model has no ability capture the ultimate load capacity of the beam.

With the application of guidelines for mechanically jointed timber beams, an analytical approach was used to estimate the bending stiffness of steel-CLT composite beams. This approach led to the conclusion that a prediction of behaviour is achievable. However, it should be noted that there is a margin of error just north of 10% in the bending stiffness. The deviation can be an over- or underestimation. This variability is theorised to be a result of the simplification of the connection with a single parameter in the analytical approach. An in-depth discussion of the analytical approach, its limitation and assumptions is done in the Discussion (Section 8).

The numerical model can conclusively be called fairly precise in the level of scatter when comparing the model against experimental data in the elastic phase of steel-CLT composite beam in a four-point bending test as the bending stiffness and initial beam stiffness deviate less than 3% maximally. The most important limitation of the numerical finite element model is its inability to capture ultimate load capacity of the beam and, secondly, the level of precision in the scattering of the results significantly decreases past the elastic state. In terms of the average mean squared error of the load-deflection curve, when comparing the numerical model against experimental data, the level of precision in the scatter of results is about 5%. Similar to the analytical analysis, the level of precision and limitations of the numerical approach will be extensively discussed in Section 8. Additionally, the assumptions made in the analysis have been outlined in Section 4.



# Discussion

In this section, a comprehensive discussion of the analyses and results obtained from both the analytical and numerical investigations will be done. Two key aspects will be covered: the analytical analysis and the numerical analysis along with their respective results. These aspects aim to provide a detailed understanding of the assumptions, limitations, considerations, challenges encountered, and the evaluation of the accuracy and reliability of the models and the analyses.

Additionally, based on the literature study, insights gathered, and results from the conducted analyses, recommendations will also be provided, along with a prospectus for valuable future research that can build upon the findings of this study. Besides delving into the detailed analyses, an assessment is also provided to evaluate the accuracy and reliability of both the numerical finite element model and the analytical initial beam stiffness, including their corresponding bending stiffness. This comparative analysis was presented in Section 4.6 to establish the validity and justification for the research methodology.

Reference is made to experimental data from previous steel-CLT composite beam tests [31]. In this thesis, the experimental data was implemented by visually extracting information from figures with the assistance of software. Therefore, while the implemented experimental data is as precisely as possible, it should be noted that it is not the original data set.

Finally, since a single reference study is used for comparison with experimental data, the reliability of that research becomes crucial. Both input parameters and output results can be subject to inaccuracy, highlighting the need for additional experimental research.

## 8.1. Numerical analysis

This section encompasses a brief discussion of the numerical investigation (Section 5) conducted. It entails critical evaluation of the numerical model (Section 4) in predicting steel-CLT composite beam behaviour by looking at assumptions, limitations and considerations involved. However, most of the assumptions of the finite element model have been extensively described in Section 4. This evaluation will focus on limitations, considerations and results of the model because, as referenced in Section 4, a model is just a simplification of the world and not reality.

The main limitations of the steel-CLT composite beam model proposed in this research are the following:

- (i) Firstly, compared to the elastic phase, the numerical model captures post-elastic behaviour relatively inaccurately (Section 8.1.1).
- (ii) Secondly, the model is unable to capture the ultimate load capacity of the beam; with the proposed manner of capturing non-linear behaviour of the orthotropic CLT panel the cross-section cannot reach full plasticity before termination of the finite element analysis as seen in Section 5.2.4.



With these limitations in mind the numerical model could be considered for analysis of steel-CLT beam design as the serviceability limit state often occurs in the elastic phase of which the model is a relatively precise predictor.

### 8.1.1. Scattering of numerical results

In terms of load-deflection the experimental data[31] was compared twice against the numerical output. The mean deviation in percentage, in both comparisons, was less than 5%. However, this seemed to go both ways as the deflection of the steel-CLT beam with a more flexible connection (Fig. 4.18a) was underestimated by the numerical model while the deflection with a more stiff connection (Fig. 4.18b) was overestimated by the finite element analysis.

The load-deflection comparison considered both the elastic and post-elastic phases. Fig. 4.18 reveals a decrease in scattering of the results during the post-elastic phase of the material. Taking this into account, a detailed analysis focused on the elastic phase was conducted by comparing the initial beam stiffness ( $K_{b,ini}$ ) and corresponding initial bending stiffnesses ( $EI$ ) of both the numerical and analytical analyses with the experimental data.

The numerical model demonstrated remarkable low amount of scatter of the results in the elastic phase, with a deviation of -0.4% for the steel-CLT beam with a more flexible connection (Fig. 4.18a) and a deviation of -2.9% for the deflection of the beam with a stiffer connection (Fig. 4.18b) when compared to the experimental data. This suggests that the numerical model captures the initial behavior of the steel-CLT composite beam with a precise level of scatter. The percentages shown are arguably within the error margin of the previously mentioned fact that data was visually extracted.

## 8.2. Analytical analysis

The analytical analysis discussion focuses on explaining the underlying assumptions, limitations, and considerations involved in the analysis. By examining these aspects, we gain insights into the reliability and applicability of the analytical approach in capturing the complexities of the investigated system and thus the accuracy of the results.

The analytical analysis employed in this research is a 2 step process:

1. Equivalent cross-section of the CLT panel
2. Application of guidance for 'Mechanically jointed beams'(EN1995-1-1 Annex B[19]) on steel-CLT composite beams

Firstly, the equivalent cross-section of the CLT panel is determined using the Gamma method (described in EN 1995-1-1 Annex B[19] and Section 3), as proposed in 'The CLT Handbook'[26]. This methodology explains the calculation for equivalent CLT cross-sections for CLT panels with 3 and 5 layers. However, in this thesis, the methodology has been simplified due to the symmetry of the CLT panel. When employing this method, the calculation is influenced by the reference length of the span. In the case of steel-CLT composite beams, the reference length of the beam is impacted by the support conditions. In practical applications, a beam-end connection partially restricts rotation, thus reducing the reference length.

Secondly, the design guidelines for mechanically jointed beams (EN 1995-1-1 Annex B[19]) for jointed timber beams are applied to steel-CLT composite beams, which are also mechanically jointed. This design method is based on the theory of linear elasticity and is used in this thesis solely to compare the analytical results to the numerical results in the elastic phase.

Regarding the boundary conditions, the beams, in the guidance, are simply supported, and the reference length, similar to the use of the Gamma method for the equivalent cross-section of the CLT, needs to be adjusted if the boundary conditions require it. Furthermore, the load acts vertically in the z-direction on the beam, resulting in a sinusoidal or parabolic moment  $M(x)$  in the guidance for analytical analysis of the beam. This differs from the load scenario analysed in Section 5, where the beam is loaded using a four-point bending test, resulting in a linear increase of moment until the load application point with a constant moment distribution between the loading points. Thus, this possibly results in

inaccuracy in the comparison of effective bending stiffnesses by both analyses. More over, this analytical approach assumes the beam is subjected to pure bending, neglecting other potential load scenarios.

Lastly, the analytical approach captures the behaviour of the steel-CLT composite connection with two parameters in EN1995-1-1 Annex B[19] and does not account for potential joint slip or relative movement between members, which can affect the stiffness and behaviour of the beams.

- The individual parts are connected to each other by mechanical fasteners with a slip modulus  $K$ .
- The spacing  $s$  between the fasteners

By implementing only two parameters the gamma method provides a simplified approach and but may not capture all the complexities and variations in mechanical joint behaviour accurately. For comparison, the implementation of the characteristics of the steel-CLT composite connection is done much more extensively in the numerical analysis where full load-slip behaviour is expressed. In addition, the scatter of the analysis results depends on the quality and reliability of the input data from which the stiffness modulus arises  $K$ .

To overcome this limitation the gamma factor could possibly be determined for different joint configurations, considering the specific joint type and design, size, and the CLT panel.

### 8.2.1. Scattering of analytical results

The scattering of the analytical analysis, although less precise compared to the numerical model, still provides useful insights and estimations. The deviations observed in the analytical analysis indicate that the results are within the order of magnitude of correctness and could potentially be employed in hand calculations. Specifically, the steel-CLT beam with a more flexible connection exhibited a deviation of -11.7% (Fig. 4.18a), while the beam with a stiffer connection showed a deviation of +10.0% (Fig. 4.18b) when compared to the experimental data. This indicates a similar overestimation of the beam with a stiffer connection when compared to the more flexible connection as noted in the numerical load-displacement results.

While these deviations signify a discrepancy, they do provide a rough estimation of the elastic behavior of the steel-CLT composite beam. It is important to consider these limitations when interpreting the results obtained from the analytical analysis.

## 8.3. Recommendations and future research

The present study on steel-CLT composite floor systems has shed light on several important aspects of their design and behaviour. However, further investigation and improvement are still warranted to advance the topic and address unanswered questions. This section presents two categories of future research directions that can build upon the findings of this study, identifying areas for further investigation and improvement.

The first category focuses on the development and implementation of novel steel-CLT composite connections, aiming to activate composite interaction between individual CLT panels and a single steel beam without the use of grout. While the current study explored the performance of existing connections, there is a need to design and test new connections that can facilitate easier implementation of steel-CLT floor systems in circular construction. By investigating the execution and practicality of such steel-CLT composite floor systems along with the newly proposed connection, a more easily implementable floor system with repetitive layout and enhanced utilisation of composite action can be achieved. This research direction will address unresolved questions related to material efficiency, cost-effectiveness, and sustainability in steel-CLT composite floor system execution.

Future research suggestions in regards to steel-CLT composite floor systems and connections:

- Explore and design a novel steel-CLT composite connection capable of activating composite interaction between two individual CLT panels resting on a single steel beam without the use

of grout. This innovative connection would facilitate the implementation of steel-CLT floor beams in floor systems and promoting circular construction practices as there would be no use of grout.

- Investigate the practical implementation and execution of steel-CLT floor systems utilising the aforementioned composite connection. Focus on developing an easily implementable floor system with a repetitive layout that efficiently utilises composite action without relying on grout.
- Conduct a comprehensive comparative study of steel-CLT composite floor systems and traditional systems, evaluating various aspects such as (i) material usage, (ii) performance, (iii) cost, and (iv) life cycle analysis. This study will provide valuable insights into the practical application and advantages of steel-CLT composite floor systems in everyday construction scenarios.

The second category focuses on the analysis of steel-CLT composite beam behaviour, aiming to refine numerical and analytical predictive methods. Although the current study employed numerical finite element models and analytical guidelines, further research is needed to improve their preciseness and reliability. Developing a more advanced numerical finite element model that precisely captures the post-elastic behaviour of steel-CLT beams, including local disruptions and damage, will provide a more comprehensive understanding of their structural response past the elastic state and will highlight the ultimate capacity of a steel-CLT composite beam.

Additionally, exploring analytical approaches that incorporate detailed data on the specific steel-CLT composite connection used, going beyond the limited characterisation of connection behaviour by a single stiffness value ( $K$ ), will enhance the predictive capabilities of analytical methods. This research direction will address the need for more precise and practical tools for analysing steel-CLT composite beams, essential for wide implementation in the built environment.

Future research recommendations for the analysis of steel-CLT composite beam behaviour:

- Develop a numerical finite element model that precisely captures the post-elastic behaviour of steel-CLT beams. Consider utilising solid elements in the model to capture local disruptions and damage, thereby providing a more comprehensive representation of the beam's response.
- Explore possibilities for analytically predicting the behaviour of steel-CLT composite beams. Enhance current analytical approaches by incorporating detailed data on the specific steel-CLT composite connection used, moving beyond the characterisation of the connection behaviour with a single stiffness parameter ( $K$ ) as outlined in current guidelines such as EN1995-1-1 Annex B.
- Research analytical determination of plastic bending moment capacity of the steel-CLT composite cross-section and possibly compare with experimental test as this thesis offers no conclusive insights on ultimate capacity of steel-CLT composite beams.

In summary, these two categories of future research directions offer avenues for further investigation and improvement in the topic of steel-CLT composite floor systems. By addressing the identified areas and building upon the findings of this study, researchers can contribute to the advancement of sustainable construction practices and the widespread adoption of steel-CLT composite floor systems which will enable construction with environmentally friendly and materially efficient solutions.

# References

- [1] J.R. Aira et al. "Static and kinetic friction coefficients of Scots pine (*Pinus sylvestris* L.), parallel and perpendicular to grain direction". In: *Mater. Construcc.* 64 (2014), p. 315.
- [2] Y. A. Ali et al. "Studying the effect of shear stud distribution on the behavior of steel–reactive powder concrete composite beams using ABAQUS software". In: *Journal of the Mechanical Behavior of Materials* (2022). doi: 10.1515/jmbm-2022-0046.
- [3] C.G. Bailey. "Efficient arrangement of reinforcement for membrane behaviour of composite floor slabs in fire conditions". In: *Journ. Constr. Steel Res.* 59 (2003), pp. 931–949.
- [4] T. Bogensperger, M. Augustin, and G. Schickhofer. "Properties of CLT-Panels Exposed to Compression Perpendicular to their Plane". In: *Inter. Council for Research and Innovation in Build. Constr. Working Commission W18 Timber Structures* (2011).
- [5] R. Brandner. "Production and Technology of Cross Laminated Timber (CLT): A state-of-the-art Report". In: *Euro. Conf. on CLT 1* (2013).
- [6] R. Brandner et al. "Cross laminated timber (CLT): overview and development". In: *Eu. Journ. Wood and Wood Prod.* 74 (2016), pp. 331–351.
- [7] A. Ceccotti et al. "SOFIE project - 3D shaking table test on a seven-storey full-scale cross-laminated timber building". In: *Earthquake Eng. Struc. Dyn.* 42 (2013).
- [8] W. S. Chang et al. "Development of all-wood connections with plywood flitch plate and oak pegs". In: *Adv. Struc. Eng.* 14 (2011), pp. 123–131.
- [9] A.A. Chiniforush et al. "Dimensional stability and moisture-induced strains in spruce cross-laminated timber (CLT) under sorption/desorption isotherms". In: *Constr. Build. Mat.* 356 (2022).
- [10] I.P. Christovasilis et al. "Evaluation of the mechanical properties of cross laminated timber with elementary beam theories". In: *Constr. Build. Mat.* 122 (2016), pp. 202–213.
- [11] Dassault Systèmes. *ABAQUS 2021*. Version 2021. Vélizy-Villacoublay, France, 2021. url: <https://www.3ds.com/products-services/simulia/products/abaqus/>.
- [12] C. Dickof, S. F. Stierner, and S. Tesfamariam. "Wood-Steel Hybrid Seismic Force Resisting Systems: Seismic Ductility". In: *12th World Conference Timb. Eng.* (2012).
- [13] C. Dickof et al. "CLT-Steel Hybrid System: Ductility and Overstrength Values Based on Static Pushover Analysis". In: *Journ. of Perf. Constr. Facil.* 28 (2014).
- [14] F. V. Emperger. "Die bulbeisendecke, system pohlmann". In: *Beton und Eisen* 3.3/4 (1904), pp. 159–235.
- [15] *Eurocode - Basis of Structural Design*. European Standard. EN 1990:2002+A1:2005/AC:2009. European Committee for Standardization (CEN), 2005.
- [16] *Eurocode 1: Actions on structures - Part 1-1: General actions - Densities, self-weight, imposed loads for buildings*. European Standard. EN 1991-1-1:2002+A1:2014/AC:2014. European Committee for Standardization (CEN), 2002.
- [17] European Committee for Standardization. *EN 1994-1-1: Eurocode 3: Design of steel structures - Part 1-1: General rules and rules for buildings*. EN 1993-1-1. 2004.
- [18] European Committee for Standardization. *EN 1994-1-1: Eurocode 4 - Design of composite steel and concrete structures - Part 1-1: General rules and rules for buildings*. EN 1994-1-1. 2004.
- [19] European Committee for Standardization. *EN 1995-1-1: Eurocode 5 - Design of timber structures - Part 1-1: General - Common rules and rules for buildings*. EN 1995-1-1. 2004.

- [20] European Committee for Standardization (CEN). *Eurocode 5: Design of timber structures - Part 1-1: General - Common rules and rules for buildings, ANNEX B*. EN 1995-1-1. 2004.
- [21] European Committee for Standardization (CEN). *Timber Structures - Joints Made with Mechanical Fasteners – General Principles for the Determination of Strength and Deformation Characteristics*. Standard. Brussels, Belgium, 1991.
- [22] European Committee for Standardization (CEN). “Timber Structures – Glued Laminated Timber and Glued Solid Timber – Requirements”. In: *NEN-EN* (2013).
- [23] M. Flaig and H. J. Blaß. “Shear strength and shear stiffness of CLT-beams loaded in plane”. In: *CIB-W18 46* (2013).
- [24] Proceedings of the GBEN Conference. *Global Built Environment: Towards an Integrated Approach for Sustainability*. Corporation Street, Preston, PR12HE: Global Built Environment Network c/o Department of Built Environment at University of Central Lancashire, 2006. isbn: 978-1-84728-396-2.
- [25] M.C. Green and J.E. Karsh. “TALL WOOD - The case for tall wood buildings”. In: *Vancouver: Wood Enterprise Coalition* (2012).
- [26] A. Gustafsson et al. *The CLT Handbook*. Swedish Wood: Föreningen Sveriges Skogsindustrier, 2019.
- [27] M. I. Hamakareem. *Design Procedure of Reinforced Concrete T-beam with Example*. <https://theconstructor.org/structural-engg/design-procedure-reinforced-concrete-beam/225363/>. 2023.
- [28] A. Hassanieh, H. Valipour, and M. Bradford. “Composite connections between CLT slab and steel beam: Experiments and empirical models”. In: *Journ. of Constr. St. Res.* 138 (2017), pp. 823–836.
- [29] A. Hassanieh, H. Valipour, and M. Bradford. “Development of steel-timber composite system for large scale construction”. In: *World Conference on Timber Engineering* (2016).
- [30] A. Hassanieh, H. Valipour, and M. Bradford. “Experimental and analytical behaviour of steel-timber composite connections”. In: *Constr. Build. Mat.* 118 (2016), pp. 63–75.
- [31] A. Hassanieh, H. Valipour, and M. Bradford. “Experimental and numerical investigation of short-term behaviour of CLT-steel composite beams”. In: *Eng. Structures* 144 (2017), pp. 43–57.
- [32] A. Hassanieh, H. Valipour, and M. Bradford. “Experimental and numerical study of steel-timber composite (STC) beams”. In: *Journ. of Constr. St. Res.* 122 (2016), pp. 367–378.
- [33] A. Hassanieh, H. Valipour, and M. Bradford. “Load-slip behaviour of steel-cross laminated timber (CLT) composite connections”. In: *Journ. of Constr. St. Res.* 122 (2016), pp. 110–121.
- [34] A. Hassanieh, H.R. Valipour, and M.A. Bradford. “Bolt shear connectors in grout pockets: Finite element modelling and parametric study”. In: *Constr. Build. Mat.* 176 (2018), pp. 179–192.
- [35] G. Hochreiner, J. Füssl, and J. Eberhardsteiner. “Cross-laminated Timber Plates Subjected to Concentrated Loading”. In: *Strain* 50 (2014).
- [36] International Energy Agency. “Global Status Report for Buildings and Construction”. In: (2021).
- [37] J. Jacob and O. Barragán. “Flexural Strengthening of Glued Laminated Timber Beams with Steel and Carbon Fiber Reinforced Polymers”. In: *Dept. Civ. Env. Eng. Chalmers University of Technology* (2007).
- [38] R.-A. Jöbstl et al. “A Contribution to the Design and System Effect of Cross Laminated Timber”. In: *CIB W18 39* (2006).
- [39] M. Kaestner and K. Rautenstrauch. “Efficient shear transfer in timber-concrete composite bridges by means of grouting with polymer mortar”. In: *World Conference on Timber Engineering* (2016).
- [40] N. Khorsandnia, H. R. Valipour, and K. Crews. “Experimental and analytical investigation of short-term behaviour of LVL-concrete composite connections and beams”. In: *Constr. Build. Mater.* 37 (2012), pp. 229–238.

- [41] N. Khorsandnia, H. R. Valipour, and K. Crews. "Nonlinear finite element analysis of timber beams and joints using the layered approach and hypoelastic constitutive law". In: *Eng. Str.* 46 (2013), pp. 606–614.
- [42] D. Lam, K.S. Elliott, and D.A. Nethercot. "Parametric study on composite steel beams with precast concrete hollow core floor slabs". In: *Journal of Constructional Steel Research* 54 (2000), pp. 283–304. doi: 10.1016/S0143-974X(99)00072-9. url: <https://www.sciencedirect.com/science/article/pii/S0143974X99000729>.
- [43] C. Loss and B. Davison. "Innovative composite steel-timber floors with prefabricated modular components". In: *Eng. Struc.* 132 (2017), pp. 695–713.
- [44] C. Loss, M. Piazza, and R. Zandonini. "Connections for steel-timber hybrid prefabricated buildings. Part I: Experimental tests". In: *Constr. Build. Mater.* 122 (2016), pp. 781–795.
- [45] C. Loss, M. Piazza, and R. Zandonini. "Connections for steel-timber hybrid prefabricated buildings. Part II: Innovative modular structures". In: *Constr. Build. Mater.* 122 (2016), pp. 796–808.
- [46] C. Loss, M. Piazza, and R. Zandonini. "Experimental tests of cross-laminated timber floors to be used in timber-steel hybrid structures". In: *13th World Conference Timb. Eng.* (2014).
- [47] R. Masoudnia, A. Hashemi, and P. Quenneville. "Predicting the Effective Flange Width of a CLT Slab in Timber Composite Beams". In: *ASCE* 144 (2018).
- [48] S. Moreira et al. "Experimental behavior of masonry wall-to-timber elements connections strengthened with injection anchors". In: *Eng. Struc.* 81 (2014), pp. 98–109.
- [49] P. Muller. "Decke aus hochkantig stehenden Holzbohlen oder Holzbrettern und Betondeckschicht". In: *Patentschau aus dem Betonbau und den damit verwandten Gebieten, Auszüge aus den Patentschriften, Beton und Eisen* 17 (1922), S. 244 (in German).
- [50] K. S. Naraine. "Slip and Uplift Effects in Composite Beams". Master's thesis. Hamilton, Ontario, Canada: McMaster University, 1984.
- [51] J. H. Negrão et al. "Numerical and experimental study of small-scale moment-resistant reinforced concrete joints for timber frames". In: *Constr. Build. Mat.* 118 (2016), pp. 89–103.
- [52] NEN (Netherlands Standardization Institute). *National Annex to NEN-EN 1991-1-1+C1+C11: Eurocode 1 - Actions on structures - Part 1-1: General actions – Densities, self-weight, imposed loads for buildings*. Technical Report. Part of Eurocode 1: EN 1991-1-1:2002+A1:2014/AC:2014. 2014.
- [53] D. Nethercot, ed. *Composite Construction*. London: Spon Press, 2003. isbn: 0-415-24662-8.
- [54] M. P. Newcombe et al. "Section analysis and cyclic behavior of post-tensioned jointed ductile connections for multi-story timber buildings". In: *Eng. Struc.* 12 (2008), pp. 83–110.
- [55] Y. Nie, A. Karimi-Nobandegani, and H.R. Valipour. "Experimental behaviour and numerical modelling of timber-timber composite (TTC) joints". In: *Constr. Build. Mat.* 290 (2021).
- [56] F. Nouri and H.R. Valipour. "Semi-rigid partial-strength steel-timber composite (STC) connections with mechanically anchored steel rods". In: *Journ. Constr. Steel Res.* 158 (2019), pp. 560–575.
- [57] A. Romero et al. "Numerical investigation of steel-LVL timber composite beams". In: *Mater. Construcc.* 64 (2022), p. 315.
- [58] R. Sathre and J. O'Connor. "A Synthesis of Research on Wood Products and Greenhouse Gas Impacts 2nd Edition". In: *FPIInnovations TR-19R* (2010), p. 117.
- [59] J. Schneider et al. "Damage Assessment of Connections Used in Cross-Laminated Timber Subject to Cyclic Loads". In: *Journ. Perf. Constr. Facil.* (2013).
- [60] M. K. Schober, W. Becker, and J. Weber. "Grouted joints in timber engineering". In: *World Conference on Timber Engineering* (2016).
- [61] E. Serrano and B. Enquist. "Compression strength perpendicular to grain in cross-laminated timber (CLT)". In: *World Conference on Timber Engineering* (2010).

- [62] S. Shulman and C. Loss. "High-performance grout-reinforced shear connectors for hybrid steel-cross-laminated timber building systems: Experimental study". In: *Journ. Build. Eng.* 67 (2023).
- [63] H. Valipour et al. "A simple strategy for constitutive modelling of timber". In: *Constr. Build. Mat.* 53 (2014), pp. 138–148.
- [64] V. Vigneri, C. Odenbreit, and A. Romero. "Numerical study on design rules for minimum degree of shear connection in propped steel–concrete composite beams". In: *Eng. Struc.* 241 (2021).
- [65] Ronald Wagner. "ABAQUS Tutorial: Damage for Fibre-Reinforced Composites - Material Model Explained - Hashin Damage". In: (Mar. 2021).
- [66] F. Wanninger and A. Frangi. "Experimental and analytical analysis of a post-tensioned timber connection under gravity loads". In: *Eng. Struc.* 70 (2014), pp. 117–129.
- [67] B.H. Xu, A. Bouchaïr, and P. Racher. "Mechanical behavior and modeling of dowelled steel-to-timber moment-resisting connections". In: *Jour. Struc. Eng. ASCE* 141 (2015).
- [68] R. Yang et al. "Mechanical behaviour of steel timber composite shear connections". In: *Constr. Build. Mater.* 258 (2020).
- [69] D. Yeoh et al. "Experimental tests of notched and plate connectors for LVL-concrete composite beams". In: *Journ. of Struc. Eng.* 137 (2011), pp. 261–269.
- [70] D. Yeoh et al. "State of the Art on Timber-Concrete Composite Structures: Literature Review". In: *Journ. Struc. Eng.* 137 (2011).
- [71] Miguel Yurrita and José Manuel Cabrero. "On the need of distinguishing ductile and brittle failure modes in timber connections with dowel-type fasteners". In: *Eng. Struc.* 242 (2021).
- [72] H. Zhang and Z. Ling. "Finite Element Modeling on Shear Performance of Grouted Stud Connectors for Steel-Timber Composite Beams". In: *Materials* 15 (2022).
- [73] Yong Zhao et al. "Experimental study on shear performance of steel-timber screw connectors with grout pockets". In: *Eng. Struc.* 266 (2022).